2012

Understanding Controlled Evaporation Of Microdroplets Towards Scalable Micro/Nano Manufacturing

Taye Dickson Esho
North Carolina Agricultural and Technical State University

UNDERSTANDING CONTROLLED EVAPORATION OF MICRODROPLETS TOWARDS SCALABLE MICRO/NANO MANUFACTURING

by

Taye Dickson Esho

A dissertation submitted to the graduate faculty
in partial fulfillment of the requirements for the degree of
DOCTOR OF PHILOSOPHY

Department: Industrial and Systems Engineering
Major: Industrial and Systems Engineering
Major Professor: Dr. Salil Desai

North Carolina A&T State University
Greensboro, North Carolina
2012

ABSTRACT

Esho, Taye Dickson. UNDERSTANDING CONTROLLED EVAPORATION OF MICRODROPLETS TOWARDS SCALABLE MICRO/NANO MANUFACTURING. (**Major Professor: Dr. Salil Desai**), North Carolina Agricultural and Technical State University.

This research investigates the controlled evaporation of microdroplets to the nano scale regime for scalable micro/nano manufacturing. A customized direct write inkjet printing system was utilized to generate monodisperse microdroplets of different fluid types. Two novel approaches were employed to achieve the research objective. The first approach incorporated a convective heat source (i.e. resistive heated ring) to induce controlled heat flux for microdroplet evaporation after ejection from the inkjet system. The temperature of the heated ring was varied to observe reduction of the microdroplet via heat transfer to its lateral periphery. The second approach employed a radiative source (i.e. CO_2 laser) which enabled the droplet to be completely encapsulated by the lasing beam for controlled evaporation. The significance of lasing power, lasing frequency, nozzle size, and fluid type were assessed by statistical hypothesis testing. Volumetric reduction analysis of the two approaches demonstrated that the radiative source exhibited higher reductions of microdroplets under equivalent experimental conditions as compared to the convective source. Direct write inkjet printing of carbon nanotube colloids was employed to fabricate functional electronic devices (i.e. flexible thin film transistors) towards large scale manufacturing. Based on the findings of the droplet reduction experiments, two fluids namely, nanotube colloid and dye-saturated aqueous solution were evaluated for spread behavior at different lasing power outputs. Significant reductions in droplet volumes and spread behavior were observed over the power

modulation range demonstrating scalable features with high repeatability. This research provides a framework for achieving controlled evaporation of features at the micrometer range with the aim of transforming those features to the nanoscale.

School of Graduate Studies
North Carolina Agricultural and Technical State University

This is to certify that the Doctoral Dissertation of

Taye Dickson Esho

has met the dissertation requirements of
North Carolina Agricultural and Technical State University

Greensboro, North Carolina
2012

Approved by:

_____	_____
Dr. Salil Desai Major Professor	Dr. Steven Jiang Committee Member
_____	_____
Dr. Daniel Mountjoy Committee Member	Dr. Silvanus Udoka Committee Member
_____	_____
Dr. Paul Stanfield Department Chairperson	Dr. Sanjiv Sarin Associate Vice Chancellor of Research and Graduate Dean

DEDICATION

This dissertation is dedicated in loving memory to my late grandmother, who was very instrumental in my upbringing. She raised me along with my twin brother, who is currently a medical student, to be the men that we are today. She instilled principles such as honesty, hard work, discipline, and most importantly the love of God in us. And to my lovely parents, my siblings, and the rest of the family, I love you all and I thank you all for your support and encouragement.

BIOGRAPHICAL SKETCH

Taye Dickson Esho was born on May 6, 1986, in Ibadan, Nigeria. The first of twin boys, Taye immigrated to the United States at the tender age of 10 along with his twin brother to reunite with their father in Maryland. He received his high school diploma from Frederick Douglass High School in Upper Marlboro, MD in June 2004. He received the Bachelor of Science degree in Industrial and Systems Engineering from North Carolina Agricultural and State University in May 2008 and enrolled in the Doctoral program the following semester as a direct-track student. He is a candidate for the PhD in Industrial and Systems Engineering with a concentration in Manufacturing and Service Enterprise Engineering.

ACKNOWLEDGEMENTS

Glory to God for His many blessings in enabling me to finish this dissertation. I thank God for the favor, mercy, grace, love, and peace that He faithfully provided to me throughout every facet of my studies.

I am also thankful to my advisor, Dr. Desai, for his support both academically and financially over the last four years. I am also grateful for the faith that he showed in me by trusting me to work on an innovative research for which he has intellectual property filed. Furthermore, I appreciate his willingness to come to the lab to provide assistance and support whenever I experienced technical issues with equipments. He worked tirelessly over the years in ensuring that I had everything I needed to ensure my success in the lab and for that I am very thankful. I also thank my committee members (Dr. Jiang, Dr. Mountjoy, and Dr. Udoka) for their willingness to be on my committee despite their busy schedules and their support and encouragements over the years dating back to my years as an undergraduate student.

Special thanks go to Dr. Park who was the chair of our department when I was finishing my bachelor's degree in 2008. My intention was to attend graduate school as a master's student and to obtain employment after completion. However, Dr. Park informed me that I should consider joining as a direct track PhD candidate, which I was unaware was even possible at the time. Hence, I am so thankful that he thought enough of me to inform me of the opportunity and I now realize that it was well worth it. Dr. Park also helped me in getting the Sloan fellowship which has provided financial assistance to me during my doctoral work for which I am so thankful.

I also thank other faculty members (excluding those already mentioned) in the department who has helped me along the way since my undergraduate years in terms of sharing their knowledge with me through courses I took with them and for helping me during their office hours. They also provided me with recommendation letters and served as references whenever I needed them. Furthermore, they provided words of encouragement while also advising and challenging me along the way. Hence I am truly appreciative for Dr. Ram, Dr. Ntuen, Dr. Stanfield, Professor Oneyear, and Dr. Davis. I also thank the mother of our department, Mrs. Brooks, for being tremendously helpful over the years.

I also thank all of my colleagues for their support and encouragements over the years. Specifically those in my research group, Mr. Ravi Kaware, have always been very supportive of me. He always encourages me to stay focused as well as for his prayers and well wishes. He assisted me with the initial phase of this research and for that I am truly grateful. I am thankful to Ms. Jessica Perkins for her assistance with the UV spec machine. I also thank Mr. Kwame Adarkwa for his assistance in experimental setup as well as his availability to assist with experiments. I also acknowledge past members of the research group for helping me in my early years in the group. I also thank Ms. Svitlana and Mr. Rueben for assisting me in IRC with the SEM machine. I thank everybody that has assisted me in any capacity including in courses taken together over the years and/or for giving me advice.

I also thank my family for their support and continual prayers for me. They have always being there for me. I thank both of my mothers for their unconditional love and

encouragement. I also thank my siblings (Kenny, Maxie, Dee Dee, Larry, Tony, and Adeola) for their support as well as my uncles (Uncle Johnson, Uncle Mike, Uncle Samson, Uncle Thomas, and Duni) for the love that they have always provided to me. I am also thankful for the support of my girlfriend (Fran) and her prayers. I am so thankful that God provided me with such a Proverbs 31 woman, whom I love dearly and can't wait to marry. I am also grateful to my church family (Mount Zion Baptist Church), especially the young adult ministry which I have been a part of for about two years now, for their encouragement and prayers. I have grown so much spiritually, emotionally, and mentally since being connected to a church where the presence of God resides. Particularly, I am so appreciative of my mentor and young adult pastor (Pastor DeJuan Harris and his lovely wife, First Lady Sannyu) for being there for me and keeping me covered in prayer. He is truly a man of God and the epitome of what a Godly man should strive to be. I love them so much and will be sadden when I have to relocate for work.

I am truly thankful to everybody and I apologize if I failed to mention your name, it was not intentional. Thanks to Ms. Norma Smith in the financial aid office for finding scholarships for me during those financially difficult undergraduate years. I truly appreciate all of your efforts.

Last but not least, I am grateful for the opportunities and experiences that I had here at one of the best universities in the world, North Carolina Agricultural and Technical State University, **AGGIE PRIDE!**

TABLE OF CONTENTS

LIST OF FIGURES

FIGURE **PAGE**

LIST OF TABLES

TABLE **PAGE**

CHAPTER 1

INTRODUCTION

1.1 Brief Overview of Miniaturized Manufacturing

Many of the recent manufacturing efforts are focusing on the fabrication of small scale features to form a product at similar dimension scales as its components. There are numerous examples of such products, i.e., iPods and iPads, cell phones, integrated circuits, mini laptops, etc., that can readily serve as a basis for this shift in the manufacturing paradigm. Perhaps the major enabler of this paradigm change can be attested to the technological advances that realize the manufacturing of products at smaller length scales. In addition, the ever-increasing demand of consumers to have portable, light-weight products as opposed to products manufactured several decades ago have similarly contributed to this observed shift in manufacturing. Consequently, there are many stakeholders avidly interested in the development of such products and systems. Mahalik (Editor: *Micromanufacturing and Nanotechnology, 2006)*, aptly states the following statement to capture the essence of this trend:

> Many industries in conjunction with academic institutions and R&D sectors are active in this multiphysics-mulitengineering sector so that the manufacturing of smaller parts, components, products and systems at the level of micro/nanoscale with more functionalities and capabilities can easily be realised (Mahalik, 2006, pg.1).

Mahalik goes further to describe manufacturing, regardless of level (i.e. macro or micro/nanoscale), as the basis of the economic growth of many industrialized nations; thus insinuating the significance of manufacturing and the obligation to continue its progression so long as technological advancements enable us. As technology continues to

evolve, the manufacturing trend will continue towards the development of smaller products with increased functionality at much lower cost due to less materials usage and operating costs. Hence, tremendous interests have been generated in both academe and industry research that focus on the development and application of nanoscale devices. These miniaturized components produce novel products with applications across many fields including automotive, aerospace, computers and electronics, medicine (e.g. lab-on-a chip), and so forth (Mahalik, 2006). An example of such systems is micro-opto-electromechanical systems (MOEMS), a miniaturized system fabricated via several micromanufacturing techniques, provides a combination of optics, micromechanics, and microelectronics based on the application and device type (Mahalik, 2006).

Miniaturize means to design or construct in small size (Merriam Webster online dictionary). Therefore, miniaturized manufacturing can be defined as the fabrication of devices, products and/or systems ranging from the nanometer to micrometers scale size. Richard Feynman, during his renowned lecture in 1959, was one of the first scientists to propose the prospect of manufacturing at the micro and nano scale (Feynman, 1961). There are numerous advantages for manufacturing at such length scales including but not limited to accuracy and precision, reduction in the material usage, reduction in costs associated with manufacturing processes based on their mass production capability, faster production rates, and so forth. In spite of these promising benefits, the realization of miniaturized manufacturing is in jeopardy until the core scientific principles are systematically investigated. Busnaina (2007) stated that a lack of understanding of barriers to manufacturing at the nanoscale has hindered the transfer of its execution into

technology. This highlights the difficulty of manufacturing realizable products at such small scales. There are several reasons for this impediment including the variable nature of forces (e.g. gravitational, friction, stiction, electrostatic, etc.) that are negligible at the micro/nano scale (Chen et al., 2007) but are significant at the macroscopic level. Materials have be known to exhibit superior properties at the nanoscale such as increased mechanical, electrical, and magnetic properties as compared to macro scale counterparts. Carbon nanotubes are exemplary materials that exhibit such superior properties of mechanical (Salvetat et al., 1999), mechanical and thermal (Ruoff and Lorents, 1995), and thermal (Hone, 2004). Consequently, it is essential that the concepts of micro and nano manufacturing are thoroughly explored for their transition to realizable entities.

1.1.1 Micromanufacturing.

Micro-manufacturing, synonymous with microfabrication, is the development or creation of features and/or components at micrometer ranges. Microfabrication is generally associated with manufacturing of microelectronic devices such as integrated circuits (Grochowski et al., 1997), MOEMS (Hornak et al., 1997), microsensors (Mohr et al., 1991), microelectromechanical systems (MEMS) (Fujita, 1997), thin film transistors (TFTs) (Brody, 1984), just to name a few; these devices are infamous to the semiconducting industry since many of the devices are formed on semiconducting substrates, i.e., silicon (Reichl, 1986), glass (Ren et al., 1998), polymers (Ko et al., 2007), among others because most are not freestanding (i.e. standalone) devices. MEMS are exemplary of microelectronic devices that are fabricated via micromanufacturing processes (Yoon et al., 1998). MEMS further exemplify the vast applicability of

micromanufacturing technologies through their applications across several sectors such as automotive (Eddy and Sparks, 1998; Müller-Fiedler and Knoblauch, 2003), biomedical (Li et al., 2004; Polla, 2001), aerospace (Jang and Liccardo, 2007), defense (Tang and Lee, 2001), and many more. Piezoelectrically-driven micronozzles used in printing applications are an example of MEMS. These nozzles involve the coupling of multiple fields including electrostatic, structural and fluidic resulting in the formation of a precise monodisperse microdroplet. The significance of micro-sized nozzles to this research will be later revealed in much detail as it is the primary source in one of the technologies discussed in the methodology chapter.

Given that micro-devices are fabricated using micromanufacturing processes, a few micromanufacturing processes will be discussed below. Additionally, it should be mentioned that micromanufacturing methods are also referred to as top-down manufacturing approach (Mijatovic et al., 2005). Moreover, top-down manufacturing methods are typically based on patterning or modification of a large scale (i.e. macroscale) material such that reductions in the microscale range are attained and at times even further reduced towards nanoscale. However, bottom-up manufacturing approaches are associated with nanomanufacturing since it aims to assemble atom-by-atom to achieve precise and specific products and systems at the nanoscale, i.e., 1-10nm. The latter approach will be discussed in the ensuing section. Photolithography, chemical vapor deposition, and plasma etching are the micromanufacturing technologies that are briefly discussed. The intention here is to briefly highlight different examples of micromanufacturing technologies rather than delve into each process in its entirety.

1.1.1.1 Photolithography.

Photolithography, also known as optical lithography, is a patterning technique that enables patterns to be placed on the surface of a desired substrate. The technique can be further described as the process of transferring shapes (i.e. patterns) on a mask to the surface of a silicon wafer. Guijt and Breadmore (2008) explained it as the basis for microfabrication processes. The objective of the process is to selectively remove parts of a thin film using light as the media to transfer a geometric pattern from a photomask to a photoresist. The steps, sequentially, in the process are wafer cleaning, barrier layer formation, photoresist application, soft baking, mask alignment, exposure and development, and hard-baking. In the initial step (wafer cleaning), the wafer is chemically cleaned and then silicon oxide is deposited on the wafer, serving as the barrier layer. The photoresist is then applied as a thin film layer, which can be either positive or negative. A positive photoresist when exposed to ultraviolet (UV) light will enable the underlying material to be removed whereas a negative photoresist enables the opposite. Hence, in negative photoresist, the exposed area remains on the substrate while material from the unexposed areas are removed. Soft baking comprises of the removal of most of the material of the photoresist coating. Mask alignment ensures that the mask is aligned with the wafer prior to the exposure and development step, which applies UV light to develop patterning on the substrate. Lastly, the hard baking step involves hardening of the photoresist and improves the adhesion of the resist to the wafer. An illustration of the photolithography process is depicted below in Figure 1.1.

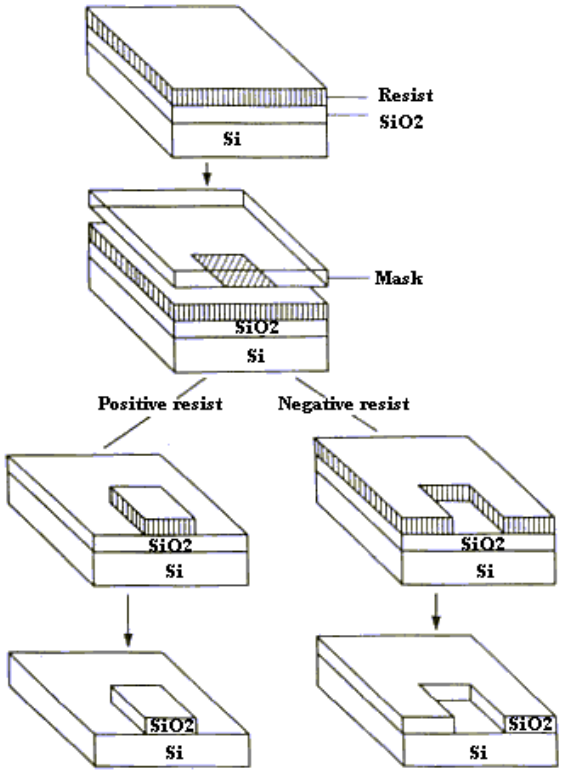

Figure 1.1. Depiction of photolithography process (courtesy: http://www.ece.gatech.edu/research/labs/vc/theory/photolith.html).

1.1.1.2 Chemical Vapor Deposition.

Another microfabrication technique widely used in the microelectronics industry is the chemical vapor deposition (CVD) process. CVD is a chemical process used to produce solid thin-film materials (Creighton and Ho, 2001). The process is also regarded as a material processing technology with most of its applications concentrated in the semiconductor industry. The process includes introducing a precursor gas or gases into a chamber containing one or more heated objects to be coated. Chemical reactions subsequently occur on or near the heated surface to enable deposition of a thin film onto the substrate (i.e. silicon wafer). The process is flexible since several different chemical

elements can be deposited. The elements that have been deposited thus far by researchers are shaded in Figure 1.2. There are also many different variants of the process due to differences in the operating pressure (atmospheric, low-pressure, or ultra-high vacuum), vapor (aerosol assisted or direct liquid injection), plasma methods (microwave plasma assisted, plasma enhanced, or remote plasma enhanced), and so forth. Figure 1.3 shows the fabrication process for an optoelectric integrated circuit in which the CVD process was employed by Furukawa et al. (2007).

PERIODIC TABLE

IA	IIA	IIIA	IVA	VA	VIA	VIIA	VIII			IB	IIB	IIIB	IV	VA	VIB	VIIB	O
1 **H** 1.008																	2 **He** 4.003
3 **Li** 6.941	4 **Be** 9.012											5 **B** 10.81	6 **C** 12.01	7 **N** 14.01	8 **O** 16.00	9 **F** 19.00	10 **Ne** 20.179
11 **Na** 22.990	12 **Mg** 24.305											13 **Al** 26.98	14 **Si** 28.05	15 **P** 30.97	16 **S** 32.06	17 **Cl** 35.45	18 **Ar** 39.948
19 **K** 39.098	20 **Ca** 40.08	21 **Sc** 44.956	22 **Ti** 47.90	23 **V** 50.942	24 **Cr** 51.996	25 **Mn** 54.938	26 **Fe** 55.847	27 **Co** 58.933	28 **Ni** 58.70	29 **Cu** 63.546	30 **Zn** 65.39	31 **Ga** 69.72	32 **Ge** 72.61	33 **As** 74.92	34 **Se** 78.96	35 **Br** 79.90	36 **Kr** 83.80
37 **Rb** 85.468	38 **Sr** 87.62	39 **Y** 88.906	40 **Zr** 91.22	41 **Nb** 92.906	42 **Mo** 95.94	43 **Tc** (99)	44 **Ru** 101.07	45 **Rh** 102.905	46 **Pd** 106.4	47 **Ag** 107.868	48 **Cd** 112.4	49 **In** 114.8	50 **Sn** 118.7	51 **Sb** 121.8	52 **Te** 127.6	53 **I** 126.9	54 **Xe** 131.30
55 **Cs** 132.905	56 **Ba** 137.33	57 **La** 138.9	72 **Hf** 178.49	73 **Ta** 180.941	74 **W** 183.85	75 **Re** 186.2	76 **Os** 190.2	77 **Ir** 192.22	78 **Pt** 195.09	79 **Au** 196.966	80 **Hg** 200.59	81 **Tl** 204.37	82 **Pb** 207.2	83 **Bi** 209.0	84 **Po** (210)	85 **At** (210)	86 **Rn** (222)
87 **Fr** (223)	88 **Ra** (226)	89 **Ac** 227.0															

LANTHANIDES	57 **La** 138.9	58 **Ce** 140.115	59 **Pr** 140.1	60 **Nd** 144.2	61 **Pm** (145)	62 **Sm** 150.4	63 **Eu** 152.0	64 **Gd** 157.2	65 Tb 158.9	66 **Dy** 162.5	67 **Ho** 164.9	68 **Er** 167.2	69 **Tm** 168.9	70 **Yb** 173.0	71 **Lu** 174.96
ACTINIDES	89 **Ac** 227.0	90 **Th** 232.0	91 **Pa** 231.0	92 **U** 238.0	93 **Np** 237.0	94 **Pu** (244)	95 **Am** (243)	96 **Cm** (247)	97 Bk (247)	98 **Cf** (251)	99 **Es** (252)	100 **Fm** (257)	101 **Md** (256)	102 **No** (259)	103 **Lr** (257)

Figure 1.2. Elements (shaded) deposited by CVD
(courtesy: Creighton and Ho, 2001).

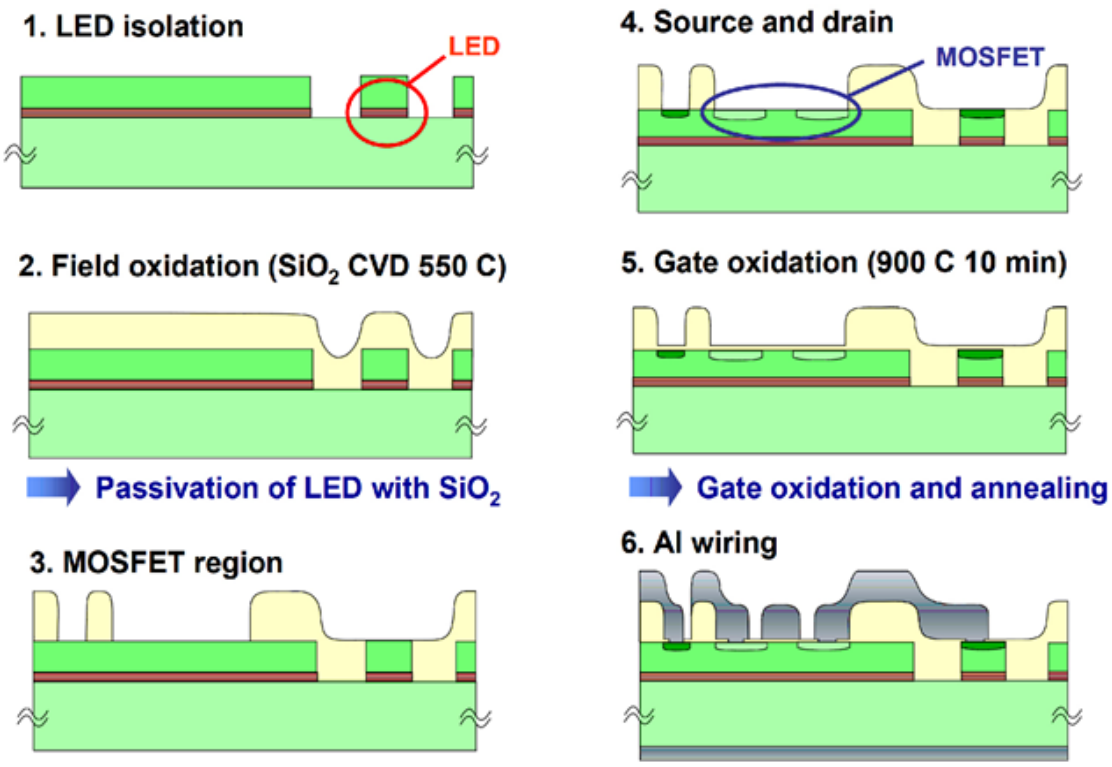

Figure 1.3. Depiction of an optoelectronic integrated circuit fabricated via CVD (courtesy: Furukawa et al., 2007).

1.1.1.3 Plasma Etching.

Plasma Etching is another micromanufacturing/microfabrication process that is associated with the microelectronic industry. This process is used to fabricated integrated circuits and involves plasma (high speed glow of gas mixture) fired in pulses upon a sample. The intention of this process is to modify the physical properties of the target (i.e. sample) from the chemical reactions between the elements of the etching material and those generated by the plasma; the chemical reaction is formed on or slightly below the substrate. The process is capable of being utilized to produce patterns at both the micro and nanometer scales (Cardinaud et al., 2000). A schematic of a device fabricated using the plasma etching process is displayed in Figure 1.4.

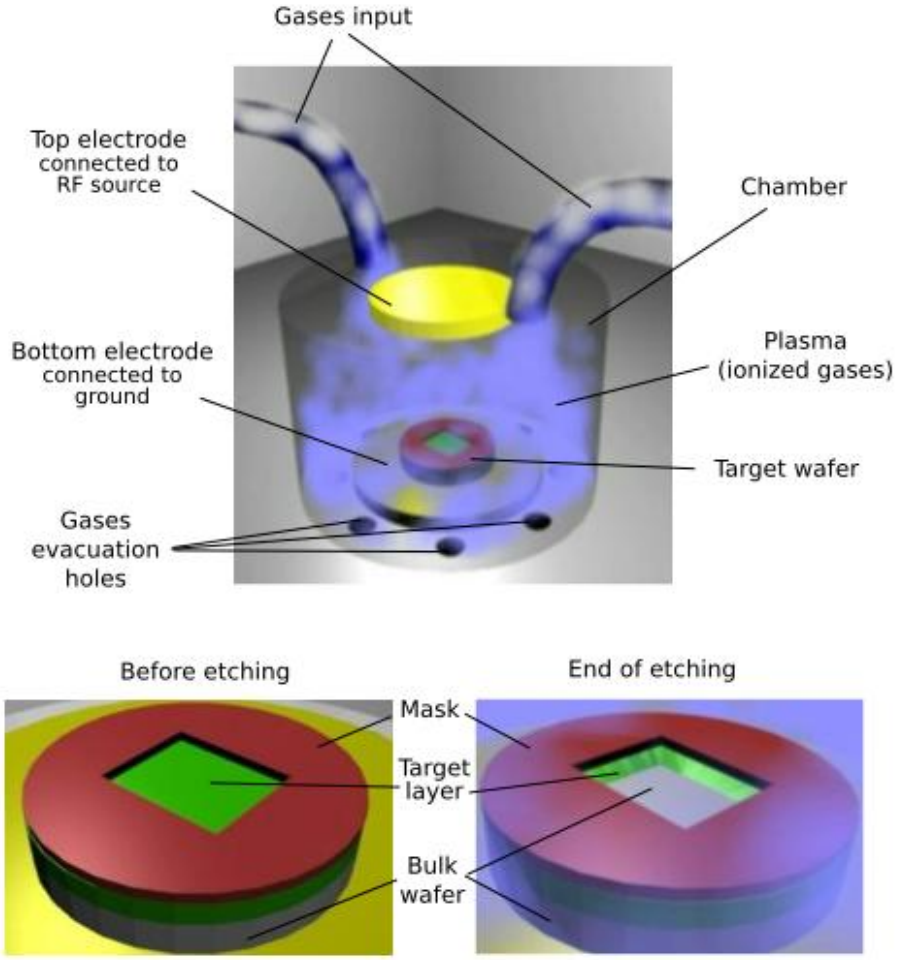

Figure 1.4. Schematic of plasma etching (courtesy: http://matthieu.lagouge.free.fr/microtechnology/microtech_pict/etching/pe-principles.png).

1.1.2 Nanomanufacturing.

Nanoscale manufacturing has been practiced as a top-down process (Chen et al., 2007) that reduces macrosized material into a desired form as commonly observed with nanoelectronic products. As a bottom-up approach, it has played significant roles in the pharmaceutical, chemical, and advanced materials industries (Chen et al., 2007). Additionally, Chen et al. (2007) suggested a hybrid of both approaches (i.e. a

combination of top-down and bottom-up) in conjunction with high-rate and high-yield nanomanufacturing towards achieving economically viable commercial products. This notion is being proven by plasma etching capability of producing micro- and nanoscale patterns. Nanomanufacturing of nanosized features have implications of resulting in novel and improved properties of products in areas such as nanobiotechnology and pharmaceuticals (e.g. new drugs and their therapeutic delivery), nanodevices (e.g. advanced semiconductors and spintronics), measuring manufacturing devices/tools, security technology (e.g. sensors) and nanoelectromechanical systems (NEMS) (Chen et al., 2007).

There are a few challenges that hinder manufacturability at the nano regime. This is due to the inability to control size dimensions, conductivity, chirality (Chen et al., 2007), etc. such that the production process is suitable for mass production. An example, (Chen et al., 2007) is the production of carbon nanotubes (CNTs) with repeatable structure, diameter and chirality, limiting its process scalability. Another challenge is the lack of manufacturing tools that would allow precise control and high production throughput to process readily available materials, structures, and/or concepts proposed by researchers. The transition of scientific research/discoveries into commercial practicality can at times be an insurmountable feat since issues such as production volumes, reliability, process robustness, and integration of the nanoscale products into micro and macroscale will need to be first addressed (Busnaina, 2007). Therefore, the lack of expertise in a specific arena due to novelty of the area (i.e. “unchartered ground”) can also contribute to the reluctance towards manufacturing that is unfamiliar to researchers.

The removal of defects and contaminations from manufactured nanostructures is identified by Busnaina (2007) as a critical challenge since surfaces would need to be free of particulates as to not destroy or disturb the assembled nanoelements. As has been observed, there are several hindrances to manufacturing at the nanoscale; however, the advantages in addition to economic and societal implications (Busnaina, 2007) outweigh the aforementioned challenges. The following three nanomanufacturing processes will be briefly expounded upon, Dip Pen Lithography, Nanoimprint Lithography, and Pulsed Laser Deposition. These methods include both bottom-up and top-down approaches as described below.

1.1.2.1 Dip Pen Nanolithography.

Dip-pen nanolithography (DPN) is a scanning probe microscopy-based nanofabrication technique that uniquely combines direct-write soft-matter compatibility with the high resolution and registry of atomic force microscopy (AFM) (Salaita et al., 2007). DPN is a powerful bottom-up nanomanufacturing process for depositing soft and hard materials in the form of stable and functional architectures on a variety of surfaces. DPN enables patterning of the surface in the sub 100 nm range. Further, DPN is a direct write technology in that the deposition material are molecular inks and can be directly written on surfaces at the molecular length scales. Figure 1.5 below shows an illustration of DPN.

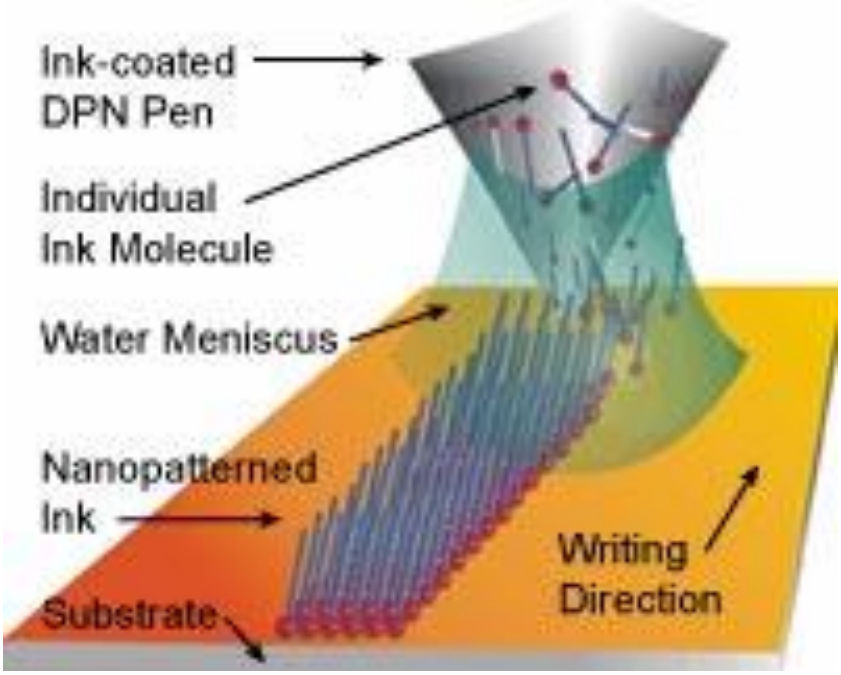

Figure 1.5. DPN schematic (courtesy: http://mark-nano.blogspot.com/2007_05_01_archive.html).

1.1.2.2 Nanoimprint Lithography.

Nanoimprint Lithography (NIL) is a top-down nanoscale fabrication patterning method. The process (shown in Figure 1.6) creates patterns by mechanically deforming the imprint resist and the subsequent processes. NIL is regarded by Chou et al. (1996) as the most successful technique for nanoscale patterning. The first step in NIL is referred to as the imprint step; it creates the thickness pattern contrast in the resist by duplicating the nanostructures on the mold in the resist film. The second step involves the pattern transfer and it enables removal of the residual resist from the compressed area; thus, the thickness contrast pattern is transferred into the entire resist. Finally, the exposed substrate areas are deposited with appropriate material to produce functional nanostructures.

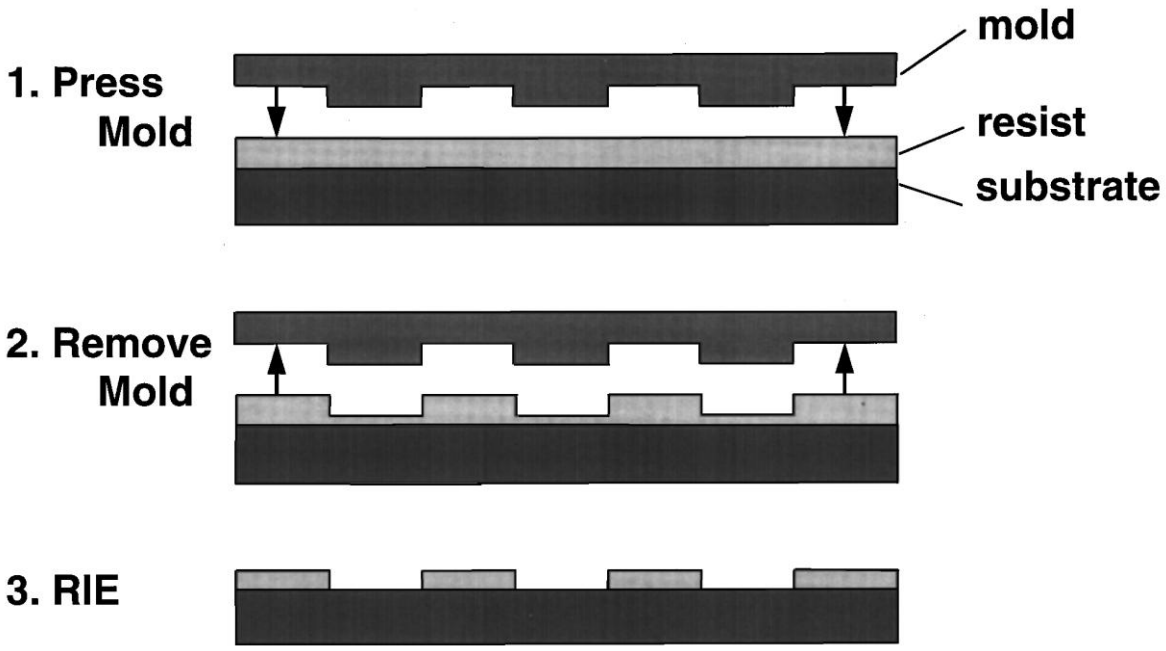

Figure 1.6. NIL schematic (courtesy: Chou et al., 1996).

1.1.2.3 Pulsed Laser Deposition.

Pulsed Laser Deposition (PLD) is a physical vapor deposition technique that enables thin films to be deposited onto a substrate using a high power pulsed laser beam. The laser beam is focused inside a vacuum chamber to strike the target material to be deposited on the substrate. Venkatesan and Green (1996) described PLD as a process that transports elements from one location to another by supplying the energy needed to transport onto a surface to be coated. PLD is a good technique for depositing extremely pure films especially given that most processes have contaminants on the films. A schematic of PLD is depicted below in Figure 1.7.

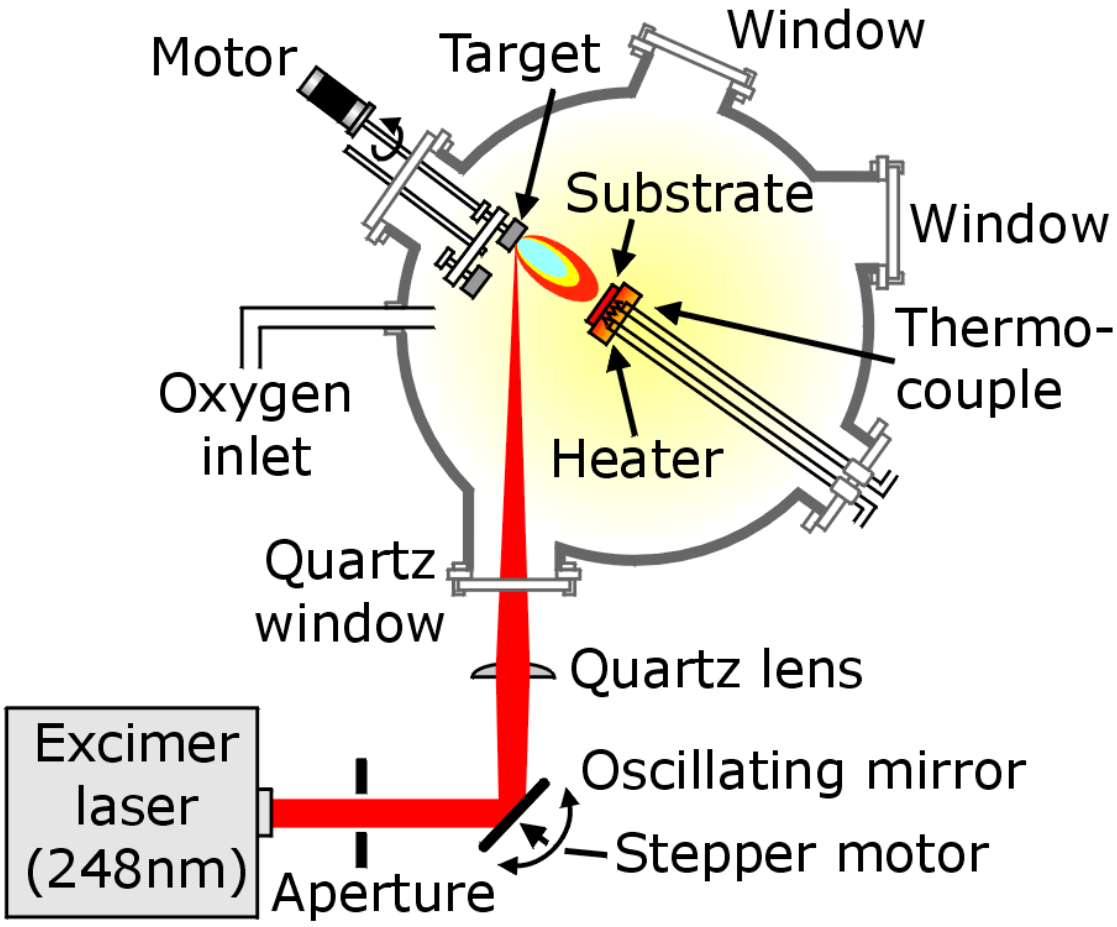

Figure 1.7. PLD schematic
(courtesy:http://www.physics.colostate.edu/groups/PattonGroup/systems/img/setup/diagram_pld_b.png)).

1.1.3 Laser Usage in Manufacturing.

The acronym 'LASER' stands for Light Amplification by Stimulated Emission of Radiation (Acronym Finder) has long been applied in numerous sectors, e.g., micromanufacturing, instrumentation, imaging, medicine, communications, as well as others (Mahalik, 2006). In micromanufacturing, lasers offer benefits such as noncontact processing, little to no tool wear, machining of hard and brittle materials, automation, and

capability of remote processing (Mahalik, 2006). Additionally, lasers are employed in manufacturing because of the accuracy and precision that they provide on the microscale since its beam can be focused onto a very small area that would otherwise be difficult to achieve with only mechanical processes. Applications of lasers in micromanufacturing, (Mahalik, 2006), are based on thermal or chemical changes in the workpiece due to the absorption of the laser light by the workpiece. Further, their application requires an understanding of the changes (i.e. thermal, physical, and chemical) during laser beam interactions with materials and their variations with respect to key laser parameters (i.e. wavelength, pulse width, and energy).

Laser technology due to its high power focusing capabilities has been used for the manufacturing of miniaturized biosensors (Hohn et al., 2008). The application of lasers for miniaturization purposes are readily seen in electronics manufacturing (Bieri et al., 2004). An example of these efforts is in a laser-induced chemical vapor deposition technique employed to repair electronic circuitry (Han and Jeong, 2004).

Due to their high output power, CO_2 lasers have been widely used in industry (i.e. manufacturing) and research (Mahalik, 2006). Thus, the CO_2 laser was employed in the second phase of the experiments presented in this work. The following section provides the motivation of the research.

1.2 Motivation

"Nanoscale devices and equipments provide benefits in terms of smaller carbon footprint, miniaturization, efficiency and resource consciousness" (Mahalik, 2006, pg.12). Chen et al. (2007) further mentioned the need for scalable nanomanufacturing

platform to enable multi-scale integration from nano to micro- and macroscale given the inability of nanometer products to communicate and interface at the micro/macro level (e.g. MEMS). The objective of this research was to demonstrate manufacturing of scalable nano/micro sized features based on controlled evaporation of microdroplets in two phases. The first phase incorporated utilization of a resistive heated ring in tandem with the direct write inkjet printing technology whereas the latter phase integrated a laser source with the inkjet system. The proposed two stage approach hypothesizes the transformation of microsized droplets into nano dimensions. Thus, this research provided the foundation for generating particulate loaded droplets (e.g. colloids, nanotubes, biomedia, etc.) towards scalable micro and nanomanufacturing in the electronics, semiconductor, biomedical, and other industrial sectors as shown by (Brinley et al (2007), Girshick (2008), and Greiner et al. (2006). Key foreseeable challenges of this research are discussed in the subsequent section.

1.3 Technical Challenges

The requirement for cost-effective large-scale production (Mahalik, 2006) has been a major hindrance in the progression of nanotechnology - a term first used by (Taniguchi, 1983) to categorize integrated manufacturing technologies and machine systems that provided ultraprecision machining capabilities in the order of 1nm, as well as other enabling technologies necessary to manufacture at the miniaturized levels. It was further mentioned by Mahalik (2006) that the increasing need to miniaturize logical circuitries is reaching the physical limit of the metal oxide semiconductor field effect transistors (MOSFET). This fact demonstrates the need for the continuation of research

that either creates the technology necessary to enable miniaturization and/or effectively utilize the current state-of-the-art technology to enhance such systems. Lastly, the difficulty in achieving scalable, reliable, and controllable production of nanostructures is a significant challenge that must be met in order to extract the benefits of manufacturing at such scales. Nevertheless, better understanding is crucial to expand upon this paradigm shift towards nanoscale manufacturing. The research objectives are discussed in the ensuing section.

1.4 Research Objectives / Hypotheses

The objective of this research was to investigate controlled evaporation of microdroplets towards scalable droplet based manufacturing. The microdroplet evaporation dynamics was studied using LED strobe based high speed photography. A customized direct-write ink-jet printing setup was used for generating monodisperse microdroplets of different fluid types. There were two phases employed towards achieving the objective of this investigation; first, the microdroplet was evaporated using convective heat transfer through a resistive ring fixture through the application of heat flux around the droplet's periphery. The first investigation provided sufficient evidence that the concept of controlled microdroplet evaporation was realizable. Effects of nozzle size, fluid type and surface to volume ratio on microdroplet size reduction were examined. Given the success of the first phase, the second phase subsequently aimed to achieve even further reduction by employing a CO_2 laser. Due to the ability to focus the lasing beam onto microdroplets upon ejection from the nozzle tip, rapid ('on-the-fly') transformation of microdroplets was achieved and further volumetric reductions were

observed as compared to the first phase. This research was one of the first attempts for achieving scalable micro/nano manufacturing with high repeatability based on understanding the transformation of monodisperse microdroplets to the nano range. The three primary objectives of this research were:

1. Transition of micro to nano droplets via convective and radiative heat sources (i.e. resistive heat ring and CO_2 laser, respectively).
2. Controlled deposition of droplets on substrates via the use of a motion controller to facilitate patterning of miniaturized features.
3. Demonstrate fabrication of functional devices (i.e. flexible thin film transistors) using direct-write inkjet method towards large scale manufacturability.

CHAPTER 2

LITERATURE REVIEW

Numerous attempts are being directed into micro and nanomanufacturing; needless to say the implications of such technologies across a host of industries are very promising; thus, justifying the level of interests that it has garnered over the past decade. However, in order to readily apply these concepts into realizable (i.e. practical) products and/or systems requires more attention and better control of the processes. The significance of maintaining control was seen by (Skrabalak and Xia, 2009) in which emphasis was placed on the synthesis and assembly of shape- and size- controlled nanocrystals towards the development of a potential device that exhibits strong performance and reproducibility. The aforementioned work correlates to the work herein since the objective of this study was to experimentally demonstrate controlled evaporation of microdroplet prior to deposition on the substrate. The transition to the nanoscale has been initially attempted via a convective heat transfer approach that used a resistive ring fixture to control the heat flux around the periphery of microdroplets (Desai et al., 2010 and Desai et al., 2011). This attempt revealed promising results for transition at the micron scale whereas the intent of our current effort is to achieve better control of the process in order to obtain higher reduction of the microdroplet to the nanoscale. It is hypothesized that by utilizing a CO_2 laser, it is possible to transform microsized droplets to nano dimensions since the lasing beam can be directly focus to completely encapsulate the microdroplet. Thus, enabling transition from micro features to the nano regime with the goal of attaining scalable micro-to-nano manufacturing. The direct write inkjet

printing method was employed as the platform technology for generating microsized, monodisperse droplets. This technology was used in conjunction with both the convective aspect of the research (resistive heat ring investigations) as well as the radiative portion (CO_2 laser source experiments) of this research. An overview of the direct write technology and several research efforts utilizing the technique for various applications is provided below.

2.1 Direct Write Manufacturing

Direct write technologies such as the inkjet printing method has many advantages; the most significant of which is its ability to deposit on the exact locations on the substrate (i.e. controlled deposition). Instances of utilizing direct writing techniques as the basis for developing scalable, industrial (i.e. manufacturing) applications are readily available (Ng et al (2009)). The technique has been used as the chief technology to produce features and/or patterns at the micron and submicron dimensions. A depiction of a typical direct writing inkjet setup is illustrated in Figure 2.1.

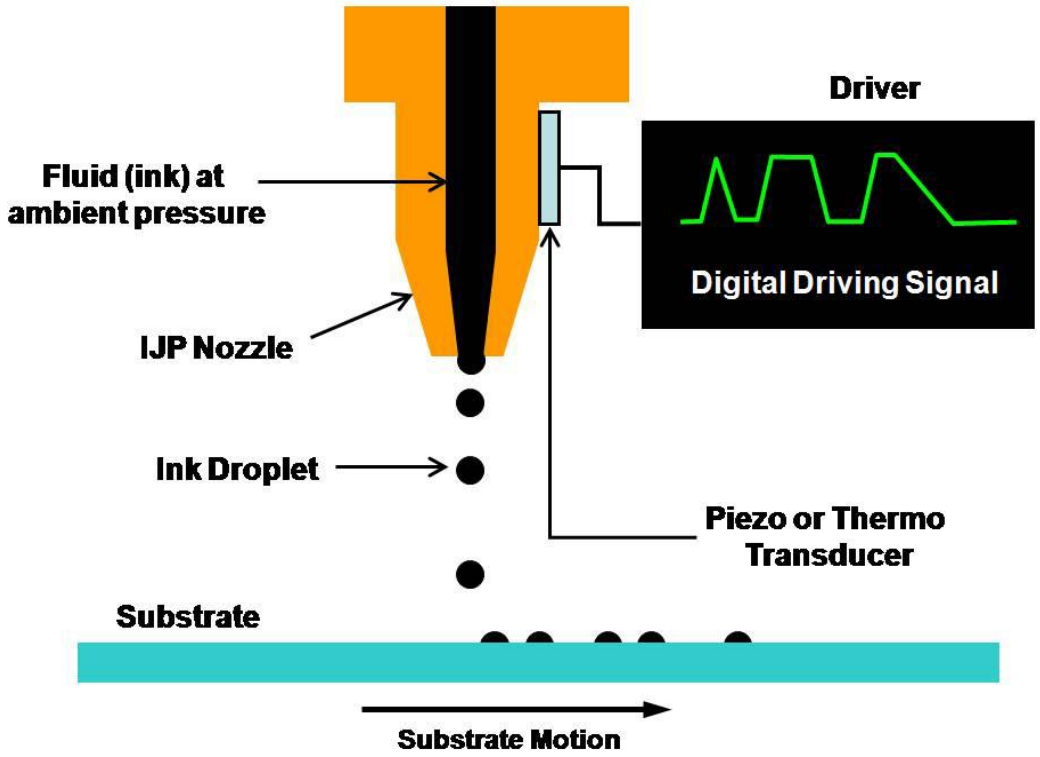

Figure 2.1. Depiction of direct write inkjet printing (courtesy: Xu et al, 2007).

Drop-on-Demand, a controlled printing direct write method, was employed in conjunction with laser curing to print electrically conducting microdroplet line patterns from a suspension of gold nanoparticles (Bieri et al., 2004). Laser irradiation was utilized by these authors to evaporate the solvent, melt the nanoparticles and sinter the lines on the substrates. There has been several investigations conducted towards the evaporation of monodisperse droplets as well as the utilization of droplet- and laser-based direct write techniques. These techniques will be reviewed in detail in the ensuing sections.

2.1.1 Droplet Based Manufacturing.

Droplet-based manufacturing, a bottom-up manufacturing approach, has shown its potential to impact emerging manufacturing fields, including biomanufacturing (Huang et

al., 2007). In the past, research efforts have been focused on the microdroplet formation, stabilization, and substrate impingement characteristics. Pique and Chrisey (2002) outlined several direct-writing techniques to form fine patterns ranging from micro- to nanoscales. The direct-writing technique has been lauded due to its waste and cost reductions while simultaneously maximizing efficiency (Chrisey, 2000). Li et al. (2005) investigated the charge-stability limits of microdroplets suspended in an electrodynamic balance. Yatsuzuka et al. (1998) and Palm and Nilsson (1998) have explored the stability of microdroplets during flight. Heston (2004) investigated the use of a linear electrodynamic quadrupole to focus the trajectories of microdroplets prior to deposition onto a substrate. Fong et al. (2007) reported experimental results on the fission of an electrically charged liquid droplet. Jones et al. (2001) developed an experimental technique to use high-speed Dielectrophoresis actuators to deposit water droplets as small as 7 nL. Lu et al. (2009) observed the dynamic behavior of deionized water droplets on three different substrates. Bortolani and Dorey (2009) investigated the use of gas heating and direct heating to remove solvents and produce spherical shaped lead zirconate titanate (PZT) nanoparticles using the electro-hydrodynamic atomization process. As can be deduced from this review of the existing literature, the focus has been on charge limits, in-flight dynamics, and atomization of droplet clusters for specific applications.

In continuing with the concept of achieving control in droplet-based processes, a focus of the work of Lee et al. (2009) was of the implementation of an electrohydrodynamic jet (e-jet) printing method that is capable of controlling the width of a printed line by toggling on/off for each nozzle in the nozzle array. The e-jet printing

technique (Park et al., 2007) uses electric fields as opposed to thermal, acoustic, or piezoelectric forces as in inkjet printing (the method used herein) to provide the necessary fluid flow of inks to substrates. Furthermore, the control of gaps between printed droplets has also been investigated by Stutzmann et al. (2003), Sele et al. (2005), and Wang et al. (2006). Although e-jet is not the jetting technique used in this work, it is nevertheless a very important technique for printing patterns for utilization in functional devices such as electronics. Liu et al. (2003), Sirringhaus et al. (2000), Szczech et al. (2002), Burns et al. (2003), Shimoda et al. (2006) and Sirringhaus and Shimoda (2003) have explored printing methods for application in various electronic devices. These efforts provided basic understanding of the droplet formation, deposition, and dynamics as it relates to droplet based manufacturing techniques. However, lasers were not employed in conjunction with the direct write printing method as intended in this study. Similar hybrid approaches similar to that proposed herein of direct-writing and laser have been employed by Pena et al. (2010) and Lin et al. (2007); Although their objectives were different from those of this research, it nevertheless provides insight on how lasers are utilized in manufacturing at the miniaturized dimensions. Instances of laser based manufacturing techniques are briefly discussed in the ensuing section.

2.1.2 Laser Based Manufacturing.

One such application in which laser is employed in conjunction to the direct write printing technique is the matrix-assisted pulsed laser evaporation direct writing (MAPLE DW) method. This method was investigated by Lin et al. (2009) to explain droplet formation of glycerol-water solution. The authors mentioned that better understanding of

droplet formation and its size control are challenges that must be overcome in order to make MAPLE DW feasible for manufacturing. Their objective was to study the effects of laser fluence and glycerol-water concentration on the glycerol-water droplet diameter during MAPLE DW using an excimer laser (λ=193nm). Both laser fluence and glycerol concentrations were varied and their effects on droplet formation were examined. Within the study, water was considered as the main laser energy absorption material because its absorption coefficient was much larger than that of glycerol once heating started. The authors found that droplet formation was caused by pressure from the thermoelastic elastic stress and the phase explosion. Also, they revealed that droplet diameter increased as the laser fluence increased as well as an increase in droplet volume as the laser fluence increased at larger values. Furthermore, droplet volume was not found to have a "systematic relationship" with glycerol concentration (in other words, the diameter first increased as concentration increased but decreased as the concentration continued to increase). In addition as the concentration ratio increased, viscosity and density increased causing the droplet diameter to decrease ("decreasing surface tension helps increase the droplet diameter as in ink-jetting"). The combined effects of laser fluence and glycerol concentration ratio revealed that the droplet diameter increased as laser fluence and concentration increased until the concentration ratio reached 65% ("transitional value"). Beyond which it was found to be more effective to control droplet size by adjusting the laser fluence level rather than the concentration ratio. It was revealed that the transitional value for the largest drop to be different at various laser fluence values (the transitional ratio generally increased as the fluence increased). Lastly, the authors acknowledged that

MAPLE DW and nozzle-based jetting share common process characteristics in that both are governed by fluid dynamics (i.e. obeying mass, momentum, and energy conservation laws); however, two primary differences were mentioned. The first of which is the droplet formation mechanisms; in MAPLE DW, droplets are formed discretely pulse by pulse once laser fluence is higher than the threshold required for droplet formation. However, Rayleigh instability is responsible for droplet formation in nozzle-based jetting. The other difference is the droplet formation boundary, in MAPLE DW there are no constraints since the droplet is formed from a free surface; however, in nozzle-based jetting, it is constrained by the nozzle geometry. Figure 2.2 depicts a schematic of a MAPLE DW experimental setup.

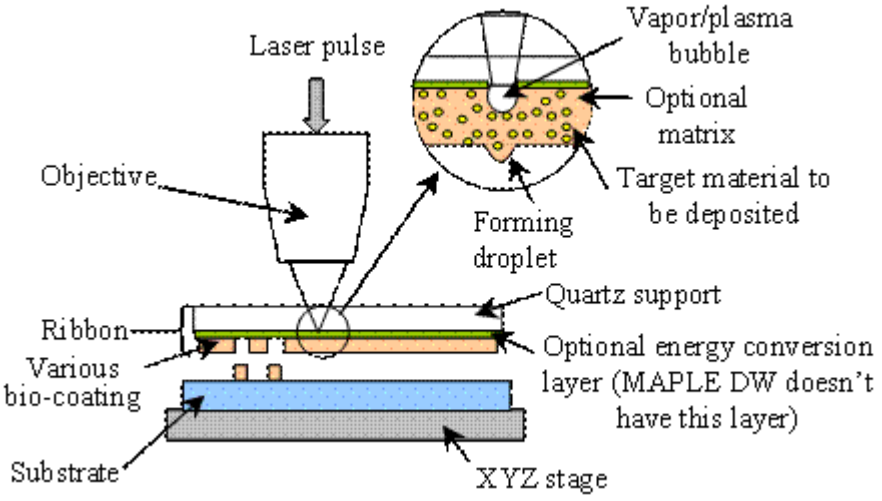

Figure 2.2. MAPLE DW schematic.
(courtesy:http://www.clemson.edu/ces/camsil/Edu_Biomanufacturing.htm).

There have been other applications of lasers to direct write technologies, of which a fair amount has been geared towards bioengineering and biomedical applications (Odde

and Renn, 1999; Kaehr et al., 2006; Arnold et al., 2007). For instance, a laser-guided direct writing approach was employed to control the placement and patterning of cells onto planar substrates (Odde and Renn, 2000). Other applications in which lasers were used as a control/manipulation mechanism in the biomedical realm include but not limited to those in plant cells and sub-cellular structures (Hoffmann, 1996). Nelson and Berns (1989) also utilized lasers in clinical applications for biomedicine; viruses and bacteria were optically trapped and manipulated by Ashkin and Dziedzic (1987). Berns et al. (1991) directed their efforts with lasers towards cell biology while Neev et al. (1996) utilized lasers for hard tissue ablation. Some of these examples were discussed to demonstrate the vast applicability of lasers towards control and manipulation of features, a primary objective for this research.

Laser micromachining has been touted as the most popular form of laser-based direct writing technique (Zhang and Xu, 2004). However, the technique removes material (i.e. via decomposition of the material by the laser's beam intensity) and does not allow for selective deposition of materials. Laser-guided direct writing, on the other hand, is a more specific form of direct writing that has found applications in the biological arena due to its additive nature; thus enabling selective deposition of biological material, a key requirement in many bio-related applications (Duocastella et al., 2010). Laser induced forward transfer (LIFT) is also another additive direct writing laser-based techniques that has been applied across a vast of areas within the bio-related regime. For instance, Colina et al. (2006) studied the droplet ejection process via their experimentation with laser induced forward transfer of liquids; Kattamis et al. (2007) also induced forward transfer

using thick film laser for materials that were thermally and mechanically sensitive; Colina and colleagues (2005) deposited DNA using the LIFT method. The LIFT technique, depicted in Figure 2.3 below, is very similar to that of inkjet printing since both are microprinting methods with the exception that the droplet size in the latter are predicated on the dimension of the nozzle whereas they are determined in the former based on the beam's diameter (Colina et al., 2006). Furthermore, the LIFT technique surpasses the inkjet printing method since it is not subjected to nozzle clogging, a major setback, with the latter (Sirringhaus and Shimoda, 2003). Some of the reviewed experimental studies utilizing lasers are described below.

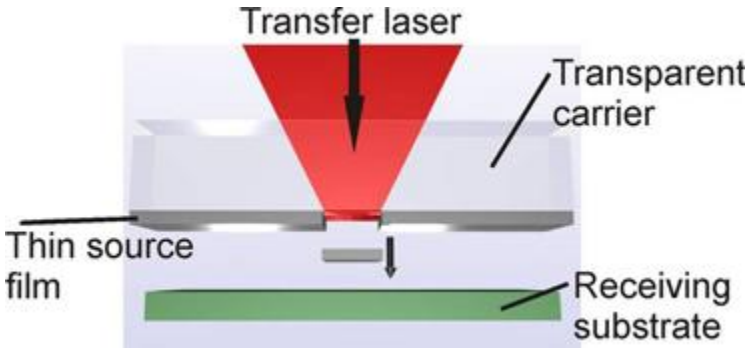

Figure 2.3. Illustration of LIFT technique (courtesy: http://www.orc.soton.ac.uk/lift.html).

2.1.2.1 Laser Characterization of Evaporated Droplets.

Several researchers have explored methods of evaporating monodisperse droplets as well as employing lasers towards understanding spreading characteristics, droplet-to-droplet interaction, measurements, and so forth. A few of these investigations were reviewed and are presented subsequently.

Some application of lasers in conjunction with microdroplets has thus far been utilized as an optical and/or characterization method to determine evaporation as well as to obtain certain properties from the observed droplets. For instance, Kiefer et al. (1997) studied Mie and Raman light scatterings (elastic and inelastic, respectively) from laser trapped microdroplets; the Raman data provided the chemical structure as well as size and refractive index of droplets. Consequently, the authors applied the trapping technique to achieve chemical reactions and evaporation of droplets; the droplet of interest in their study was a 1:1 mixture of catechol and diethylene glycol in which they found that the former component of the mixture evaporated faster than its counterpart.

The work by Garcia et al. (2010) focused on characterization of particles obtained from low temperature desolvation of monodisperse microdroplets as well as suspensions for nanoparticle calibration in inductively coupled plasma spectrometry. The authors introduced Peclet number as the ratio of droplet's evaporation rate over the diffusion coefficient; moreover, they concluded that a high Peclet number correlates to liquid droplets whereas a low number was typically observed with solid particles.

Ray and Devarakonda (1998) explored resonance-based light scattering techniques to measure evaporation rates of monodisperse droplets mixture containing ethanol and methanol generated through a modified vibrating orifice aerosol generator (VOAG). Their results revealed that pure methanol's evaporation rate is twice as much as that of pure ethanol droplets, which according to the authors was expected due to higher volatility of methanol as compared to ethanol.

Efforts by Tay and Edirisinghe (2002) involved the evaporation (i.e. shrinkage) of zirconia ink droplets. Two substrate types were evaluated in their experiments, the first type, silicone release paper, had lower surface energy when compared with the surface tension of the ceramic ink. The second substrate type, acetate sheet, had higher surface energy. Wettability studies which included observations of variations in the contact angle and width of ink-substrate interface as well as variations in droplets' height. The shrinkage in droplet volume was consequently calculated. The authors revealed that all of the aforementioned measures were expedited on the latter substrate type. It was further revealed that the average volumetric shrinkage observed in both substrate types was approximately 70% after 160s for type 1 and 90s for type 2. However, the deposition on the second substrate type shrank about twice as fast as those deposited on the first type.

Maqua et al. (2008) explored droplet-to-droplet interaction by conducting experimental studies for monodisperse droplet heating and evaporation while they attempted to validate these studies by using it as input for the numerical model. Ethanol and acetone droplets were utilized due to their low and high volatility, respectively. Two modes were investigated, the first of which was pure heating and evaporation of droplets in a flow of air of prescribed temperature. The latter was in a flame produced by previously injected combusting droplets. Two-color laser induced fluorescence was used to estimate droplet temperature. Their results suggested that the experimentally measured temperature was close to the numerical model's predicted average temperature for relatively small droplets (i.e. those with initial radii of about 65μm). On the contrary, the experimental temperatures were close to the predicted temperature at the droplet's center

for larger droplets (initial radii of about 120 μm). The authors concluded that their work provides a reliable way of evaluating droplet-to-droplet interactions.

Varghese and Gangamma (2007) investigated numerical evaporation of polydispersed water droplets via radiation in the presence of absorbing inclusions. Their studies included water droplets containing salt (NaCl) and a black-carbon core in which the authors examined the effect of radiation absorption on droplets' size distribution. The methodology expanded established single droplet equations towards polydispersed droplets to obtain mass and energy balance. The results suggested that the equilibrium of water vapor and droplets (i.e. with absorbing inclusions) were significantly affected by the absorption of solar energy. Also, the evaporation induced by absorbed energy caused modification in droplets' size; hence, the initial mean diameter of droplet distribution reduced to half the initial diameter due to the solar radiative heating. Lastly, it was also found that the evaporation caused droplets' polydispersity to be reduced.

Lim et al. (2009) used experimental studies to investigate spreading and evaporating characteristics of droplets jetted by drop-on-demand inkjet. Water and ethylene glycol droplets (17-42 μm diameter) were studied on heated silicon substrates. For water droplets the spreading ended before evaporation became significant; however, in the more viscous glycol droplets, extra wetting overlapped evaporation at high temperatures.

Davis and Ray (1978) demonstrated evaporation of low-volatility liquid submicron droplets suspended in an electric field in a polarized laser beam. Droplets' size was determined as a function of time and Mie theory was used to interpret the light-

scattering data. The intent of this study was to test available theoretical data and semi-theoretical analyses of aerosol evaporation in the diffusion-controlled and Knudsen aerosol regimes.

In the work of Roth and Fischer (1985), submicron aerosol droplets were suspended in argon and studied via shock waves at two Knudsen numbers (0.1 and 0.9). The authors used laser light scattering to measure the reduction in droplets' size during post-shock period. Furthermore, Mie theory was employed to determine time-dependent droplet size during evaporation. It was concluded that experimental results coincide with analytical results with regards to the mass flux in the transition regime.

The work of Ro and colleagues (1968), perhaps one of the earliest attempts of droplet evaporation using lasers focused on measuring evaporation rates of water droplets (dia. = 0.6mm-1.5mm) using the intensity variation of a laser beam at the droplet's center. Water droplets were studied in two modes: bead thermistor (measured surface temperature) and beaded glass fiber, which resulted in smoother results than the thermistor according to the researchers. It was mentioned that the results were in excellent agreement with Maxwell's equation (which states that evaporating droplet diameter should be inversely related to the droplet diameter); however the experimental rates were 20%-30% lower than the equation's prediction.

Jia and Qiu (2002) proposed a novel method to measure the contact diameter, profile, and volume of liquid droplets on hot substrates using scattering patterns from laser beams. Contact diameter is related to the total number of scattering fringes while a droplet's profile was related to the spatial frequency. The minimum volume that can be

measured using their optical approach is $2.48\times10-5$ mm^3, which is equal to the volume of a sphere with of 36μm diameter. Accuracies of ±1% and ±5% were achieved for contact diameter and volume, respectively. Within the study, the authors investigated evaporating ethanol and water microdroplets. They found that the evaporation process can be classified into 3 regions: constant volume heating up, constant contact diameter evaporation, and constant contact angle evaporation.

According to Lamanna et al. (2005), the D^2 law (a law stating that the square of the diameter of an evaporating droplet decreases linearly with time) was not applicable for interacting droplets based on their review of the work conducted by Sangiovanni and Labowsky (1982). The work of Lamanna et al. (2005) describes their efforts towards determining evaporation rate of single streams of monosized droplets by simultaneously measuring droplet size and speed. Low angle elastic light scattering (LAELS) technique was used to study droplet evaporation of diameter below 100μm.

Sefiane and Bennacer (2009) investigated the effects of aluminum nanoparticles on evaporation of ethanol droplets deposited on a heated substrate. A FTA 200 goniometer was used to measure droplets over time (i.e. drop shape analysis - contact angle, diameter, and volume). Based on these measurements, evaporation rate was deduced. The authors found the presence of nanoparticles to reduce evaporation rate compared to the base fluid. Evaporation rates of droplets with small radii were relatively the same for both nanofluid and for the base fluids; however, the evaporation rate of the nanofluid were lower than the base fluids for larger radii at all droplet sizes and substrate temperatures. In other words, the overall evaporation time for the base fluid was shorter

than droplets of nanofluid. Also, nanoparticles were found to influence wetting dynamics during the evaporation process (e.g. contact angles were larger for nanofluid droplets compared to base fluid droplets). Lastly, they observed that the nanofluid droplets remained pinned to the substrates longer than the pure ethanol droplets enabling faster evaporation.

Chen et al. (2006) used a "simple digital camera" system (a side view camera and a top view camera) to observe the evolution of evaporating microdroplets. Side-view images provided shape evolution of droplets before meniscuses became flat; however, once the meniscuses changed from flat to concave the side camera was no longer applicable, thus the top view camera was employed. The authors found three phases to exist during evaporation: constant baseline (first half of evaporation time- indicated by decrease in height and contact angle), constant contact angle (last half of evaporation time- indicated by a decrease in baseline and constant contact angle), and shrinking region (occurs after the previous two phases – the baseline and contact angle decrease at the same time). The average volume rate of evaporation was -1.66nl/s. Shape Drop Method (FTA®, Dynamic Contact Angle Analyzer 100) was used to calculate droplets' volume and height.

Chen and colleagues (2010) investigated the effects of nanoparticles added to deionized water on evaporation rate. Deionized water was used as the base fluid in conjunction with 3 different types of nanoparticles (laponite (type of clay), silver (Ag, pure metal), and Fe_2O_3 (metal oxide)). A Rame-Hart Model 250 Standard goniometer, with data processing software, was used for real time droplet size and volume

measurements. The evaporation rate of a single liquid droplet is governed by D^2 law which was found by Langmuir (1918), who showed the mass loss rate of a small liquid sphere to be proportional to its radius (also to its diameter):

$$D^2 = D^2_0\text{-}Kt \quad (1)$$

where

D_0 = the initial droplet diameter

K = the evaporation rate constant (in m^2/s)

t = temperature

From their experiment the following points were induced:

1. PVP (a surfactant used to stabilize the iron oxide nanofluid) helped to enhance evaporation rate of deionized water by a factor of ≈2.
2. Laponite was found to slightly reduce evaporate rate constant by ≈ 10% for the base fluid.
3. The Ag nanofluid at low concentrations without PVP did not significantly affect evaporation rate constant. However, with PVP it enhanced evaporation.
4. The iron oxide nanofluid with PVP slowed down evaporation.

Hallett and Beauchamp-Kiss (2010) evaluated measurements of droplet evaporation for mixtures of pure and denatured ethanol with No.2 fuel oil. A model representing droplets evaporation was developed and it incorporated continuous thermodynamics to describe the fuel-oil fraction. In the experiments, 1.4-1.8mm (dia.) single droplets were suspended from a quartz fiber. Their computational model was found to be in "excellent" agreement with actual experiments. They found,

remarkably, that the evaporation rate of ethanol was very similar to that of the No.2 fuel; although ethanol has much lower boiling point, its enthalpy of vaporization is nearly 3 times that of typical hydrocarbons. The authors conclude by stating that their work provides a basis for accurate continuous thermodynamics description of commercial petroleum fuel.

Tseng and Viskanta (2006) investigated the effects of radiation absorption of water droplet evaporation. Within their mathematical model, they assumed the droplet to be both spherical and semi-transparent to radiation. The objective was to compare the effects of convection and radiation on evaporation of water droplets. Two critical findings were as follows:

1. Evaporation rate increased and shorter droplet lifetime were observed for conditions in which radiation was significant as opposed to convection for droplets >100μm dia. and higher surrounding temperature.
2. An increase in the surrounding's gas velocity decreased the importance of radiation while decreasing droplet lifetime and increasing evaporation rate. However, a decrease in surroundings temperature decreased the evaporation rate and increased the droplet lifetime.

Crafton and Black (2004) studied evaporation of water (≈1mm dia.) and heptane (≈5mm dia.) droplets in order to measure the heat transfer rates once deposition on a horizontal heated surface. Aluminum and copper surfaces were used and kept at temperatures below droplets saturation points. Differences were observed in the two droplet types, heptane droplets evaporated faster than water and were found to have lower

heat fluxes than the water droplets. During evaporation, heptane drops continually decreased in diameter while water droplets remain constant; however, the height of both fluid types decreased, continually, during evaporation. Evaporation rates of water droplets were analogous for both surface types and remained constant throughout the droplets lifetime. For heptane, the diameter and height decreased during evaporation while the contact angle remained relatively constant. Also, the evaporation heat transfer rates were less than that of water for the same surface and temperature. Lastly, the experimental data was compared with an established numerical model that accounts for conduction and convection of drops. It showed that evaporation rate to be linear to droplet volume as a function of time and that small drops evaporate faster than larger ones (which follows the D2 model in equation 1).

Swindal et al (1996) introduced a non-intrusive optical method of characterizing droplet sizes and evaporation rates based on droplets' optical cavity resonances. The authors added small amounts of laser dye (Rhodamine 6G) to the droplets mixtures of ethanol and ethanol-acetone to detect droplets' wavelengths at their corresponding spectral positions of the droplet-cavity resonance. Swindal and colleagues reported that they were able to determine droplet evaporation sensitivity of 1nm in droplet radius change for droplets with initial radii of 40nm due to measurements in the cavity resonance shift. What's more, the authors were able to determine evaporation rates among leading and trailing droplets within a single segmented flowing stream, and also between closely spaced adjacent droplets.

Chemical and physical dynamics of a single aerosol droplet were characterized by Reid and Mitchem (2006) using heat and mass transfer between particle and surrounding medium, properties of multiphase droplets, and the coagulation of aerosol droplets. Furthermore, the authors explored properties of elastic and inelastic light scattering to provide information on composition, particle size, temperature and morphology. All of the aforementioned techniques were utilized by Reid and Mitchem to understand the dynamic properties of aerosol droplets.

In contrast to the aforementioned efforts, the following section will describe some attempts by majority of researchers utilizing numerous laser sources. These efforts include the use of CO_2 lasers, which is the evaporation mechanism of droplets in this research.

2.1.2.2 Laser Evaporation of Monodisperse Droplets.

A few previous attempts similar to the efforts herein of laser evaporation of microdroplets are highlighted below. Although, the efforts of the reviewed studies below do not attempt to achieve this feat of "on the fly" transition of microdroplets into the nano regime; they are however significant in that they provide a basic understanding of several laser sources and their operating modes from which we may choose to employ in our experimental studies. Nano-sized zirconia particles were produced by Michel et al. (1997) via CO_2 laser evaporation. Helium was used as the carrier gas and short laser pulses of a 4 kW CO_2 laser were employed in the study. The authors found that short laser pulses (i.e. <100 microsecs) and carrier gasses with high thermal conductivity (e.g. He) are necessary for producing ultrafine particles with diameters of the order of 1 nm.

A 2kW CO_2 laser capable of continuous and pulsed operational modes was used by Kurland et al. (2007) in their experiments, which focused on utilizing laser evaporation to produce magnetic iron oxide nanopowders. A CO_2 laser was employed, as its wavelength (λ=10.59μm) is absorbed by the raw material (ceramic powders) in high percentages (up to 90%) and due to its high power output, enabling high evaporation rates. The evaporation rates "steeply" increased with laser intensity (i.e. radiation). It was observed that pulsed radiation resulted in smaller particles than continuous mode. The experimental conditions included varying laser power, operational mode (pulsed vs. continuous), and carrier gas as well as its flow. Varying the power, carrier gas, and flow of the carrier gas did not result in significant changes in the production of nanopowders; however, changing the operational mode resulted in smaller particles when pulsed laser mode was used. The primary advantage of this study as mentioned by the authors was the high flexibility it offered as a result of the variations in experimental conditions.

A pulsed Nd:YAG laser was employed by Moras et al. (2005) as the evaporation mechanism for the production of magnetic nanopowders for ferrofluids. The target contained a combination of metallic micropowder or solid alloy in a reaction chamber with condensation of the particles in an aggregation gas (i.e. Nitrogen or Argon) under various pressures. The laser was operated at a mean power of 100W, pulse energy of 3J, and pulse length of 0.5ms while the gas pressure was varied from 20 to 200 mbar by altering gas inflow and/or the power of the vacuum pump. The results indicated a significant amount of loss due to evaporation since the Si content by chemical analysis was 2.2-4.2 wt% as reduction as compared to the 6.2wt% (used in the sheet) and 6.8wt%

of Si used in the micropowder during the preparation of the Fe-Si nanopowder target. The authors found the pressure of the aggregation gas to be significant since as the pressure increased so did the Fe intensity.

Lisenkov et al. (2009) explored the impact of laser evaporation of a stainless steel fast moving target. A CO_2 laser was employed in the research at a power density of 107 W/cm^2 and the influence of the laser's radiation on the target's surface at various ways of fast beam displacements were studied by the authors. The authors also developed a 3D numerical model which showed good agreement with the experimental results. Within the experiments, Lisenkov and colleagues operated the laser in a single pulse mode and generated pulses of radiation up to 70kW for a maximum duration of up to 1100μs. Two conditions were observed; first the target (stainless steel disk) was fixed and subsequently the target was rotated (400rpm at about 50m/s). In both conditions, the average laser power density was increased and the influence (i.e. laser plume) on fixed and moving target was observed. They found that the moving target increases the threshold of optical breakdown as oppose to the fixed target. In addition, evaporation of moving target was found at laser power of 12-24kW (avg. power density of 0.6-1.2 x 107 W/cm2).

The paper by Essien et al. (1993) is one of the first reports of lasing emission from a single, evaporating, layered microdroplet. Droplets consisted of approximately 7.9μm radius glass core were covered by a liquid shell of Rhodamine 6G dye-doped glycerin-water solution. In their experiments, an electrodynamic quadrupole trap was used to create droplets by collision of the glass core with the dyed solution. Droplets' radii were within the 7-32 μm range. Lasing emissions from the evaporated droplets were

recorded and depicted in the experimental setup. The He-Ne laser was used to illuminate the droplet (this facilitated observation via a microscope) and to obtain elastic scattering spectra. Nd:YAG pump laser was used to initiate droplet lasing. Lasing emissions were recorded at several droplet radii as the liquid shell decreased from roughly 14.5μm to about 0.4 μm, an evaporation rate of approximately 0.5μm per hr.

Hitoshi et al. (2006) investigated radiative evaporation of a single droplet of suspended alcohol fuel (ethanol) via the use of a CO_2 laser source. The droplet's evaporation behavior was monitored using a high speed video camera; variations of droplet diameter were measured and the authors observed that the slope of the temporal variation of droplet diameter to be almost constant. Additionally, Hitoshi et al. suggested that a droplet absorbs the radiative energy in proportion to its area. They also observed droplet explosions at high radiative power densities and large intital droplet diameters. Lastly, they found that the time for a droplet to reduce to half its size (referred to by the authors as the "half-diameter period") increased as the initial diameter was larger and decreases with increase in power density of the radiative laser source. Hitoshi and colleagues found that the half-diameter period was almost proportional to the initial droplet diameter at high radiative power densities.

With respects to the aforementioned authors, this research investigates the rapid transformation of microsized features into the nanoscale while maintaining controlled evaporation and deposition towards scalability in manufacturing. The methodology employed in this research is described in the following chapter.

CHAPTER 3

METHODOLOGY

3.1 Drop-on-Demand Inkjet System

The primary source for generating microdroplets of the different fluids (e.g. distilled water, acetone, blue color mixture with both acetone and water, and nanotubes solutions) used in this research is via a drop-on-demand (DOD) system. This inkjet system enables controlled deposition of droplets onto desired substrates. Specifically, the system to be employed is the direct write technique of inkjet printing with interchangeable nozzle diameters (e.g. 10 – 100μm). The DOD system has a backpressure that is instrumental in ensuring appropriate amount of pressure is applied such that microdroplets are generated. Further, the system comprises of a piezoelectric jetting head that is controlled via an electrical signal generating device (MicroFab's JetDrive III Controller), which sends frequency and voltage input data to the inkjet direct write system. The same signal generating system is used to control the strobe delay, which is a light emitting diode (LED) used in illuminating the droplets. The strobe delay is synchronous to illuminate microdroplets based on the frequency that the droplets are being generated at. The entire DOD system is installed in a clean room (class 1000); hence, the impact of contaminants such as particulates and dust particles are mitigated. The experimental setup for the preliminary work with a convective heating source is described. The ensuing section describes the experimental setup for the CO_2 laser source.

3.2 Experimental Setup for Resistive Ring

Nanopure distilled water and 99.998% filtered acetone were used as candidate fluids with specific heats of 4.19 and 2.22 kJ/kg K, respectively. The choice of these two fluids enabled the assessment regarding the significance of the specific heat (e.g., high versus low) on droplet evaporation. The other factor investigated was the impact of nozzle diameter (50 versus 30 μm) for both fluids. The use of different nozzle sizes determined the impact of the surface to-volume ratio on droplet evaporation. Both of the fluids were jetted using a customized direct-writing inkjet system (MicroFab Technologies Inc., Plano, TX) as shown in Figure 3.1. The system consisted of a JetDrive III waveform generator and amplifier, a pneumatics console, an optics system, and an MJ-AT-01-30 piezoelectric (PZT) microvalve with an interchangeable orifice (i.e., the nozzle diameters of 30 and 50 μm could be accommodated). Monodisperse microdroplets were ejected through a resistive heating ring fixture that was placed approximately 5 mm away from the nozzle tip. Controlled evaporation of the microdroplet was achieved by varying the temperature of the resistive heating ring fixture (Mid Atlantic Heater and Control Inc., SC), which was manipulated using a PID controller. Figure 3.1 depicts the direct-write inkjet system and resistive heating ring fixture with a PID temperature controller.

A working principle of the resistive ring experimental setup (phase one of this research) has been depicted in Figure 3.2. The schematic illustrates that initial microdroplets have larger diameters prior to passing through the ring; however, after

passing through the ring as energy (i.e. heat) has been applied noticeable reductions are observed in droplets dimensions via a high-speed CCD camera.

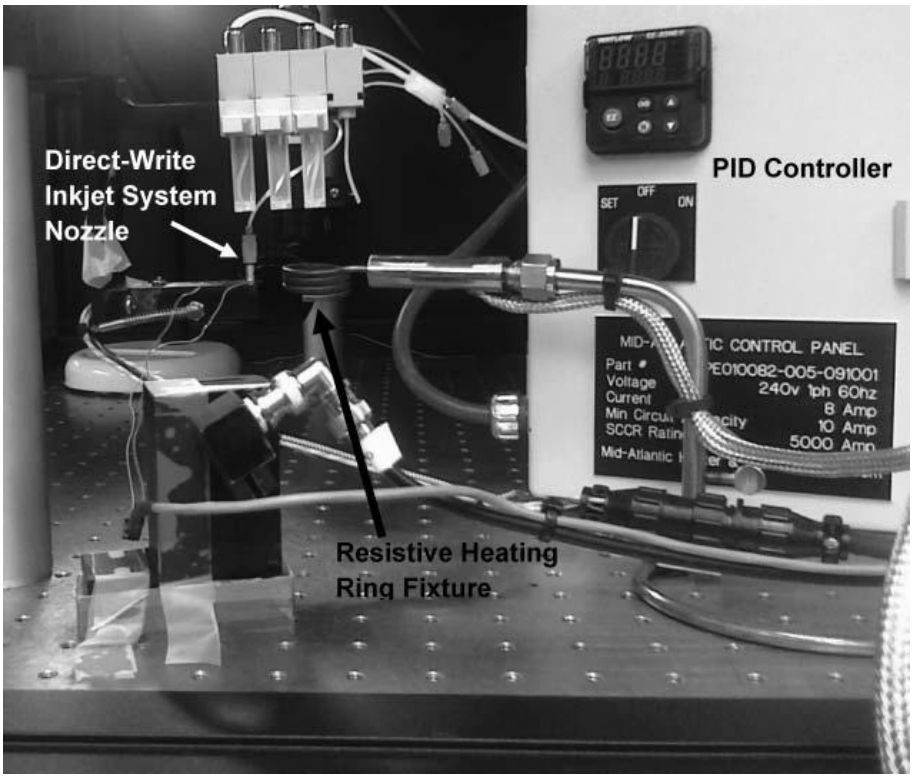

(a)

(b)

(c)

Figure 3.1. Experimental setup resistive heating ring (a) direct-write system and ring fixture with its temperature controller; (b) electrical signal generating device; (c) pressure system.

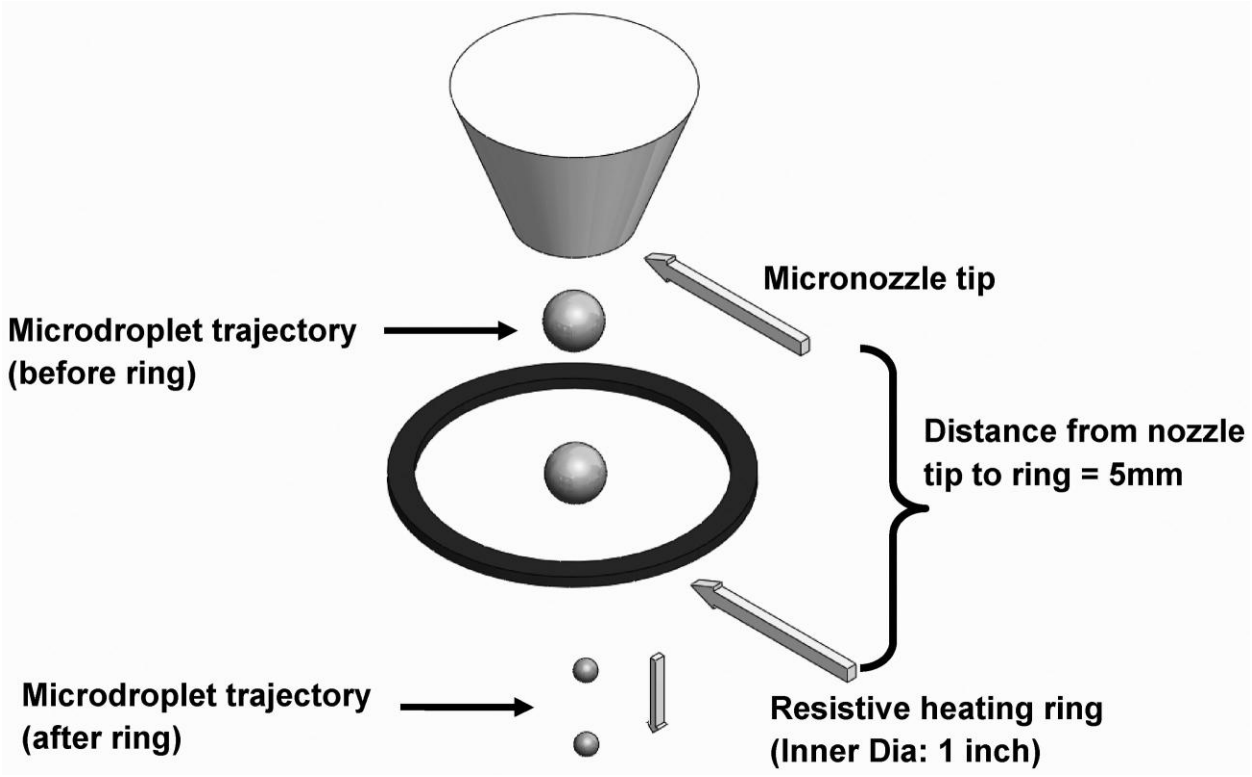

Figure 3.2. Schematic of the working principle for the resistive heating ring investigations.

3.2.1 Experimental Design.

The experimental procedure consisted of jetting both fluids (water and acetone) using two different nozzle diameters (30 and 50 μm). The temperature of the resistive heating ring fixture was adjusted to provide controlled evaporation of the droplets for each experimental condition as listed in Table 3.1. The initial droplet condition (i.e., without the heating ring) for each experiment was recorded at room temperature (25°C). The working principle of the resistive heating ring is illustrated in Figure. 3.2. The resistive heating ring was placed approximately 5 mm away from the nozzle tip to expose the microdroplet to a convective heat flux during its flight. The resistive heating ring had an internal diameter of 25 mm. Utilization of the resistive heating ring led to reductions in the microdroplet volume

relative to the before-ring condition. The temperature range varied from 200 to 400°C in increments of 50°C.

Table 3.1. Experimental conditions for resistive heating ring.

Condition No.	Nozzle Diameter	Fluid type	Ring temperature range (°C)
1	50 microns	Acetone	200-400
2	30 microns	Acetone	200-400
3	50 microns	Distilled water	200-400
4	30 microns	Distilled water	200-400

3.2.2 Image Analysis of Microdroplets.

A charged-coupled device camera with a microscopic zoom lens was used to capture the microdroplet formations and their respective flight path trajectories from the nozzle orifice (Figure 3.3). A light-emitting diode was synchronized with the inkjet's piezoelectric actuator to provide illumination for observing the droplets. Once a stable monodisperse droplet condition was achieved, the heating ring fixture was positioned to envelope the droplets for evaporation. Image acquisition software (ImageJ) from the National Institutes of Health was used to analyze the droplet evaporation (Abramoff et al., 2004). The software enabled image analysis of microdroplets (before-ring Figure 3.4(a) and after-ring Figure 3.4(b) conditions) by allowing for measurements of different dimensions (i.e., length/diameter, area, etc.). The droplet was allowed to stabilize to a spherical shape after exiting the nozzle so that reliable droplet volume calculations could be made based on the diameter of the droplet. A copper wire as shown in Figure 3.4(b) of known dimensions (68.9μm) was introduced in the frame during image capture to calibrate the microdroplet dimensions. Using the relationship of the ratio between the numbers of pixels of a known dimension, a global scale was set to measure all ensuing

images. Diameters of droplets were measured to record reduction after passing through the heated ring (sample size n = 6). Droplet surface area ($4\pi r^2$) and volume dimensions ($4/3 \times \pi r^3$), where r stands for radius of the microdroplet, were calculated. These values were recorded for each experimental condition to characterize reductions in its size with variations in the temperature.

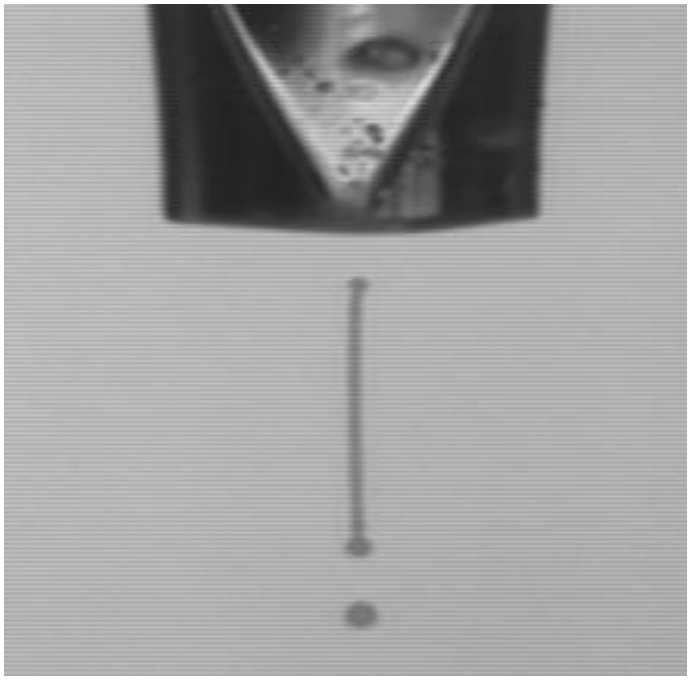

Figure 3.3. Microdroplet formation from DOD system's nozzle.

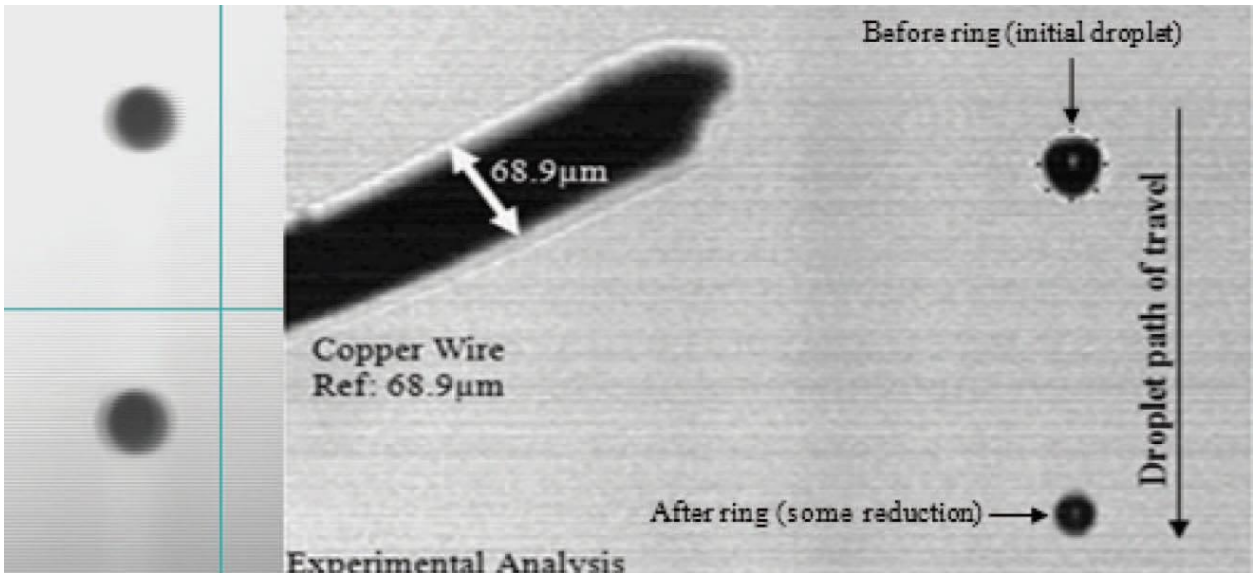

(a) (b)

Figure 3.4. Image analysis of droplet (a) before heating; (b) during path of flight after exposure to heating ring.

3.2.3 Experimental Procedure.

The experimental procedure for the conductive (i.e. resistive heating ring) experiments was as follows:

1. Generate monodisperse (i.e. single) microdroplets of candidate fluid type using the direct write inkjet printing technique
2. Utilize the CCD camera to capture several images of the microdroplets to obtain initial diameter of the droplet (at least 5 images are recommended for consistency and accuracy in measurement)
3. Place the resistive heating ring approximately 5mm below the nozzle to ensure that the microdroplet trajectory passes through the ring in order to initiate reduction (see Figure 3.2)

4. Power on the resistive heating ring device using the PID controller and set the desired ring temperature (at each temperature, capture at least 7 images for consistency and accuracy to be measured and compared to the initial diameter)
5. After concluding experiments at the desired temperature, all images should be measured in ImageJ (Note: at least 4 measurements (e.g. 2 in horizontal direction and 2 in vertical direction) in ImageJ should be obtained and averaged for the diameter for all captured images).
6. Use the diameter measurements to calculate surface area and volume for the droplets and compare initial conditions to experimental conditions.

3.3 Experimental Setup for CO_2 Laser

The methodology employed in this second phase was similar that of the first phase (i.e. resistive heating ring experiments) with the exception that this phase experimented included the use of a smaller nozzle orifice (20μm), and considered the impact of adding a color dye to both candidate fluids. It was hypothesized that the addition of a darker color would enable absorption of higher heat at a given lasing power. However, prior to the discussion of the experimental setup, the safety protocol is first briefly mentioned.

3.3.1 Laser Safety Protocol.

The laser was controlled via a UC-2000 laser controller (Synrad Inc, Mukilteo, WA) and was operated in the manual control mode. In addition, there were several safety devices utilized in conjunction with the laser setup. For instance, a diode pointer was equipped with the laser because the laser beam is invisible; hence, the pointer emitted a

visible (red color) beam to aid in accurate tracking and alignment of the laser's beam travel trajectory. The laser was operated inside a black aluminum hood enclosure (VERE, New Kensington, PA) with dimensions of 27in x 36in x 24in (LWH) (see Figure 3.5). Also, a beam dump (from VERE) with 2 and 3 inch posts was positioned inside the enclosure to obstruct unsafe travel of the laser beam. Lastly, the enclosure was equipped with an additional safety feature, an interlock switch, which prevented the laser from operating if any of the enclosure's door panels were open. An illustration of the laser experimental setup is depicted in Figure 3.5, followed by a schematic of the working principle for the laser source (Figure 3.6).

The CO_2 laser source was employed to impinge upon microdroplets after emission from the nozzle during their trajectory to the substrate, but prior to reaching the surface of the substrate. It is expected that the region of the laser's heat flux will significantly reduce the droplet's size and will be captured by a high-speed CCD camera as shown in Figure 3.6. The setup ensured that the laser source enabled microdroplet evaporation such that the reduced features were those deposited onto the substrate.

(a)

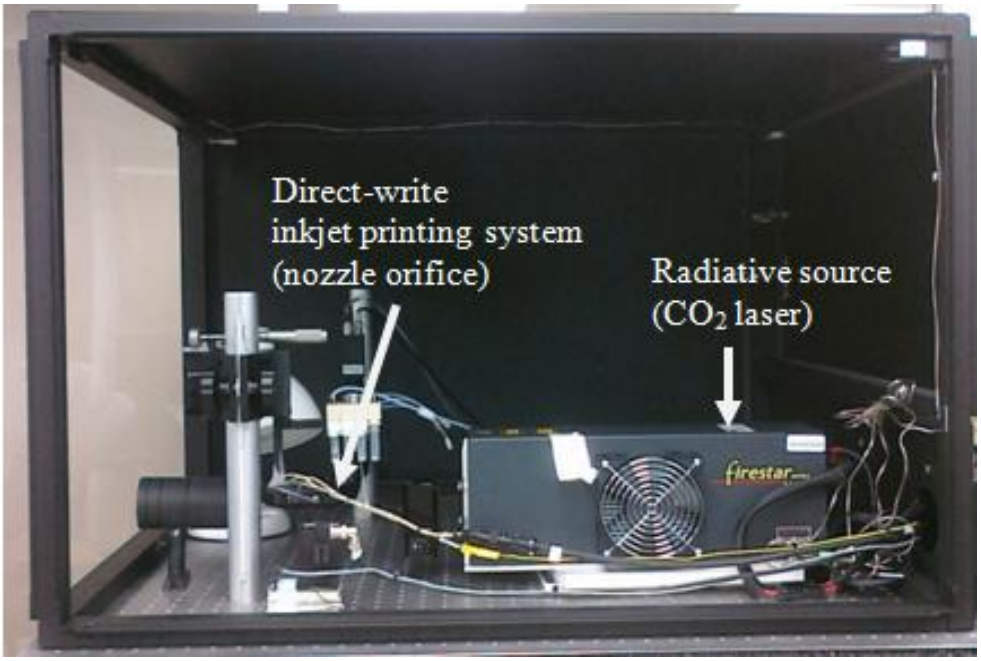
Direct-write
inkjet printing system
(nozzle orifice)
Radiative source
(CO_2 laser)

(b)

(c)

(d)

Figure 3.5. Laser experimental setup (a) black aluminum hood enclosure; (b) laser components and DOD system inside the enclosure; (c) V30 firestar series laser; (d) UC 2000 laser controller.

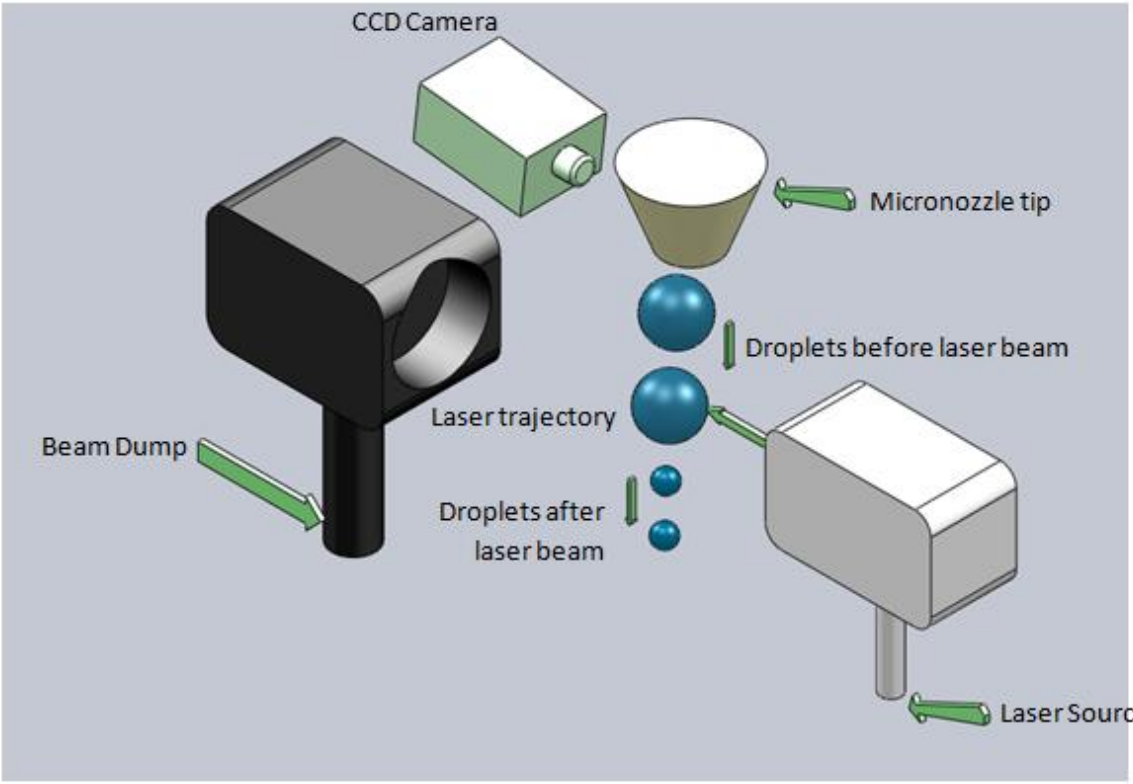

Figure 3.6. Schematic of the working principle for the CO_2 laser source investigations.

3.3.2 Experimental Setup.

The primary candidate fluids were nanopure distilled water and 99.998% filtered acetone. In addition, a blue color dye was mixed in equal concentrations with each fluid type to enable the observation it has on microdroplet evaporation given that the lasing sources operates via wavelength. The wavelengths of both fluids were measured via a UV spectrometer. Giving a total of four fluid types as presented in Table 3.2. The disparity between the fluid types is in their specific heat capacity, which measures the amount of heat required to change an object's physical property as a result of an increase in the object's temperature. The specific heat capacity of the each fluid was 4.19 kJ/kg K for

water and 2.22 kJ/kg K for acetone. An evaluation of the impact of specific heat capacity on droplet evaporation was studied. The significance of the initial diameter of microdroplets on evaporation rate was evaluated since three different nozzle orifices (50, 30, and 20μm) were utilized in the experiments to eject microdroplets of both fluids. Additionally, the effect of the lasing frequency was studied on microdroplet evaporation. Lastly, microdroplet reduction towards the nanoscale was investigated as the lasing output power (PWM) was varied. The fluids were jetted using the customized direct writing inkjet printing system (MicroFab Technologies Inc., Plano, TX) employed in the previous phase. A 30W CO_2 laser (Firestar Series V30, Synrad Inc., Mukilteo, WA) was the radiative source employed for all experimentations. Its beam was impinged to completely encapsulate monodisperse microdroplets as they were ejected from the nozzle orifice of the direct write inkjet printing system. The complete system (i.e. direct-write inkjet system and laser source) is depicted in Figure 3.5.

3.3.3 Design of Experiments.

The design of experiment for the radiative source consisted of a screening of the experimental factors to determine which factors should be considered in the experimental conditions. Furthermore, the levels within each factor were also determined to ensure that each level would have an effect towards microdroplet evaporation.

3.3.3.1 Factor Screening.

Factor screening of potential factors was evaluated to determine which factors will have the most significant impact on the response variable (i.e. microdroplet reduction). The following factors were hypothesized to have significant effect on

microdroplet evaporation based on preliminary experiments. The levels associated with each factors are noted in the parenthesis as follows:

- Fluid Type (acetone and water)
- Nozzle Size (20, 30, and 50μm)
- Laser Power (10, 50, and 95%)
- Laser Frequency (5, 10, and 20kHz)

There were a total of 54 (2x3x3x3) combinations (i.e. experiments) conducted in the screening. Each combination was replicated once to estimate error; thus providing a total of 108 experimental runs. It was assumed that the effect of each factor on droplet reduction would be both normal and random. Normality and randomness results were validated and are presented in Section 4.2.1.

3.3.3.2 Experimental Factors and Levels.

Based on the assumptions in the previous section, the four factors were considered in the experimental design in the radiative source phase. These factors were nozzle size, fluid type, lasing power, and lasing frequency. The corresponding levels for each factor were 3, 4, 5, and 3, respectively. Therefore, there were 180 (3 x 4 x 5 x 3) full factorial design experiments conducted to assess the combination of the factors and their levels. However, a factorial design was analyzed for statistical significance in the ensuing chapter to evaluate interaction effects as well as main effects of factors on percentage microdroplet volume reduction. Each factorial level was evaluated to determine its impact on droplet evaporation. Table 3.2 provides a list of the factors along with their respective levels. The most significant factor observed during preliminary experiments to

affect the evaporation of microdroplets was lasing power. However, this observation must be validated statistically in the analysis presented in the section 4.2.2.

Table 3.2. Factors and levels.

Factors	Levels
Nozzle Size (μm)	50, 30, 20
Fluid Type	acetone, distilled nanopure water, acetone and color dye, water and color dye
Pulse Width Modulation (PWM)	10, 30, 50, 70, 95
Lasing Frequency (kHz)	5, 10, 20

3.3.3.3 Experimental Procedure.

The experimental procedure consisted of jetting both the plain fluids (water and acetone) as well as the dyed-doped fluids (water with color additive and acetone with color additive) using all three available nozzle diameters (20, 30, and 50μm). The pulsed width modulation (PWM), which corresponds to the output power of the CO_2 laser source employed, was varied such that its impact can be assessed on microdroplet evaporation. The laser was operated at each of its frequency (5, 10, and 20 kHz) for all experimental conditions (see Table 3.3). For each experimental condition, five initial microdroplets (i.e. before lasing) and five closing microdroplets (i.e. after lasing) were captured. The significance of capturing pre-experimental images (Figure 3.9) of microdroplets was to obtain the average initial diameter of the microdroplet. Hence, ensuing image captures (Figure 3.10) of microdroplets during lasing were attested to evaporation caused by the laser source and compared to the initial diameter for reduction. During experimentation,

at least seven ($n \geq 7$) images of microdroplets were captured for each PWM to ensure consistency and accuracy in determining the average diameter of the microdroplet at that lasing power. Likewise, it was equally important to capture images after completion of each experimental condition because it provided assurance that the evaporation (i.e. reduction) observed was due to the lasing power; since the haze which formed around droplet's periphery during experimentation diminished once the laser was switched off and allowed to cool after several minutes. Although, post-experimental images had lower diameter values compared to the pre-experimental conditions due to the increased heat flux of the air surrounding the nozzle orifice (observed by an increase in temperature in the inkjet system's thermocouple reader); however, those diameters were generally higher than the average diameters observed during lasing. The lasing output power was adjusted from 10% to 95% in increments of 20% (i.e. 10, 30, 50, 70, and 95 %). 95% and 99% are the maximum PWM of the laser; however, 95% is the recommended setting for efficiency and greatest modulation purposes.

Table 3.3. Experimental conditions for laser source.

Condition No.	Nozzle Diameter	Fluid type	Lasing Output Power (% PWM)	Lasing Frequency (kHz)
1	50 microns	Acetone	10-95	5, 10, and 20
2	30 microns	Acetone	10-95	5, 10, and 20
3	20 microns	Acetone	10-95	5, 10, and 20
4	50 microns	Distilled Nanopure Water	10-95	5, 10, and 20
5	30 microns	Distilled Nanopure Water	10-95	5, 10, and 20
6	20 microns	Distilled Nanopure Water	10-95	5, 10, and 20
7	50 microns	Acetone and Color Additive	10-95	5, 10, and 20

8	30 microns	Acetone and Color Additive	10-95	5, 10, and 20
9	20 microns	Acetone and Color Additive	10-95	5, 10, and 20
10	50 microns	Distilled Nanopure Water and Color Additive	10-95	5, 10, and 20
11	30 microns	Distilled Nanopure Water and Color Additive	10-95	5, 10, and 20
12	20 microns	Distilled Nanopure Water and Color Additive	10-95	5, 10, and 20

In summary, the experimental procedure for the lasing experiments was as follows:

1. Generate monodisperse (i.e. single) microdroplets of candidate fluid type using the direct write inkjet printing technique
2. Utilize the CCD camera to capture several images of the microdroplets to obtain initial diameter of the droplet (at least 5 images are recommended for consistency and accuracy in measurement)
3. Ensure that the laser source is in alignment with the trajectory of droplets such that it impinges upon droplets to initiate microdroplet reduction (Note: a diode pointer enabled visibility of the laser beam trajectory prior to operation).
4. Enclose the laser in an hood enclosure for safety purposes (see Figure 3.5a)
5. Power on the laser and allow to warm up for about 5 minutes, then operate it at the desired output power and frequency (at each output, capture at least 7 images for consistency and accuracy to be measured and compared to the initial diameter)
6. After concluding experiments at the desired output power and frequency, all images should be measured in ImageJ (Note: at least 4 measurements (e.g. 2 in

horizontal direction and 2 in vertical direction) in ImageJ should be obtained and averaged for the diameter for all captured images).

7. Use the diameter measurements to calculate surface area and volume for the droplets and compare initial conditions to experimental conditions.

3.3.4 Image Acquisition and Analysis of Microdroplet Reduction.

The CCD camera was employed to capture monodisperse microdroplets (Figure 3.7) ejected from the nozzle orifice. The camera also enabled images after passing through the laser beam to be captured including the evaporation haze that formed around the nucleus of the microdroplet (see Figure 3.10). In other words, evaporation of droplets was visible via image capture especially as the lasing power was increased. However, image analysis software was later employed to accurately measure the diameter of reduced droplets. The high-speed camera, equipped with a LED strobe light, was synchronized to the frequency of the ejected microdroplets through the inkjet printing system's piezoelectric actuator; this provided the necessary lighting for observing each microdroplet. After a stable monodisperse droplet condition, the diode pointer equipped with the laser source was employed to ensure that the beam would pass through the droplet trajectory when the lasing power was triggered. This ensured that the laser's beam would impinge and encapsulate the microdroplet to facilitate evaporation. Subsequently, the experimental setup (Figure 3.5b) was enclosed and the laser was triggered to initiate droplet evaporation. The familiar image acquisition software (ImageJ) from the national institute of health (NIH) was again used in this phase to analyze droplet evaporation. Multiple measurements in the horizontal and vertical directions of each microdroplet

were taken to ensure consistency in obtaining the droplet's length (i.e. diameter). A micrometer scale (Figure 3.8) of known dimensions was introduced in the frame during image capture to calibrate the microdroplet dimensions in ImageJ. Using the calibration, droplet surface area and volume were calculated using the length obtained via ImageJ for each experimental condition to characterize reductions in its size with variations in the laser output power and frequencies.

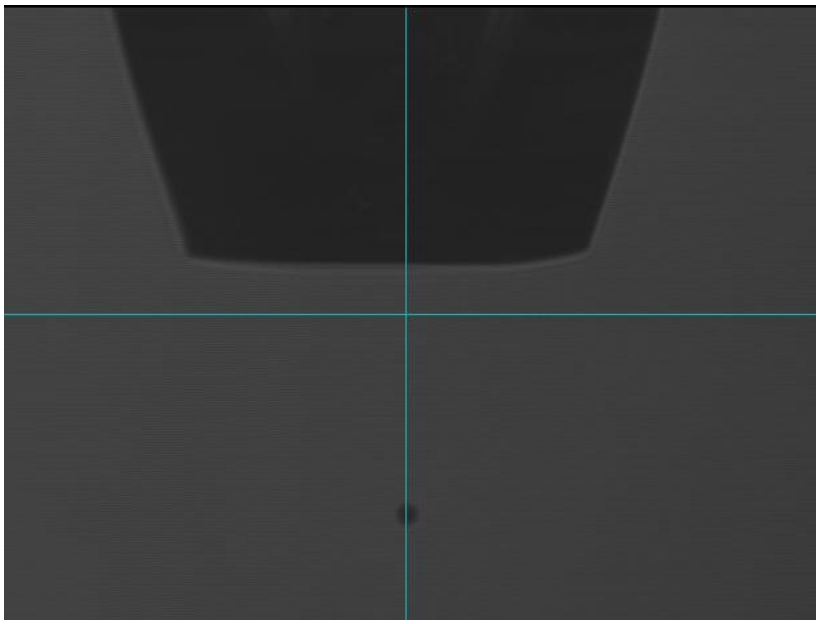

Figure 3.7. Monodisperse microdroplet formation from nozzle orifice.

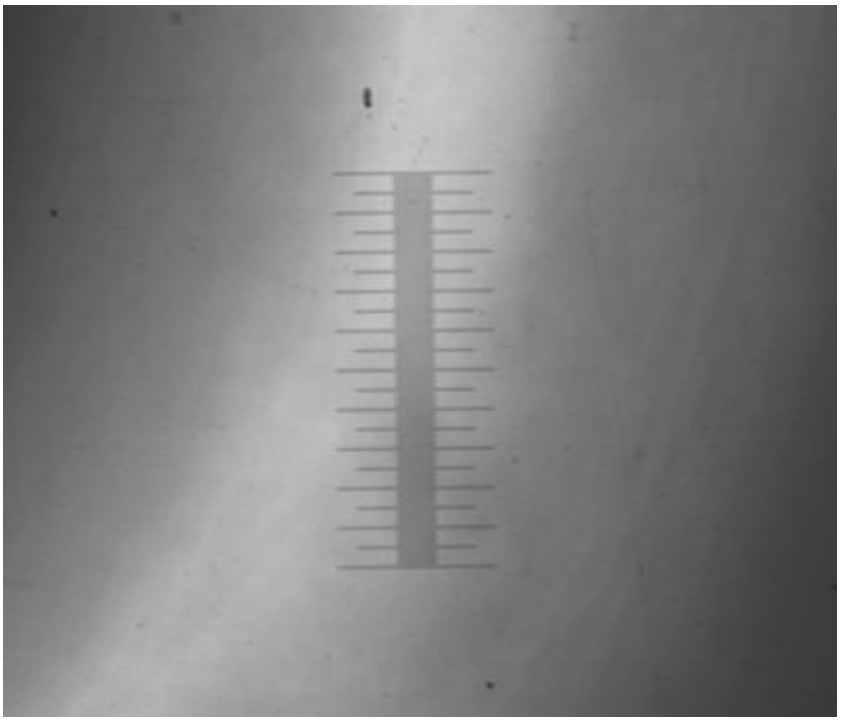

Figure 3.8. Micrometer scale used for calibration of droplet measurements in ImageJ.

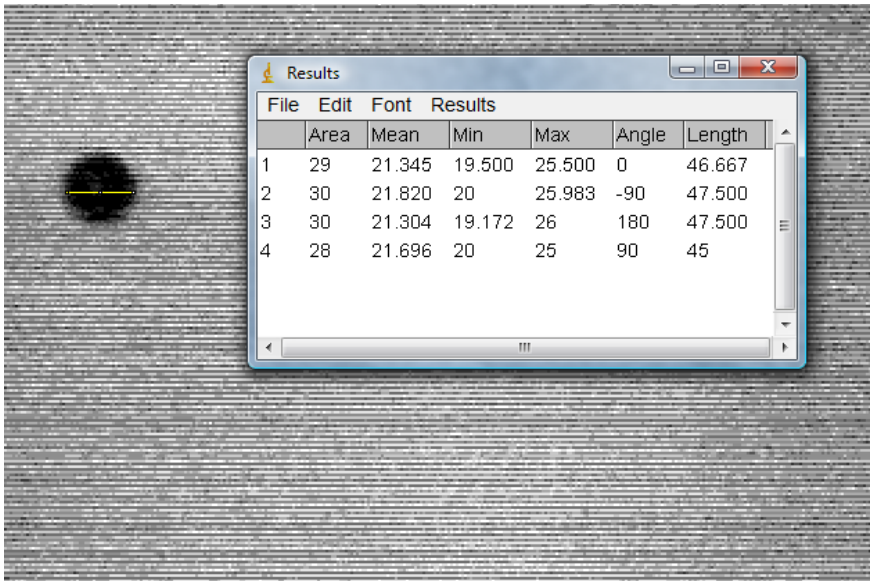

Figure 3.9. ImageJ measurements of initial diameter (acetone droplet) ejected from 50µm nozzle.

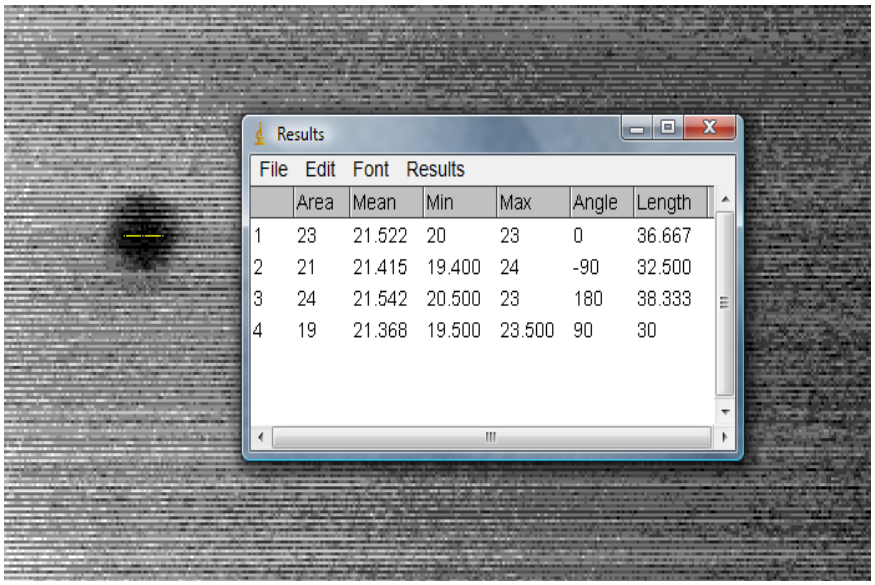

Figure 3.10. Image analysis of reduced acetone droplet ejected from 50µm nozzle at 95% PMW.

3.3.5 Characterization Techniques.

Scanning Electron Microscope (SEM) and the Atomic Force Microscope (AFM) were employed for characterization of carbon nanotube microdroplets. The AFM was utilized in Chapter 5 to characterize carbon nanotube clusters and networks. In addition, SEM was employed in Chapter 6 for characterization of the monodisperse microdroplets deposited on silicon substrate. The SEM depicted in Figure 3.11, operates by scanning the sample's surface using high-energy electron beams that interacts with the sample's atoms to produce topographic, composition, and other properties (e.g. electrical conductivity) in order to create an image. This microscopy technique was explored because of its ability to image samples within the 1-5nm range while also enabling magnification of up to 500,000 times the size of the sample. The AFM, another scanning probe microscopy, was employed to evaluate bundles of carbon nanotubes in the

investigation of fabricating thin film transistors (see Chapter 5). Operation of the AFM includes a cantilever arm with a sharp tip that is used to scan surfaces of samples in order to image, measure, and manipulate features on the substrate. Figure 3.12 below depicts a picture of the AFM employed in this research.

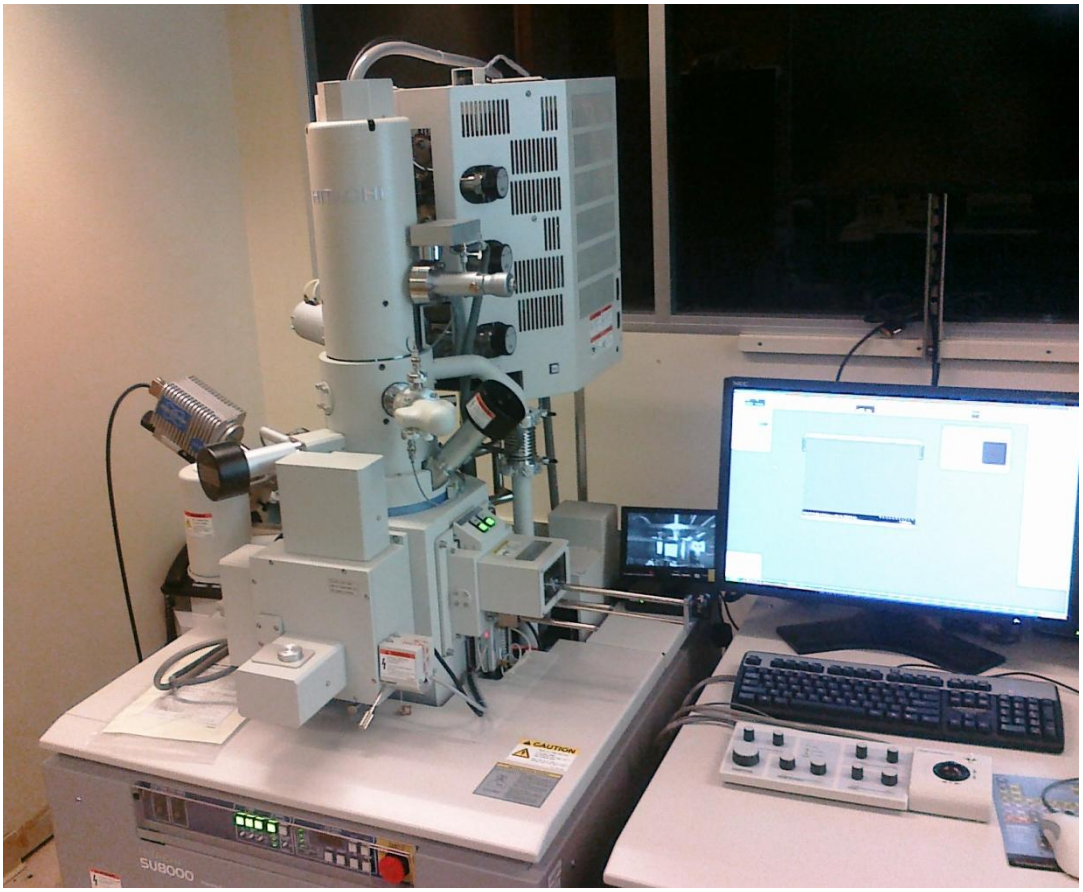

Figure 3.11. Depiction of SEM.

Figure 3.12. Depiction of AFM.

CHAPTER 4

RESULTS AND DISCUSSION

In this chapter, the results of the experiments conducted in the two phases, conductive source and radiative source are discussed, respectively. The impact of fluid type, nozzle size, and impact of the source employed were evaluated on microdroplet size reduction. Lastly, a numerical validation of results obtained from the convective experiments was conducted and showed close agreement. Furthermore, the statistical significance of experimental factors considered in the radiative source experiments was assessed to determine normality and randomness of the data as well as which factor had the most significant effect on microdroplet evaporation (i.e. percentage reduction in volume).

4.1 Resistive Ring Experiments

The initial microdroplet sizes for both fluid types (nanopure distilled water and ultra-purified acetone) prior to the introduction of the resistive heating ring differed. Water droplets (48–50µm) were closer to the size of the nozzle used, whereas the acetone droplets (30–40µm) were smaller for the same nozzle size (50µm). This can be attributed to the differences in the viscosity and surface tension of the two fluids (Table 4.1). Thus, acetone, due to its lower viscosity (0.31 cP) and surface tension (25.20 mN/m), required a lower piezoelectric activation voltage, thereby inducing smaller sized droplets. Water, due to its relatively higher viscosity (1.00 cP) and surface tension (72.80 mN/m), was shown to require higher activation voltages as compared to acetone. This resulted in larger drop sizes due to merging of satellite tails during ejection (shown in Figure. 3.3).

Table 4.1. Physical properties of experimental fluids.

Fluid Type	Viscosity (cP)*	Surface Tension (mN/m)*
Nanopure distilled water	1.00	72.80
Ultra-purified acetone	0.31	25.20

* Measurements taken at 20°C

4.1.1 Percentage Reduction in Droplet Volume.

For each of the experimental conditions, a proportional relationship between percentage volume reduction and incremental increase in temperature was observed (Figure 4.1). Furthermore, it was observed that the larger sized nozzle (50µm) yielded higher percentages of volume reductions compared to the smaller sized nozzle (30µm) for both investigated fluids. This phenomenon indicates that the microdroplets generated from the larger nozzle were subject to a higher heat flux on its periphery compared to the smaller sized nozzle. The use of a 30µm nozzle resulted in a 30% reduction in volume at 400°C for both fluid types, whereas the use of a 50µm nozzle resulted in 58 and 65% reductions in volumes at 400°C for water and acetone, respectively.

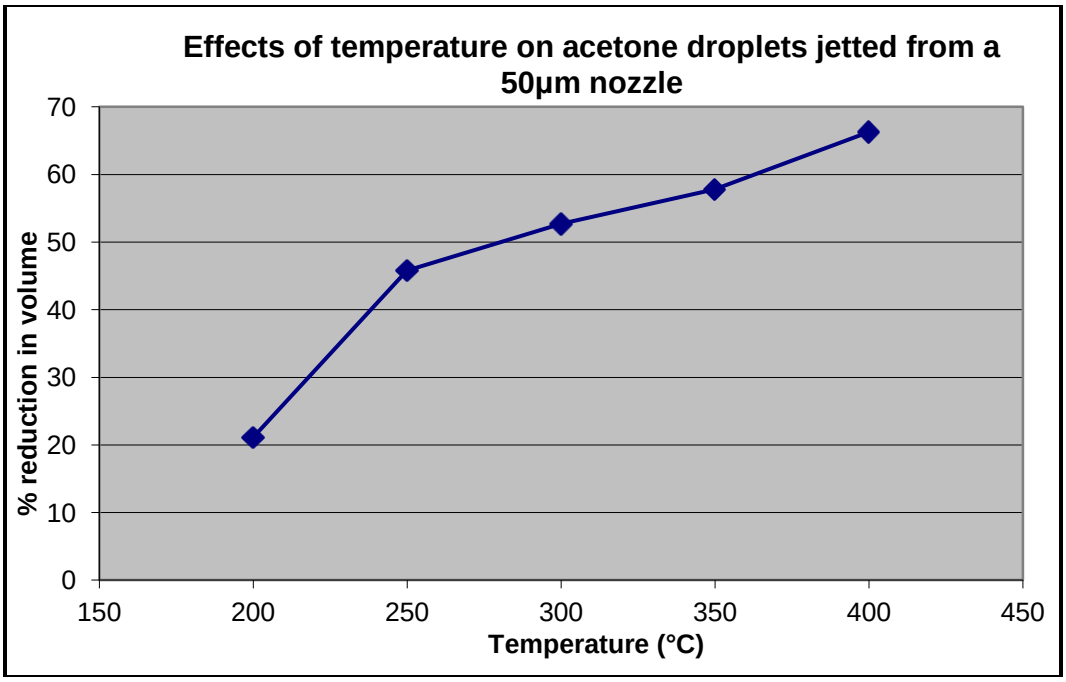
Effects of temperature on acetone droplets jetted from a 50µm nozzle
% reduction in volume
0
10
20
30
40
50
60
70
150
200
250
300
350
400
450
Temperature (°C)

(a)

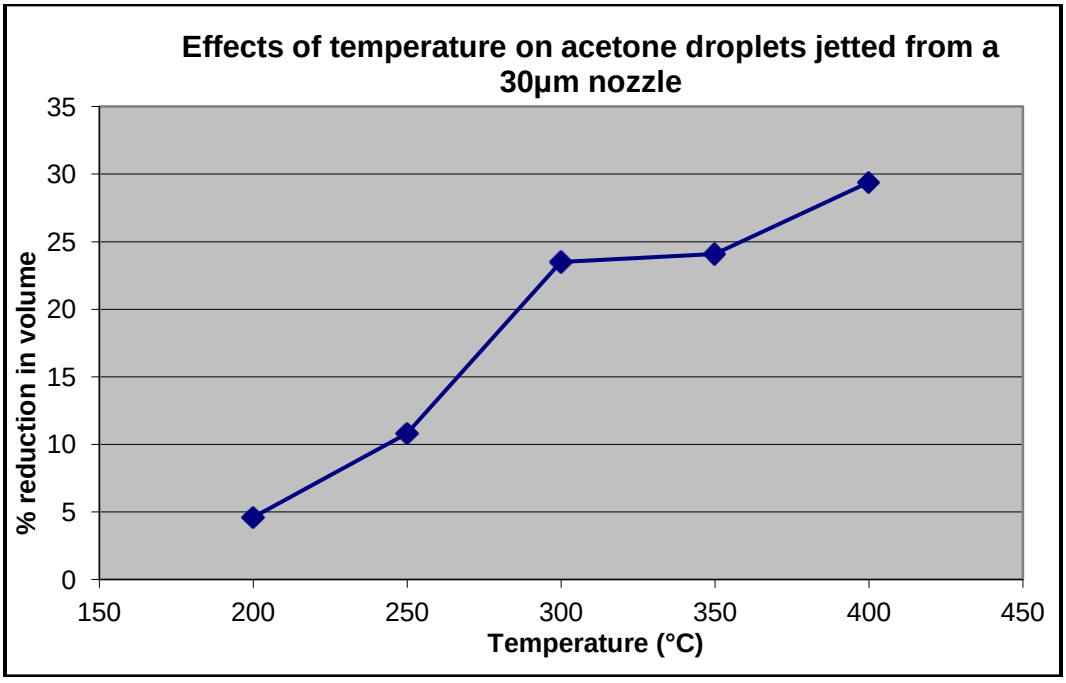
Effects of temperature on acetone droplets jetted from a 30µm nozzle
% reduction in volume
0
5
10
15
20
25
30
35
150
200
250
300
350
400
450
Temperature (°C)

(b)

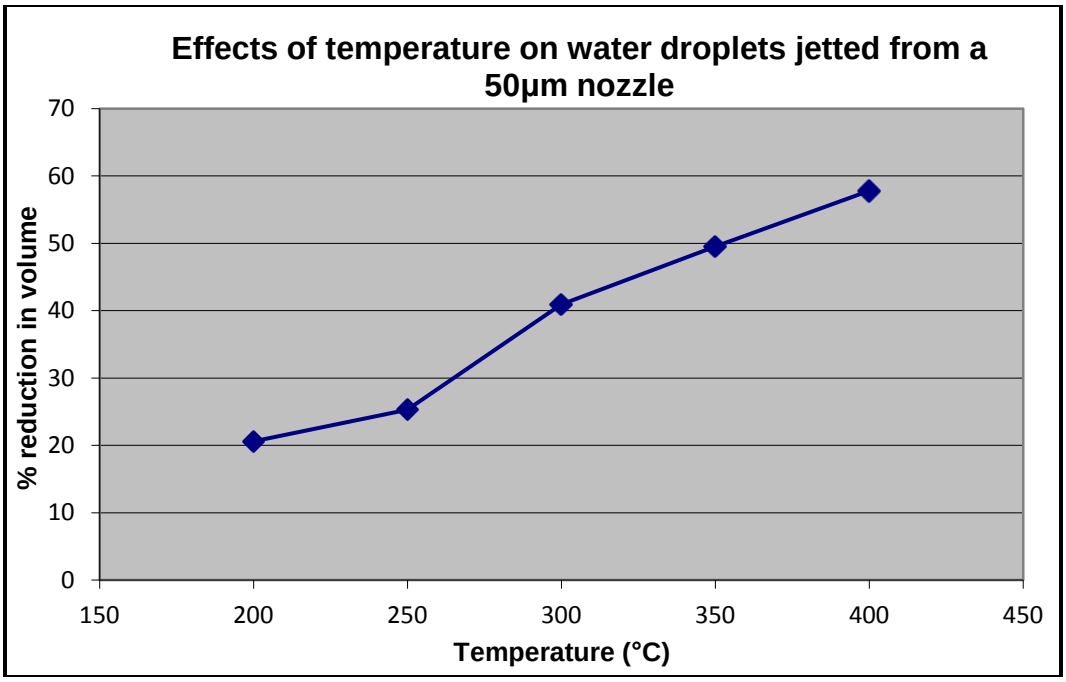

(c)

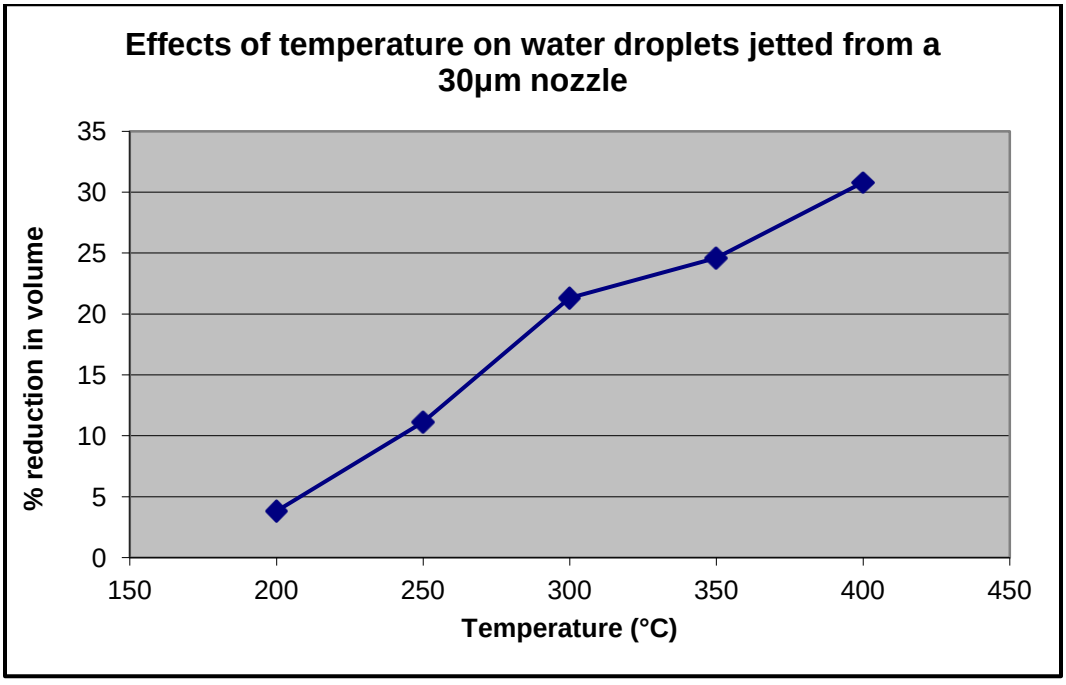

(d)

Figure 4.1. Percentage reduction in volume (a) acetone-50µm nozzle; (b) acetone-30µm nozzle; (c) water-50µm nozzle; (d) water-30µm nozzle.

4.1.2 Effect of Fluid Type

The effect of different fluids on the evaporation and shrinkage of microdroplets was studied. Acetone was observed to evaporate at higher rates compared to water with an increase in the resistive ring temperature (Figure 4.2). This can be attributed to the lower specific heat of acetone 2.22kJ/kgK compared to that of distilled water 4.19kJ/kgK. Both water and acetone microdroplets from a 50µm nozzle show higher volume reductions compared to microdroplets from the 30µm nozzle as they are subjected to a higher heat flux from the heating ring. However, the reduction of droplet volume for acetone from the 50µm nozzle was at a faster rate compared to the 30 µm nozzle due to variations in the heat flux.

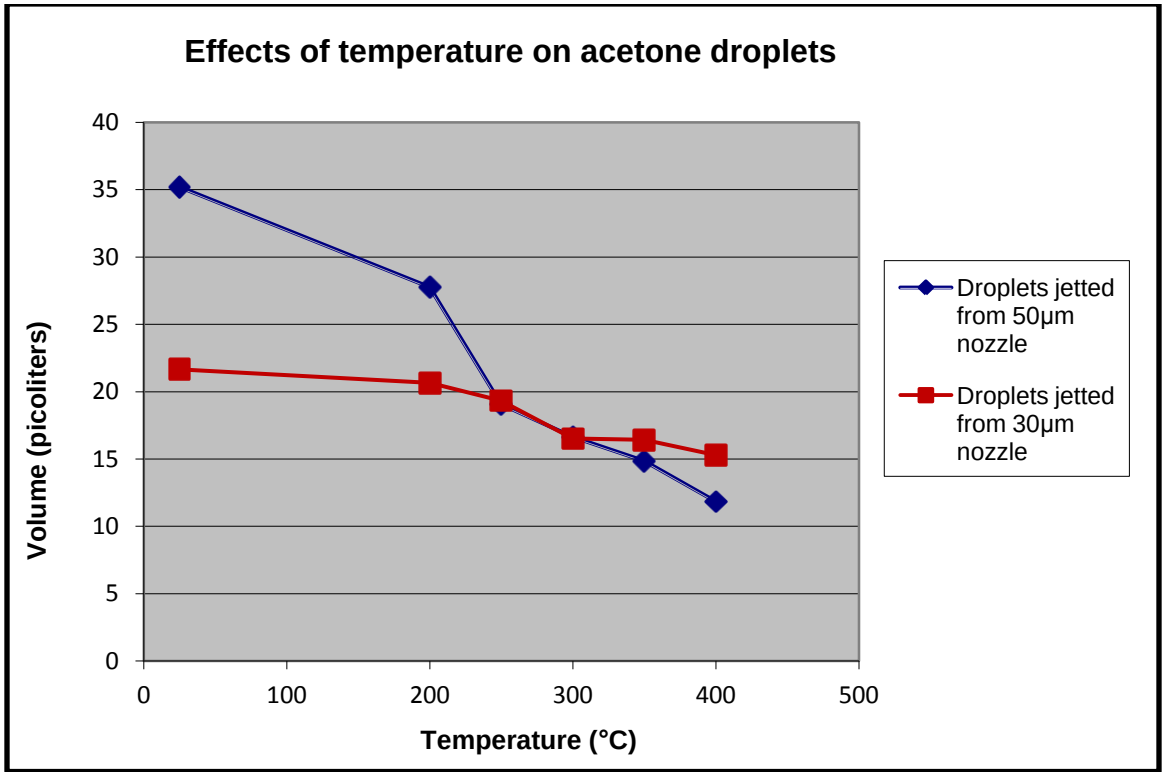

(a)

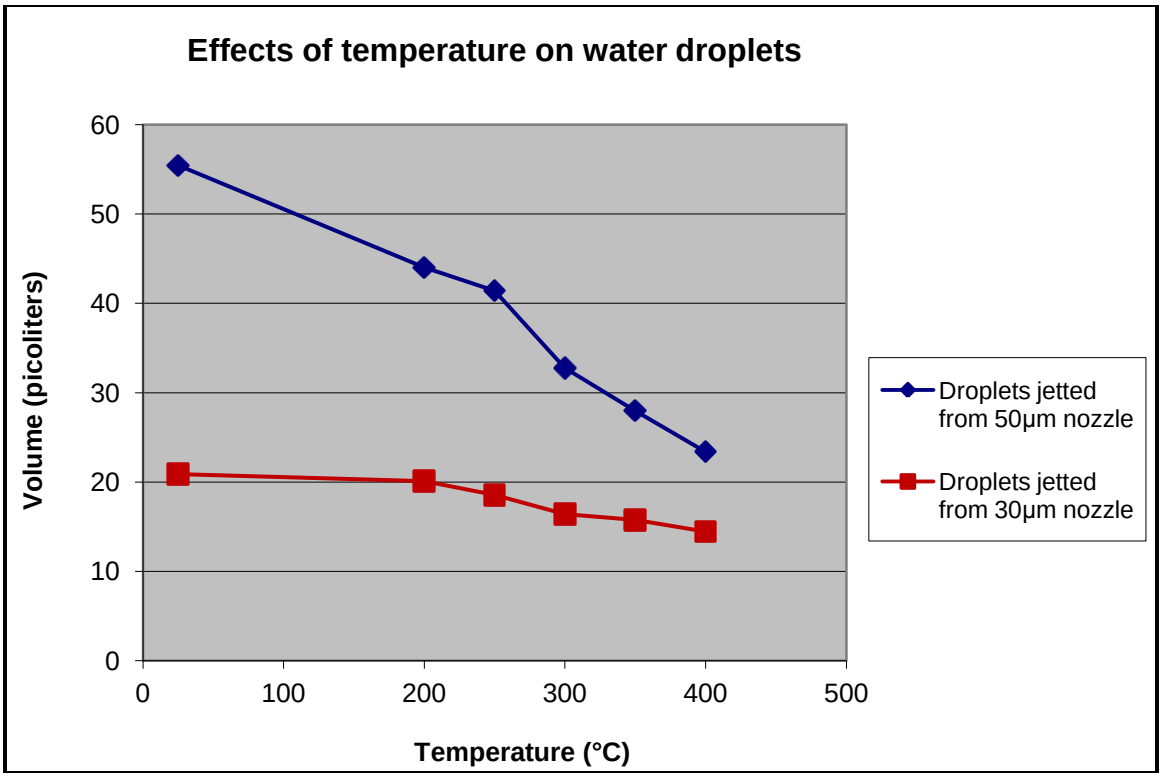

(b)

Figure 4.2. Evaporation characteristics based on fluid type (a) acetone; (b) water.

4.1.3 Effect of Surface Area to Volume Ratio.

The effect of the surface area–to-volume ratio on droplet evaporation was assessed as shown in Figure 4.3. Fluids, when jetted through the smaller nozzle size (30µm), resulted in a higher surface area–to-volume ratio compared to larger sized droplets. This can be attributed to the fact that at smaller droplet sizes there is a drastic increase in the surface area with reductions in the volumes. However at higher ring temperatures, the 50µm microdroplet of acetone was observed to have evaporated at a much faster rate in comparison with a 30µm size droplet, resulting in higher surface area–to-volume ratios at higher temperatures.

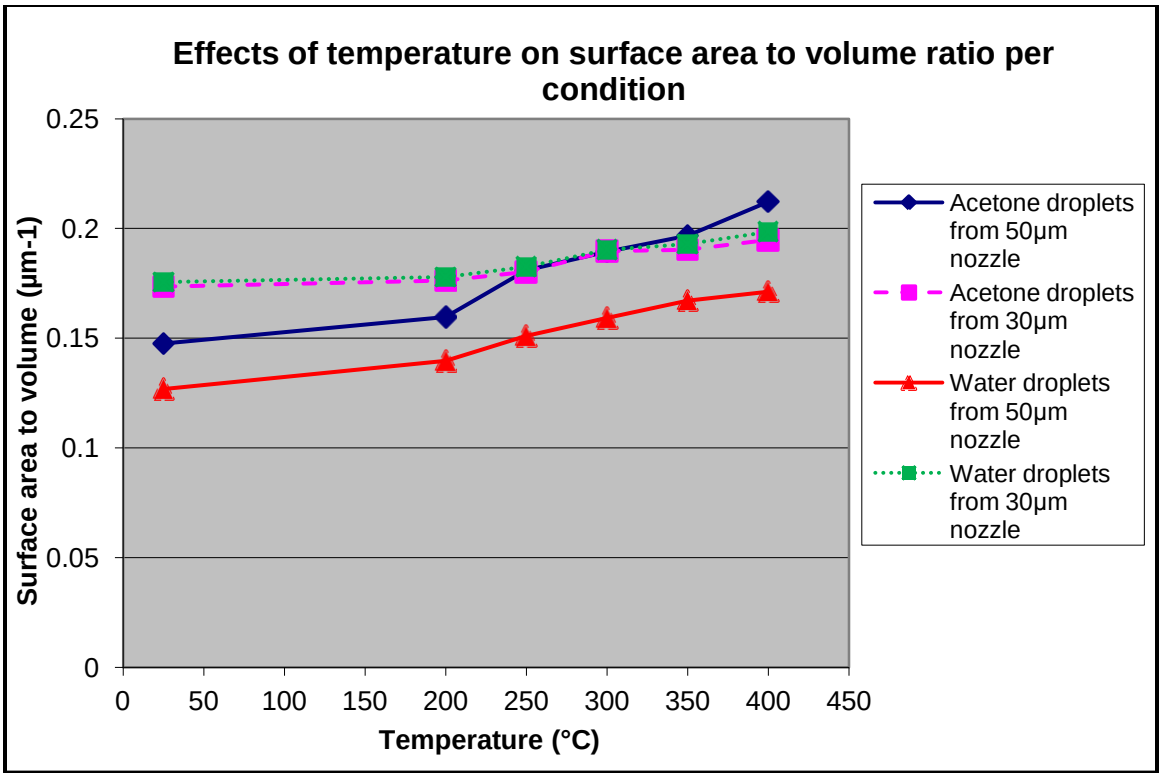

Figure 4.3. Evaporation characteristics for each condition.

4.1.4 Numerical Modeling/Validation of Phase One.

The evaporation phenomenon for microdroplets was validated using an equivalent theoretical model based on the D^2 law, which states that the time rate of change of the square of the droplet diameter, D, is constant (Mikkilineni et al., 2007) as stated in Equation (2); that is,

$$\frac{dD^2}{dt} = -K. \qquad (2)$$

This model assumes constant spherical droplet and vapor properties, and a spherical droplet with uniform temperature, K, is predicted using Equation (3) from the conservation equations to be (Faeth, 1977).

$$K = \frac{8\rho^{\mathrm{V}}\delta^{\mathrm{V}}}{\rho^{\mathrm{L}}} \ln\left[1 + \frac{8c_p^V \Delta T}{h_{LV}}\right] \quad (3),$$

where D is the droplet diameter, t is the time, K is the evaporation coefficient, h_{LV} is the latent heat of vaporization, ρ is the density, δ is the mass diffusion coefficient, ΔT is the difference between ambient vapor temperature and the droplet surface temperature, and c_p is the constant pressure specific heat. The superscripts L and V are used to show liquid and vapor properties, respectively.

The microdroplet was captured using high-speed stroboscopic photography at a distance of approximately 1 mm below the lower end of the heating ring for image analysis. The droplet's in-flight velocity was measured using the stroboscopic delay based on the type of fluid and input excitation conditions. The in-flight microdroplet velocity for water and acetone was calculated to be 1 and 3 m/s, respectively. This difference can be attributed to the variations in fluid properties such as density, viscosity, and surface tension between the fluids. The input piezoelectric waveform was adjusted to accommodate for the fluid property variations to obtain a monodisperse microdroplet. Thus, the time for evaporation from the heating ring to the image capture region was calculated to be 1 and 0.3 ms for water and acetone, respectively. This is the time difference (Δt) it takes for the initial droplet to shrink to the smaller diameter that is being captured by the high-speed camera. Using the D^2 law, we calculated the diameters of the respective droplets after size reduction for this time period (Δt) for both the fluids. The difference between ambient vapor temperature and the droplet surface temperature (ΔT) was assumed to be 100°C for water. For acetone, (ΔT) was assumed to be 10°C as the

droplets were traveling at higher speeds compared to water; thus, acetone was exposed to a lower heat flux compared to water. The D^2 law predicts the time it takes for a droplet of given initial size to evaporate completely to vapor. The theoretical size reduction based on the D^2 law was compared with the experimental results to observe differences as discussed below.

4.1.4.1 Water Droplet Size Reduction.

The experimental droplet volume reduction at 200°C was 21% with an initial water droplet size of 50µm. Percentage reduction in volume of spherical droplet (equation 4) is given by

$$\frac{4}{3} \times \pi \times \left(\frac{r_1^3 - r_2^3}{r_1^3} \right) \times 100 \qquad (4),$$

where r_1 is the radius of the droplet before heating and r_2 is the radius of the droplet after heating. Thus, using Equation (4) the water droplet size reduction after heating ring = 46.22µm. Using the D^2 law, the initial 50µm completely evaporates after 7.25 ms at ΔT =100°C. Based on Δt = 1 ms, the droplet diameter was estimated that would completely evaporate after (7.25 − 1) = 6.25 ms. The theoretical droplet size after 1 ms based on D^2 law = 46.5µm. Percentage difference between theoretical and experimental droplet radius = 0.6%.

4.1.4.2 Acetone Droplet Size Reduction.

Acetone's experimental droplet volume reduction at 200°C was observed to be 23%; its initial droplet size ejected from the larger micron nozzle (50µm) was found to be 40µm. Thus, using Equation (4) the acetone droplet size reduction after heating ring =

36.66μm. Using the D^2 law, the initial 40μm completely evaporates after 2.06 ms at ΔT = 10°C. Based on Δt = 0.3 ms, the droplet diameter was estimated that would completely evaporate after (2.06 − 0.3) = 1.76 ms. Theoretical droplet size after 0.3 ms based on D^2 law = 37μm. Percentage difference between theoretical and experimental droplet = 0.92%.

The theoretical and experimental droplet reduction values show close agreement with each other for both water and acetone. Thus, the experimental results are reliable predictors of droplet size reduction.

4.1.5 Phase One Discussion.

In this initial phase, the droplet evaporation characteristics for water and acetone were studied to understand the microdroplet size reduction phenomenon. A proportional reduction in the volume of water and acetone microdroplets was observed as the temperature of the resistive heating ring increased (i.e., increase in the heat flux). Acetone microdroplets exhibited a higher percentage volume reduction compared to water under the same conditions. This can be attributed to its lower specific heat and thus higher volatility compared to that of water. Additionally, droplets jetted with the 50μm diameter nozzle were observed to have higher percentage volume reductions than those jetted with the 30μm nozzle due to differences in the heat flux. Droplets with higher surface area–to-volume ratio evaporated at a faster rate. The experimental droplet size reductions were validated with a theoretical model (D^2 law) and showed close agreement. Hence, the experiments conducted in this phase provided the assurance that the second phase (i.e. laser) would exhibit even further reductions since the lasing beam can be

focused to completely encapsulate the microdroplet; thus, providing a more controlled evaporation towards achieving the primary objective of this research.

4.2 Laser Experiments

Prior to analyzing the experimental results from phase two (i.e. laser), statistical analyses of the factors were conducted to ensure that normality and randomness conditions were not violated. Based on the findings that there were no major violations, ANOVA analysis was subsequently conducted to examine the statistical significance of each factor in regards to its effect on droplet reduction.

4.2.1 Statistical Significance of Factors

Experimental results from the laser experiments were statistically evaluated to determine significance of factors on reducing the volume of microdroplets. Screening of the factors was conducted to establish whether or not experimental data followed a normal distribution as well as randomness. Additionally, ANOVA analysis was performed to determine the statistical significance of each factor on microdroplet evaporation as well as any interaction (i.e. combined effects) of factors. Both analyses are presented in the ensuing sections, respectively.

4.2.1.1 Factor Screening Results.

The results of the factor screening for normality and randomness suggested that the experimental data were normally distributed (Figure 4.4) as well as random in nature (Figure 4.5). Consequently, since the factors screening analysis did not violate normality and randomness conditions it validated the assumption suggested in Section 3.3.3.1 and thus validates that the factors are critical and would each have an effect on droplet

reduction. Given the results of this analysis, an ANOVA analysis was conducted as presented in the following section to determine statistical significance of each factor on volumetric reduction of microdroplets per candidate fluid type.

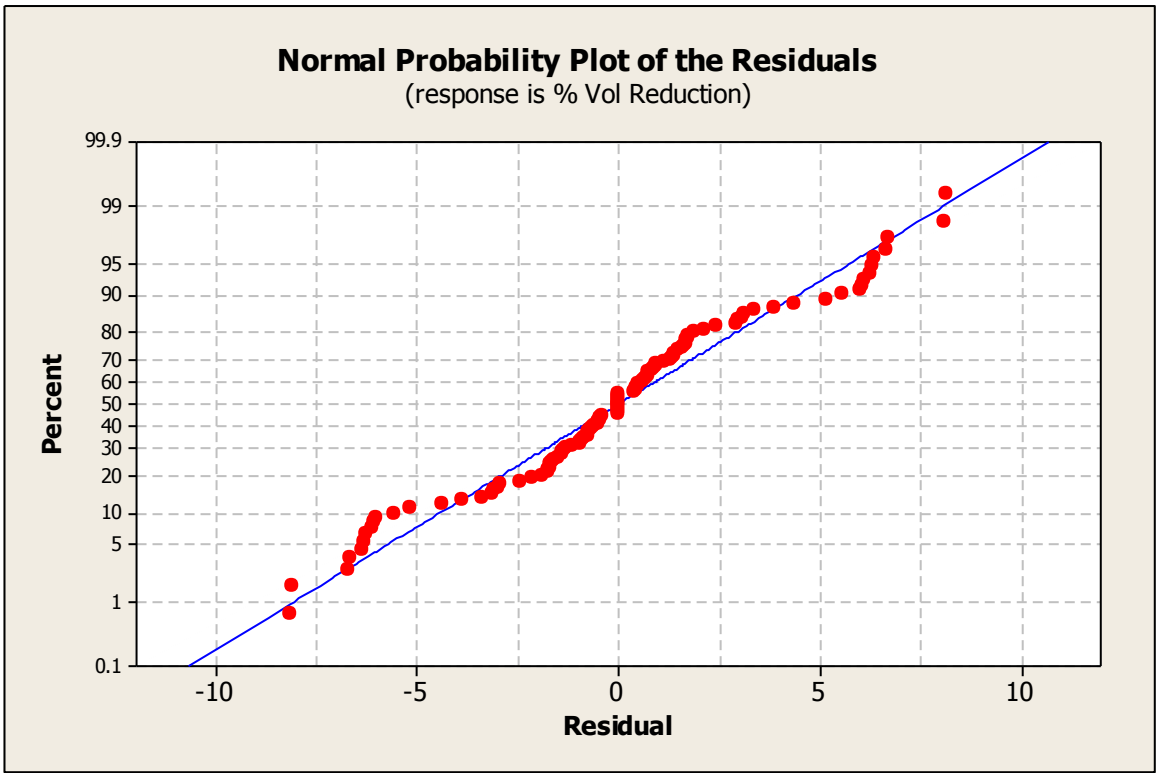

Figure 4.4. Normal distribution of experimental data.

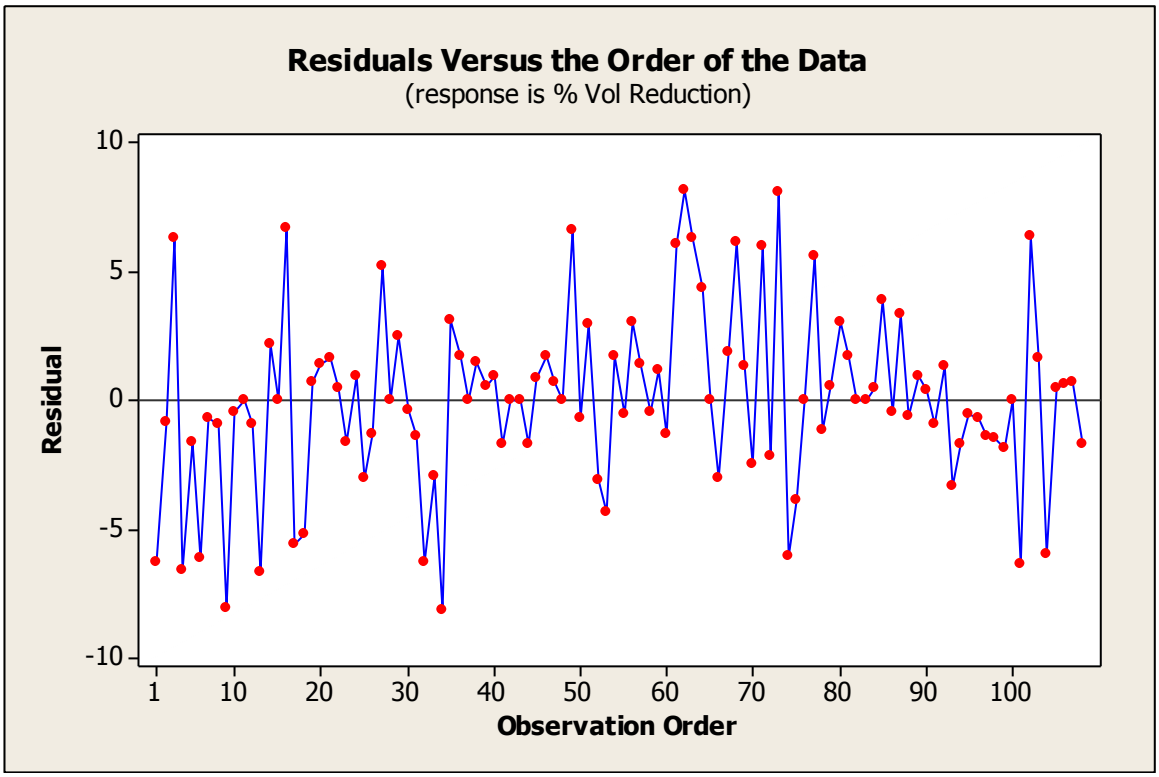

Figure 4.5. Random distribution of experimental data.

4.2.1.2 ANOVA Analysis Results.

A multilevel factorial design was conducted to evaluate the interaction effects as well as main effects of the factors employed in this experimental phase. The factors along with their corresponding levels used in the statistical analysis are presented in Table 4.2. As a result, the base run for statistical purposes provided a combination of 54 experiments (2x3x3x3). Additionally, each combination was replicated to provide an estimate for error. Analysis of Variance (ANOVA) was conducted since there was only a single depend variable (i.e. microdroplet reduction in size) to determine the effects of the independent variables (i.e. nozzle size, fluid type, lasing power and lasing frequency) on reduction. The analysis enabled the determination of whether or not average microdroplet reductions (i.e. means) were equal

as each factor varied. The assumptions of the analysis were independence of observations (i.e. no correlations between independent variables), normal distribution of data, and equality or homogeneity of variances (i.e. variance in groups are the same). The results of the ANOVA are presented in Table 4.3. The randomized multilevel factorial design is presented in the appendix.

Table 4.2. Factorial design.

No.	Factors	Levels
1	Fluid Type	Water and Acetone
2	Laser Power	10%, 50%, and 95%
3	Laser Frequency	5 kHz, 10 kHz, and 20 kHz
4	Nozzle Size	20µm, 30µm, and 50µm

Table 4.3. ANOVA analysis output.

General Linear Model: % Vol Reduct versus Fluid Type, Laser Power, ...

```
Factor           Type   Levels  Values
Fluid Type       fixed       2  Water, Acetone
Laser Power      fixed       3  10, 50, 95
Laser Frequency  fixed       3  5, 10, 20
Nozzle Size      fixed       3  20, 30, 50


Analysis of Variance for % Vol Reduction, using Adjusted SS for Tests

Source                                DF    Seq SS    Adj SS    Adj MS       F
Fluid Type                             1   1808.04   1808.04   1808.04   76.55
Laser Power                            2  24296.59  24296.59  12148.30  514.33
Laser Frequency                        2    880.43    880.43    440.21   18.64
Nozzle Size                            2   6929.95   6929.95   3464.97  146.70
Fluid Type*Laser Power                 2    139.84    139.84     69.92    2.96
Fluid Type*Laser Frequency             2     12.42     12.42      6.21    0.26
Fluid Type*Nozzle Size                 2    120.50    120.50     60.25    2.55
Laser Power*Laser Frequency            4     48.92     48.92     12.23    0.52
Laser Power*Nozzle Size                4    337.07    337.07     84.27    3.57
Laser Frequency*Nozzle Size            4     43.56     43.56     10.89    0.46
Fluid Type*Laser Power*                4      7.24      7.24      1.81    0.08
  Laser Frequency
Fluid Type*Laser Power*Nozzle Size     4     99.67     99.67     24.92    1.05
```

Fluid Type*Laser Frequency* Nozzle Size	4	24.06	24.06	6.01	0.25
Laser Power*Laser Frequency* Nozzle Size	8	49.55	49.55	6.19	0.26
Fluid Type*Laser Power* Laser Frequency*Nozzle Size	8	24.65	24.65	3.08	0.13
Error	54	1275.47	1275.47	23.62	
Total	107	36097.96			

Source	P
Fluid Type	0.000
Laser Power	0.000
Laser Frequency	0.000
Nozzle Size	0.000
Fluid Type*Laser Power	0.060
Fluid Type*Laser Frequency	0.770
Fluid Type*Nozzle Size	0.087
Laser Power*Laser Frequency	0.723
Laser Power*Nozzle Size	0.012
Laser Frequency*Nozzle Size	0.764
Fluid Type*Laser Power* Laser Frequency	0.989
Fluid Type*Laser Power*Nozzle Size	0.388
Fluid Type*Laser Frequency* Nozzle Size	0.906
Laser Power*Laser Frequency* Nozzle Size	0.975
Fluid Type*Laser Power* Laser Frequency*Nozzle Size	0.998
Error	
Total	

S = 4.86001 R-Sq = 96.47% R-Sq(adj) = 93.00% (REGRESSION FIT)

The ANOVA analysis (Table 4.3) revealed that there were no four-way and three-way interaction effects that were statistically significant because their probability values (p-value) were greater than the significance level (α) of 0.05. Thus, suggesting that the combination of all four factors or any combination of three of the factors did not cause a significant effect on the percentage volumetric reduction of the microdroplet. However, there was a significant two-way interaction effect between Laser Power and Nozzle Size with a p-value of 0.012. A depiction of the interaction effects is provided in Figure 4.6. This observation demonstrated what was observed during experimentation that the combination of nozzle size and lasing power had a significant effect on microdroplet

reduction. Furthermore, it is worthy to note that each experimental factor (i.e. main effects) was found to be statistically significant in affecting the reduction of droplets (see Figure 4.7). Each had a p-value of 0.000 that was less than the desired α level. It was observed experimentally that lasing power was most significant factor in microdroplet reduction, followed by nozzle size, fluid type, and lasing frequency. Lastly, a regression fit for the model revealed a coefficient of determination or better known as R-Square value of 0.9647. Hence, it established the goodness of fit of the data as well as implied that approximately 97% of the variation in the response variable (i.e. percentage volume reduction) was attributed to the experimental factors.

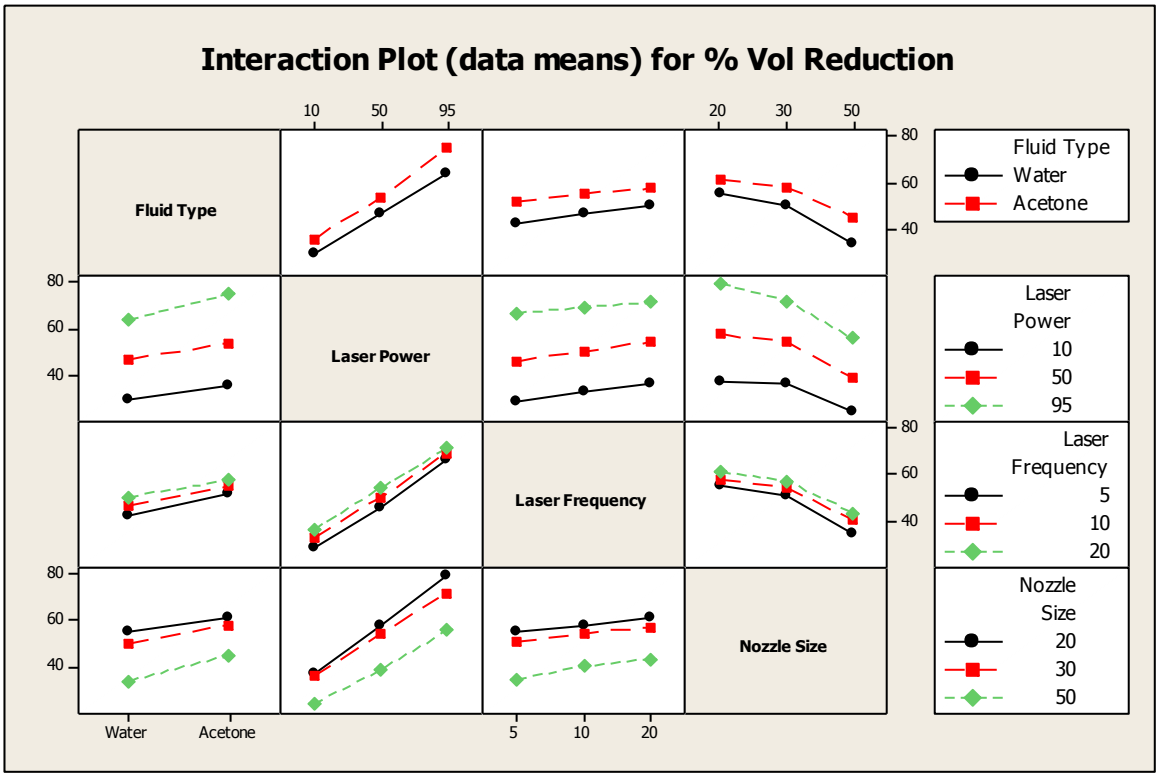

Figure 4.6. Interaction effects plot.

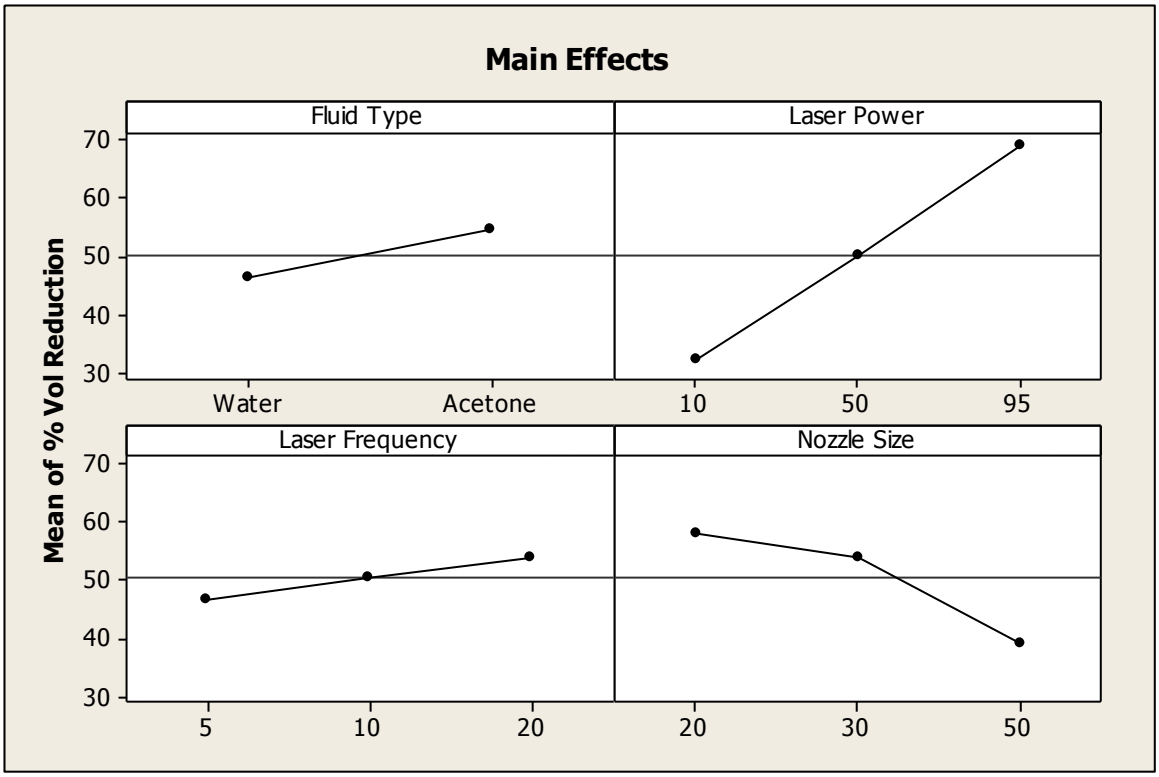

Figure 4.7. Main effects plot.

Since each of the four factors was found to be statistically significant from the factor ANOVA analysis, the experimental procedure of the radiative source was validated. Results of each of the experimental condition for the laser experiments are presented in the following section.

4.2.2 Volumetric Reduction (percentage) of Microdroplets.

The initial diameters for each of the four candidate fluid types differed since the jetting parameters (i.e. voltage, frequency, time, etc.) were dependent on external factors such as the humidity and temperature of the room. Hence, each experimental condition had its own initial microdroplet size which was consistent in size with respective to the fluid type. To normalize minor variations in initial drop sizes, microdroplet reduction

was calculated based on the difference in droplet diameter after subjection to the laser beam compared to the initial size for that experimental condition. Nevertheless, it was consistently observed that water droplets generally had larger initial diameters than acetone droplets for the same nozzle size. This observation was found to be true as well for both fluid types after the color addition. The initial diameter for each fluid type per experimental condition is presented in Table 4.4. The disparity in the initial diameter between water and acetone droplets is attributable to lower viscosity (0.31cp) and surface tension (25.2mN/m) at 20°C of acetone; whereas the values for water are 1.0cpand 72.80mN/m for viscosity and surface tension, respectively. Hence, acetone droplets eject easier (i.e. less satellite drops) from the nozzle orifice than water droplets.

Table 4.4. Microdroplet initial diameter (µm).

Lasing Frequency / **Nozzle size**	**5kHz**			**10kHz**			**20kHz**		
	50 µm	**30 µm**	**20 µm**	**50 µm**	**30 µm**	**20 µm**	**50 µm**	**30 µm**	**20 µm**
Acetone	46.67	31.15	22.50	40	32.12	20.38	40.21	33.46	21.35
Water	49.38	34.62	24.62	46.46	35.39	24.04	46.04	36.15	24.42
Acetone and Color dye	45.41	34.62	22.31	48.96	35.19	21.54	48.75	31.60	21.54
Water and Color dye	43.96	34.42	25.77	43.13	33.08	25.38	42.29	32.69	25.19

An increase in the lasing output power (% PWM) resulted in higher evaporation rates and reductions in microdroplet diameters for each nozzle size. However, the smaller nozzle orifice (20µm) had higher percentage reductions in volume as compared to the

larger nozzle dimensions of 50µm and 30µm for all candidate fluid types (acetone, water, acetone with color dye, and water with color dye). This is because smaller microdroplets (i.e. those ejected from the 20µm nozzle) have a lower mass compared to microdroplets ejected from larger nozzle orifices. Therefore, the difference in mass enables higher evaporation rates (i.e. higher volumetric reduction) for those smaller microdroplets given an equivalent amount of heat flux subjected to the droplets by the laser beam. Average percentage reduction in microdroplet volume for each fluid type based on the lasing output power and frequencies varied as presented in Tables 4.5 - 4.7. Acetone microdroplets ejected from the 50µm nozzle (see Table 4.5) revealed volumetric reductions ranging from 23% - 60%, 28% - 64%, and 31% - 65%, for 5, 10, and 20 kHz lasing frequencies, respectively as the lasing power was increased. For the same nozzle size, the average reduction in volume for acetone mixed with the blue color dye also reduced as follows: 25% - 63%, 28% - 64%, and 31% - 67% for the laser's frequency levels of 5, 10, and 20 kHz, respectively. 16% - 44% (5 kHz), 20% - 48% (10 kHz), and 24% - 54% (20 kHz), were the percentage volumetric reduction ranges for water microdroplets ejected out of the 50µm nozzle orifice. Lastly with the 50µm nozzle, the volume reduction of the mixture of blue color dye with water were on average 22% - 47%, 27% - 52%, and 30% - 57% as the output power increased at each lasing frequency, 5, 10, and 20 kHz, respectively. Higher volumetric reductions were attained as the nozzle diameter was reduced to 30µm (Table 4.6) as compared to the 50µm nozzle reductions. For 5, 10, and 20 kHz lasing frequencies, acetone microdroplets reduced in volume in the order of 35% - 77%, 39% - 78%, and 43% - 80%, respectively. Similarly, acetone and

blue dye droplets exhibited the following volume reductions 42% - 81%, 42% - 82%, and 43% - 83%, respectively at 5, 10, and 20 kHz lasing frequencies. In contrast, water microdroplets at the same nozzle size had percentage volumetric reduction in the order of 26% - 63% (5 kHz), 34% - 66% (10 kHz), and 38% - 67% (20 kHz). However, the reductions observed to water mixed with the blue color dye were slightly higher than plain water microdroplets. The percentage reductions for the dye-doped water were 27% - 67%, 31% - 74%, and 31% - 78% for 5, 10, and 20 kHz, respectively. The highest volumetric reductions were observed with the smallest nozzle orifice employed in the experiments (20μm) as displayed in Table 4.7. At 5, 10, and 20 kHz lasing frequencies, acetone microdroplets volumetric reductions ranged as follows 36% - 82%, 41% - 83%, and 42% - 83%, respectively. However, for the same frequencies, acetone with the blue color dye microdroplets reduced slightly higher as such 39% - 83%, 44% - 83%, and 45% - 84%, respectively. For the same nozzle size and in an incremental order of power and frequency, water microdroplets reduced in the range of 32% - 74%, 34% -76%, and 38% - 78%, respectively. In contrast, the mixture of blue dye and water revealed volumetric reductions in the order of 35% - 76%, 37% - 79%, and 41% - 81%, at 5, 10, and 20 kHz lasing frequencies with incremental increase in lasing output power. The reductions observed for this nozzle exceeded those of the previous nozzle sizes (50μm and 30μm) at each lasing frequency per fluid type. Each candidate fluids displayed linear trends in volumetric reductions with an increase in laser power output as well as lasing frequency (Figures 4.8-4.10).

Table 4.5. Volumetric reduction (%) for 50µm nozzle size.

Acetone			
PWM (%)	**5kHz**	**10kHz**	**20kHz**
10	22.77	27.93	30.84
30	32.49	38.11	40.86
50	38.28	47.33	48.20
70	47.68	55.56	57.08
95	59.30	63.89	64.62
Acetone & Blue dye			
PWM (%)	**5kHz**	**10kHz**	**20kHz**
10	25.01	28.13	31.26
30	32.20	34.38	38.96
50	37.27	41.94	46.45
70	47.79	50.38	50.97
95	62.98	64.43	67.43
Water			
PWM (%)	**5kHz**	**10kHz**	**20kHz**
10	16.12	20.58	24.19
30	22.17	25.12	29.70
50	27.41	32.10	37.94
70	32.40	40.06	45.84
95	43.84	48.28	53.81
Water & Blue dye			
PWM (%)	**5kHz**	**10kHz**	**20kHz**
10	21.56	26.78	30.12
30	27.76	35.19	38.10
50	35.94	42.63	46.54
70	42.28	47.13	51.03
95	47.18	52.05	57.42

Table 4.6. Volumetric reduction (%) for 30µm nozzle size.

Acetone			
PWM (%)	**5kHz**	**10kHz**	**20kHz**
10	35.10	39.17	42.52
30	44.65	46.15	49.93
50	53.24	56.35	58.11
70	61.05	63.31	65.37
95	77.17	78.07	80.15
Acetone & Blue dye			
PWM (%)	**5kHz**	**10kHz**	**20kHz**
10	41.93	41.93	42.77
30	49.46	50.83	51.34
50	58.43	60.67	60.07
70	71.08	72.60	72.50
95	81.21	82.39	83.35
Water			
PWM (%)	**5kHz**	**10kHz**	**20kHz**
10	25.74	33.58	38.35
30	35.11	40.19	45.55
50	48.25	53.26	55.99
70	56.18	58.07	59.42
95	62.63	65.68	67.28
Water & Blue dye			
PWM (%)	**5kHz**	**10kHz**	**20kHz**
10	26.77	30.98	31.27
30	36.94	41.32	44.15
50	46.29	55.81	58.31
70	57.43	62.50	64.37
95	67.16	74.52	77.73

Table 4.7. Volumetric reduction (%) for 20µm nozzle size.

Acetone			
PWM (%)	**5kHz**	**10kHz**	**20kHz**
10	36.39	40.61	42.12
30	46.95	48.24	53.02
50	56.22	57.57	66.60
70	69.79	72.35	72.71
95	81.94	83.19	83.35
Acetone & Blue dye			
PWM (%)	**5kHz**	**10kHz**	**20kHz**
10	38.77	43.54	44.57
30	47.27	53.89	53.89
50	58.53	63.28	66.66
70	70.75	71.75	71.64
95	82.76	83.04	84.16
Water			
PWM (%)	**5kHz**	**10kHz**	**20kHz**
10	32.10	34.26	37.64
30	40.76	42.26	47.39
50	51.60	53.27	58.12
70	64.65	63.29	66.73
95	74.19	75.69	78.14
Water & Blue dye			
PWM (%)	**5kHz**	**10kHz**	**20kHz**
10	35.13	37.25	40.80
30	43.90	46.68	49.24
50	51.12	55.70	59.20
70	66.03	67.27	69.69
95	75.73	78.56	80.85

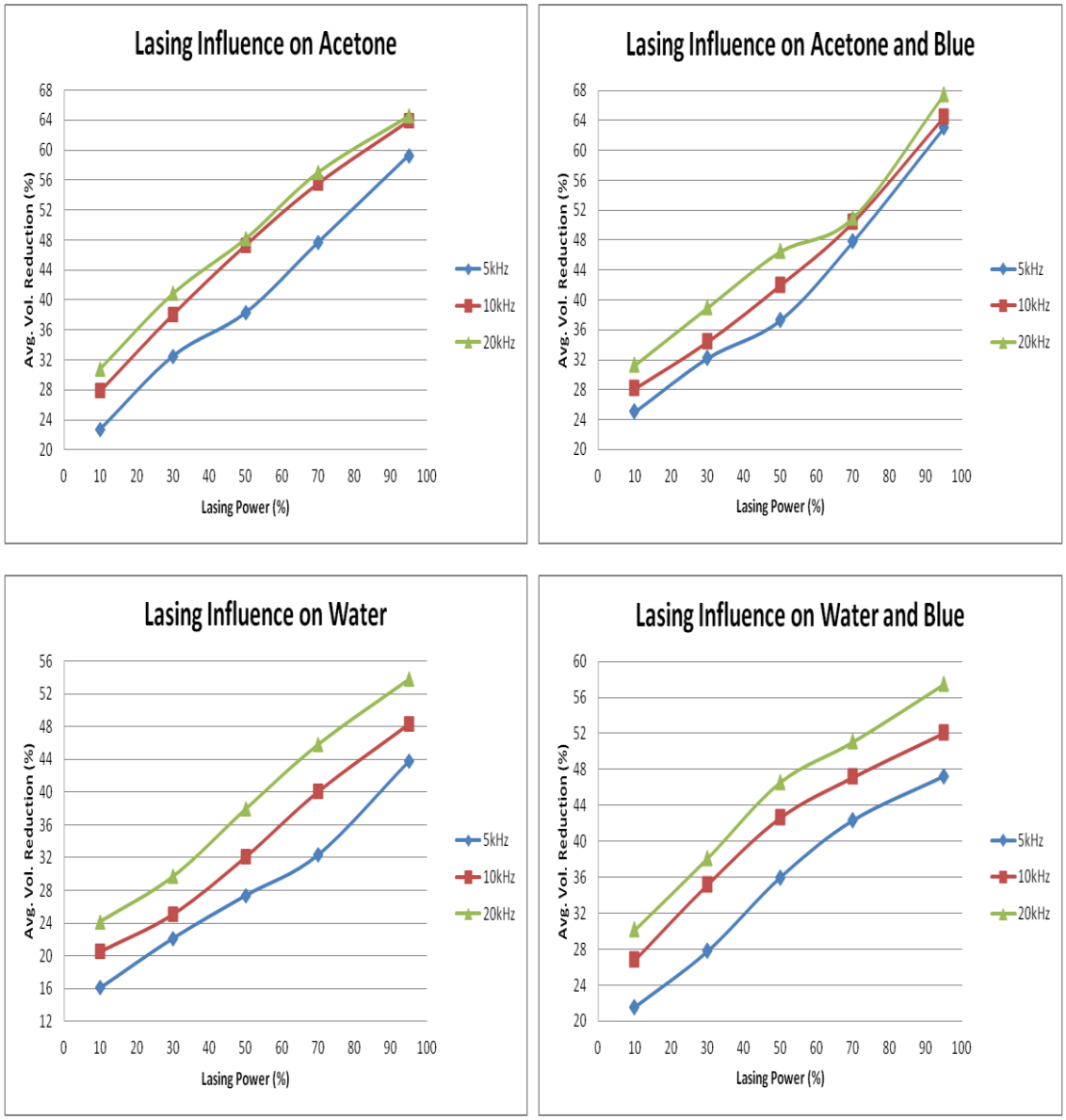

Figure 4.8. Percentage reduction in microdroplet volume for droplets ejected from 50µm nozzle per fluid type.

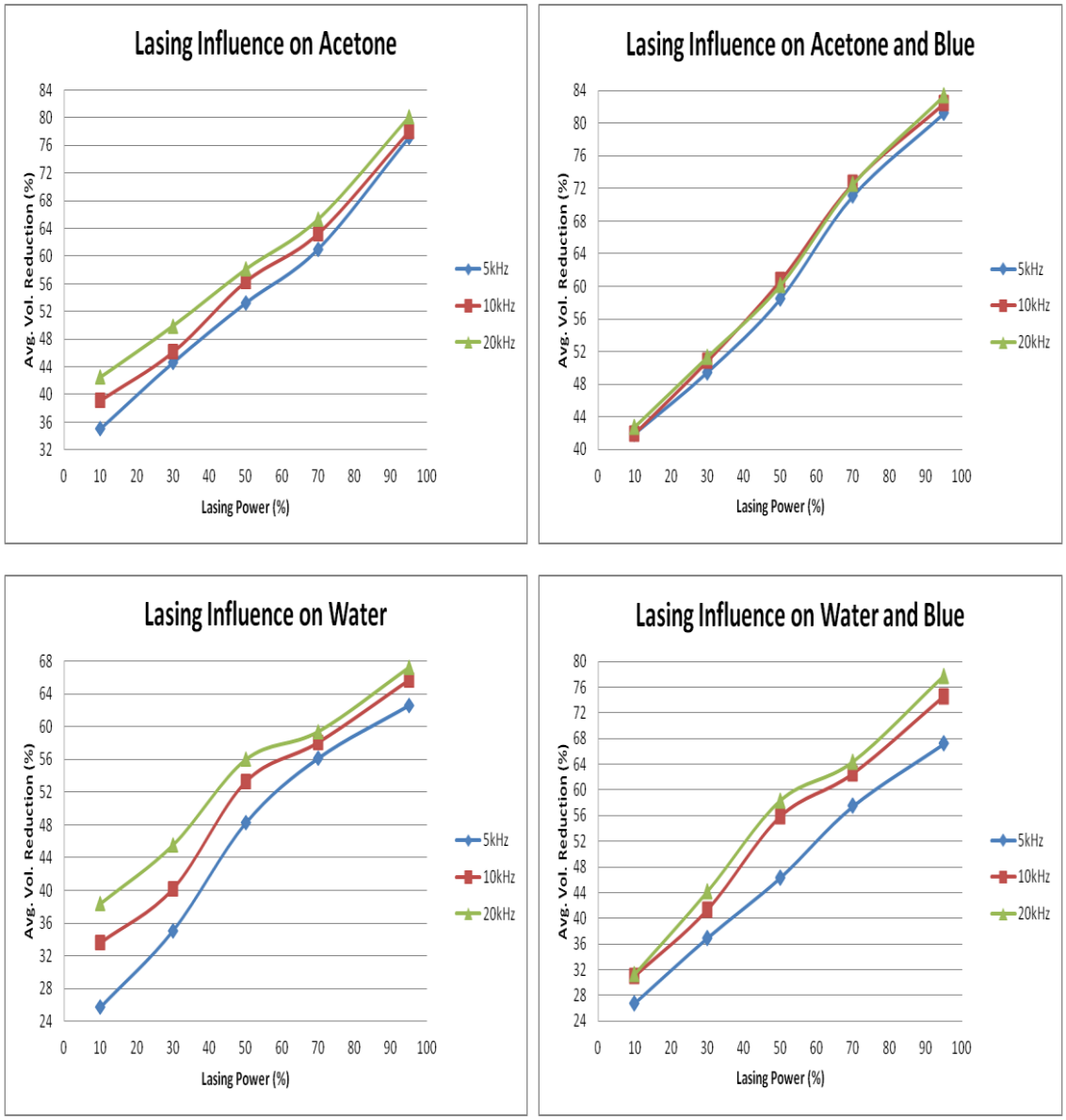

Figure 4.9. Percentage reduction in microdroplet volume for droplets ejected from 30µm nozzle per fluid type.

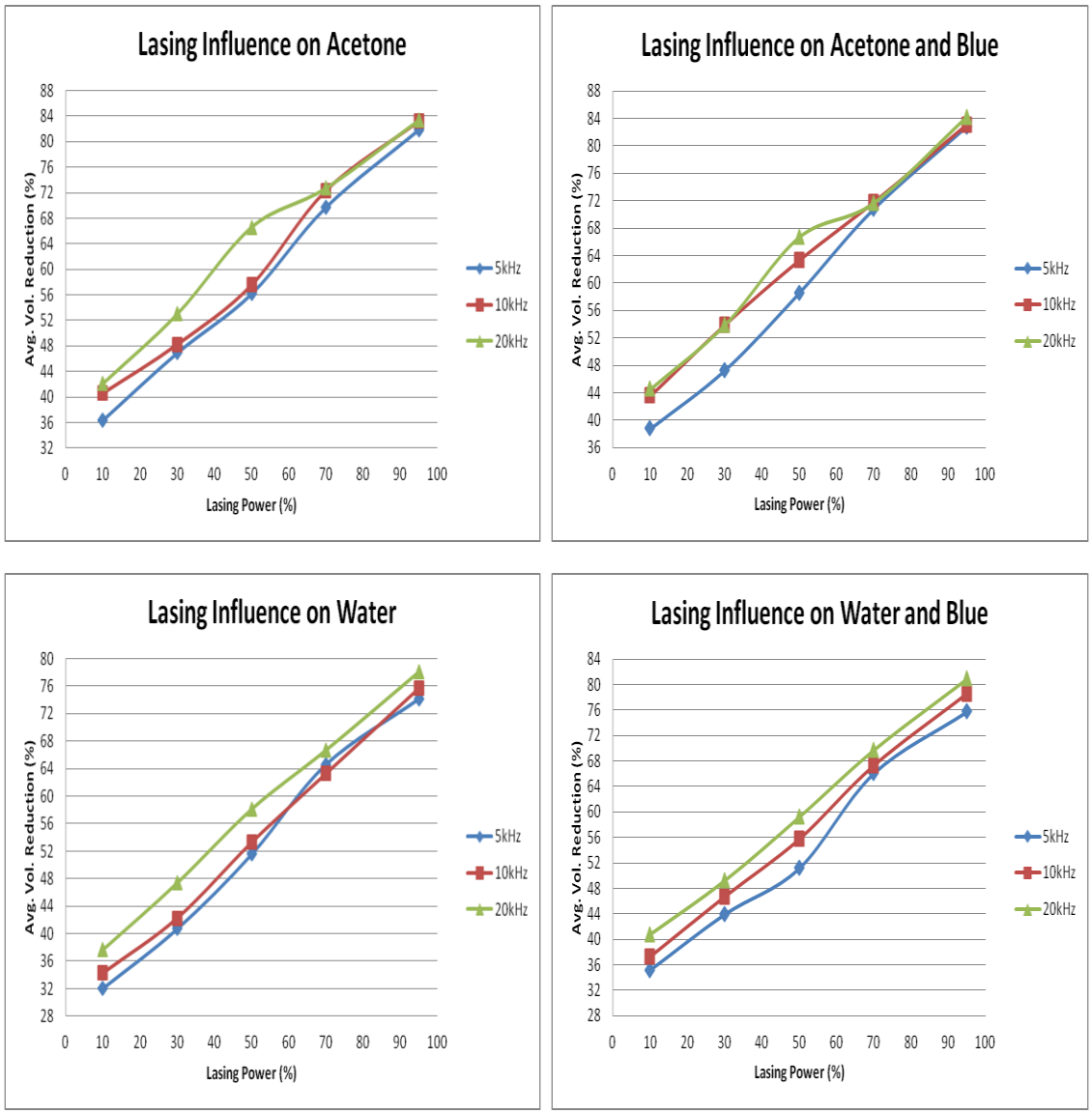

Figure 4.10. Percentage reduction in microdroplet volume for droplets ejected from 20µm nozzle per fluid type.

4.2.3 Significance of Fluid Type and Lasing Frequency on Droplet Reduction.

Acetone exhibited higher volumetric reductions when compared to that of water as both frequency and lasing power was increased. This observation can be attested to the fact that acetone is highly volatile due to its lower specific heat as compared to water. Furthermore, the observation proved to be consistent for each fluid type as the blue color

dye was added to it. However, evaporation rates were slightly higher for fluids with the color mixture when compared to their plain counterpart. The effect of the dye addition to the solvents impacted their heat absorption capacity. The dark blue dye enabled absorption of more heat from the incident laser beam which resulted in higher volumetric reductions for both dye-saturated fluids. The dominant wavelength in acetone and water after saturation of the blue dye were recorded as 208nm and 197nm, respectively (UV-Vis Spectrophotometer, Shimadzu Inc.). Furthermore, an increase in the laser beam pulses (i.e. lasing frequency) resulted in higher droplet reductions at equivalent power outputs. Figures 4.11-4.13 graphically depicts noticeable differences in volume reduction for each fluid type as the frequency and lasing output power were increased. The initial volume is denoted at 0% PWM (i.e. prior to lasing). For each fluid type, it was observed that microdroplets ejected out of the 20µm nozzle had steeper reduction in volume when compared to the other two nozzle sizes (30µm and 50µm). Furthermore, the steepness in volume reduction correlated to the nozzle orifice used in conducting the experiment. However, as the nozzle size decreased, the steepness in volume increased for the same experimental conditions. For example, at 5 kHz lasing frequency (Figure 4.11), acetone microdroplets displayed a 2.5, 4.4, and 5.5-fold decrease from 50µm, 30µm, and 20µm nozzle orifices, respectively. Consequently, more volumetric reductions were observed as the nozzle size decreased with increases in both lasing frequency and lasing power for equivalent conditions. In addition, microdroplets with the blue color dye revealed higher (i.e. more sudden) reductions in volume than their clear fluid counterparts. For instance, the mixture of water and blue color dye microdroplets jetted out of the 20µm nozzle at a

lasing frequency of 20 kHz (Figure 4.12) displayed a 5.25-fold decrease in volume as compared the 4.5-fold decrease observed with plain water droplets. Overall, acetone mixed with the blue color dye displayed the highest volumetric reductions in contrast to the remaining fluid types for each experimental condition.

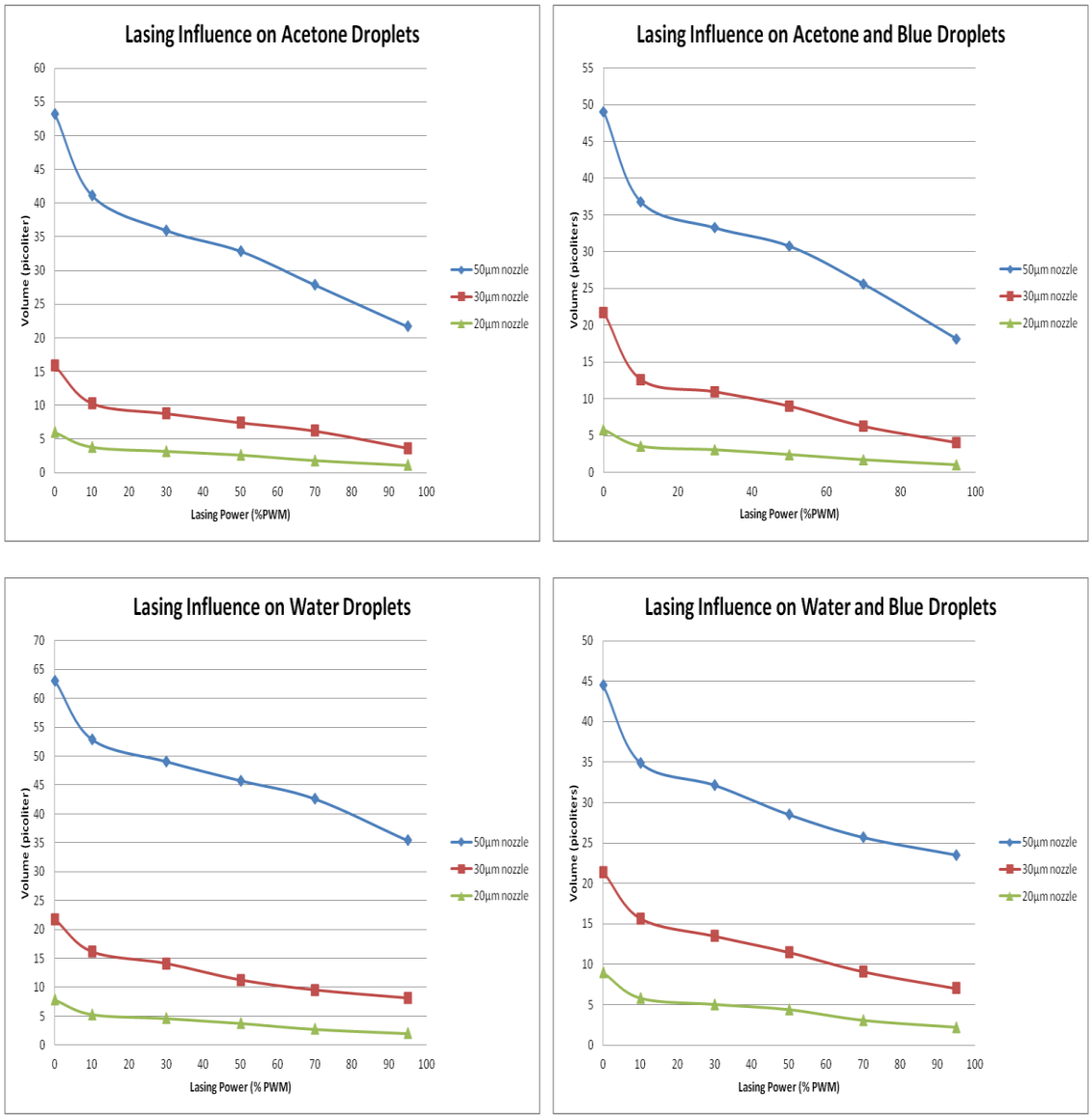

Figure 4.11. Evaporation characteristics based on fluid type at 5 kHz lasing frequency.

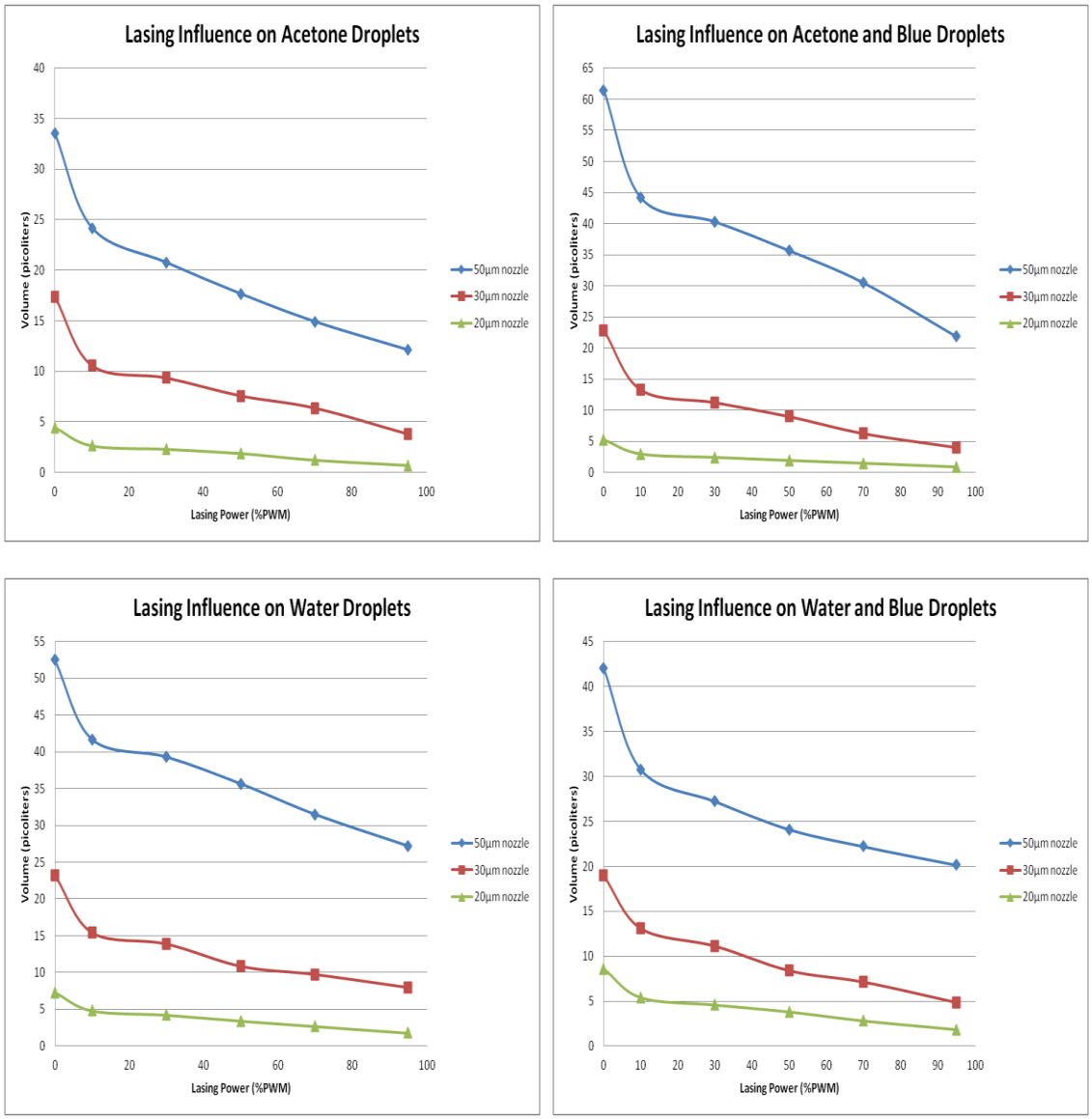

Figure 4.12. Evaporation characteristics based on fluid type at 10 kHz lasing frequency.

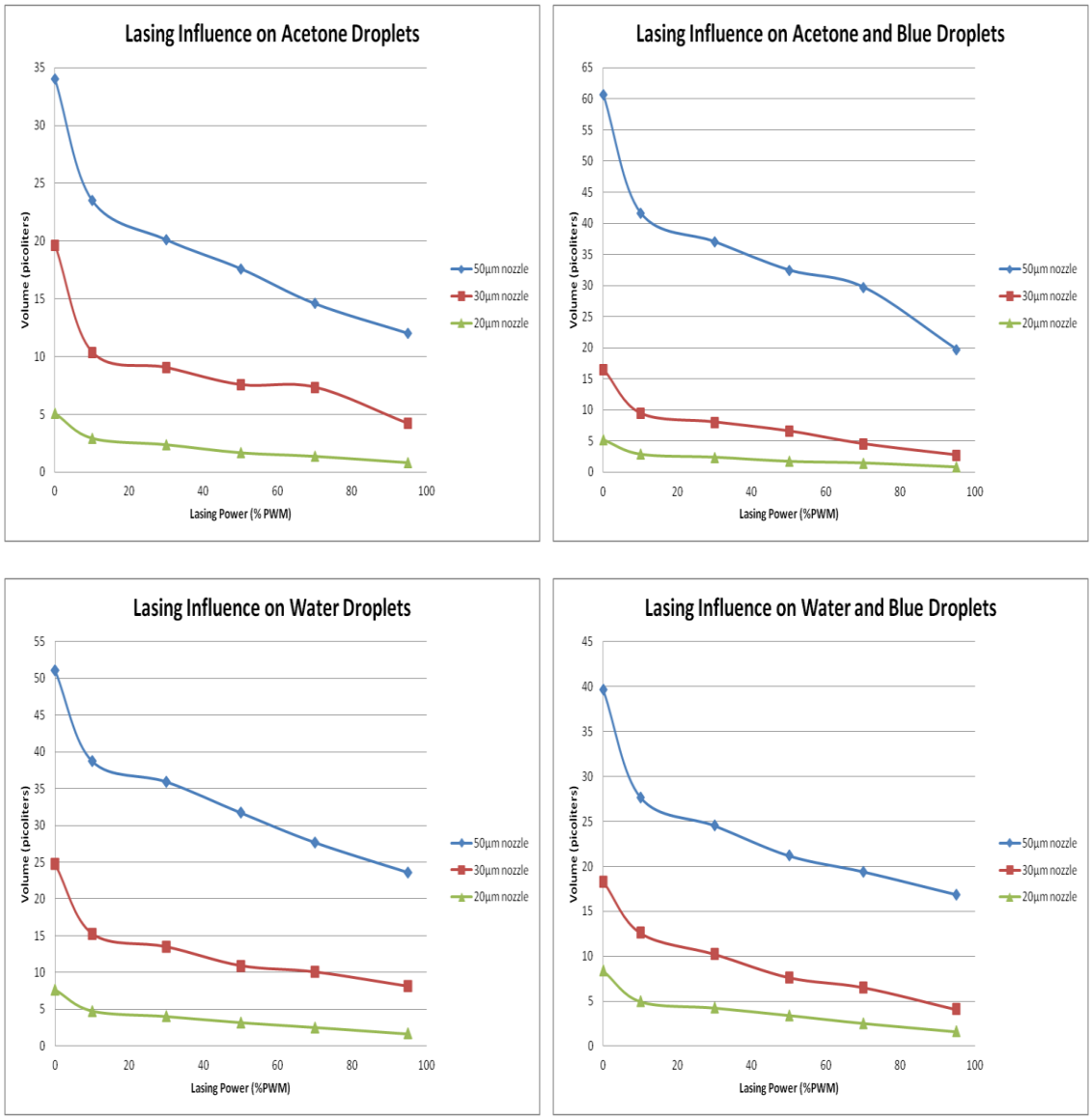

Figure 4.13. Evaporation characteristics based on fluid type at 20 kHz lasing frequency.

4.2.4 Surface Area to Volume Ratio Effect on Droplet Reduction.

The effect of surface area-to-volume ratio on droplet evaporation was observed by nozzle size and lasing frequency (Figures 4.14-4.16). Fluids when jetted through smaller nozzles size resulted in higher surface area to volume (s/V) ratio and vice versa.

However, the (s/V) ratios from this phase, radiative source (i.e. laser based experiments), have shown to be higher as compared to the previous phase (resistive heating ring), which employed a convective heating source. It was revealed that at higher lasing output power and frequency there was a rapid increase in surface area-to-volume ratio for droplets ejected from the smallest nozzle size employed in the experiments (20µm) as compared to microdroplets ejected from the 50µm and 30µm nozzles. Additionally, basic acetone microdroplets exhibited the highest surface area-to-volume ratio as compared with the remaining fluid types. This can be attested to the superheating of the fluid as the microdroplet shrinks in size.

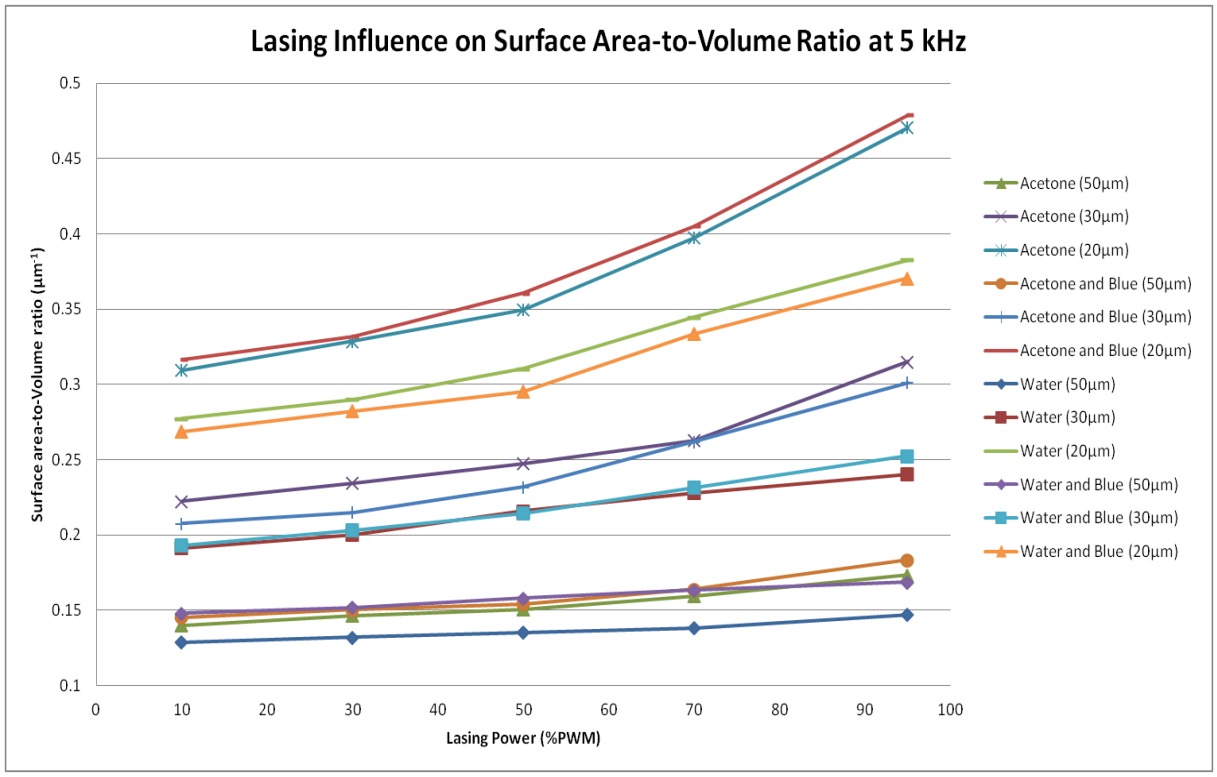

Figure 4.14. Surface area-to-volume ratio by fluid type at 5 kHz lasing frequency.

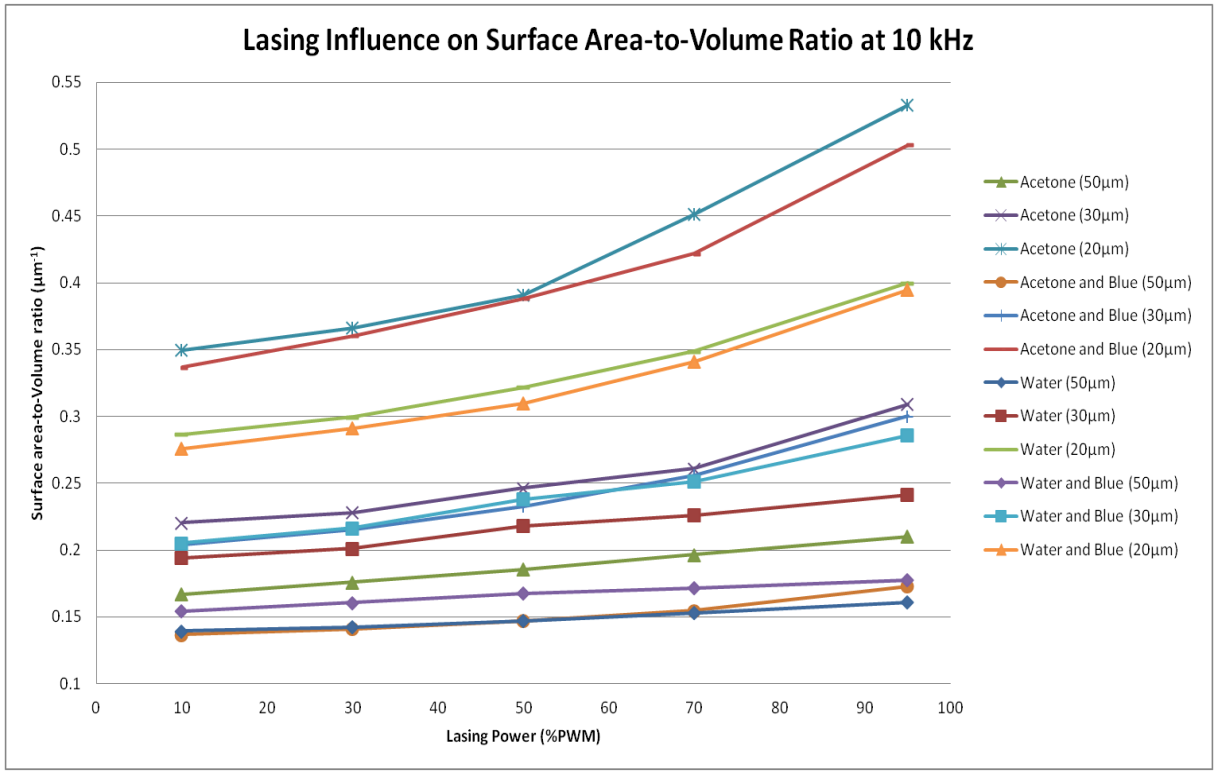

Figure 4.15. Surface area-to-volume ratio by fluid type at 10 kHz lasing frequency.

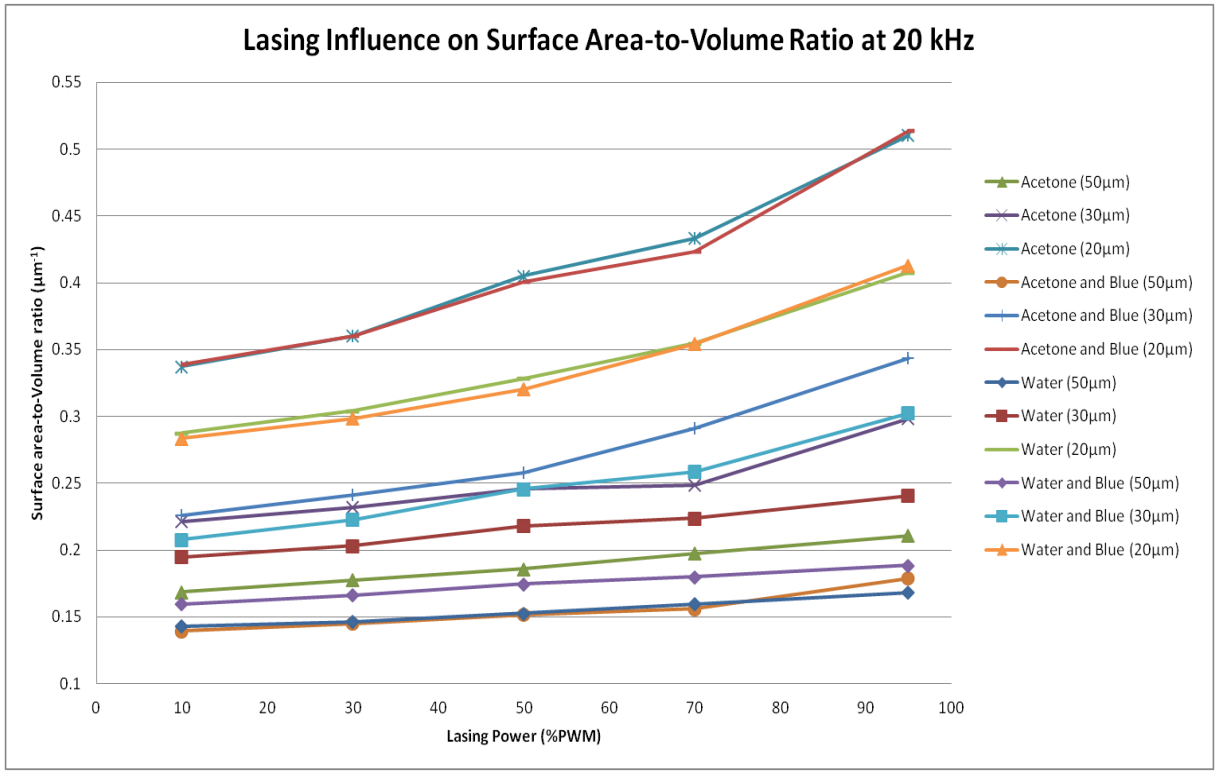

Figure 4.16. Surface area-to-volume ratio by fluid type at 20 kHz lasing frequency.

4.2.5 Phase Two Discussion.

The droplet evaporation characteristics for water and acetone were studied using laser irradiation. Furthermore, the impact of adding a color additive to these fluids was also investigated with the aim of assessing its impact on increasing the heat absorption within the microdroplet. Acetone microdroplets revealed higher percentage volumetric reductions as compared to water microdroplets under equivalent conditions. This is due to acetone's lower specific heat and thus higher volatility as compared to that of water. However, acetone droplets with the color addition reduced at slightly higher evaporation rates compared to plain acetone droplets. The saturation of liquids with blue-dye resulted in a higher absorption of heat from the incident laser beam. This demonstrated that the

presence of a darker color dye within the fluid media enables the laser source to exhibit further reduction of microdroplet. Droplets ejected from a smaller nozzle size (20µm) had higher percentage reductions in volume as compared to the larger nozzle sizes of 50µm and 30µm for all fluid types. This is attributed to the lower mass of the smaller microdroplets thereby resulting in faster evaporation rates for the equivalent amount of heat flux subjected by the laser beam. At both higher lasing output power and lasing frequency there was a rapid increase in surface area-to-volume ratio for droplets ejected from the smaller nozzle orifice (20µm) due to superheating of the fluid. In contrast to the initial phase (resistive heating ring experiments), significantly higher reductions in microdroplet volumes were realized using CO_2 lasers. The use of laser beam enabled "on-the-fly" manipulation of the microdroplet size based on modulation of parameters. This phase enabled the investigation of depositing nanotube solutions onto a substrate for scalable manufacturing of functional devices. Specifically, the fabrication of thin film transistors is later discussed in the ensuing chapter.

CHAPTER 5

FABRICATION OF FLEXIBLE THIN FILM TRANSISTORS (f-TFTs)

5.1 Introduction

The unique properties (electrical, mechanical, thermal, etc.) of carbon nanotubes (Salvetat et al., 1999) entail them an advantage over traditional materials for different industrial applications that encompass semiconductor electronics. Carbon nanotubes are flexible (Ruoff and Lorents, 1995), have high current carrying capacity, excellent thermal conductivity (Hone, 2004), low thermal expansion coefficients, and are less susceptible to electromigration than conventional interconnect materials such as copper, tungsten and aluminum. Enriched semiconducting single walled carbon nanotubes (s-SWNT) possess electronic properties for the fabrication of flexible thin film transistors (F-TFTs). Several researchers (Snow et al., 2005, Zhao et al., 2009, Han et al., 2007, Wang et al., 2009, LeMieux et al., 2008, and Ono et al., 2010) have utilized carbon nanotubes to fabricate TFTs with different synthesis routes and processing methods. Carbon nanotube colloidal inks are inherently more flexible than their metallic counterparts and the ability to dispense them using an additive technology makes them a primary candidate for large area electronics as well as flexible circuitry. Until recently, a method to separate large quantities of SWNTs into individual metallic and semiconducting fractions was inexistent (Tanaka et al., 2009). When approaching large scale flexible arrays, the problem of depositing source, drain, and gate electrodes with conventional metal pads arises. After enough flexing, the metal begins to crack and the contact to the transistor is lost. A

scalable additive process can be implemented to realize the full potential of SWNT based flexible transistors. This research demonstrated the applicability of direct-write inkjet printing as a patterning mechanism for SWNTs on substrates towards the fabrication of functional devices (i.e. f-TFTs). Many of the conventional manufacturing processes require multiple steps to make patterns during the fabrication process (e.g. transfer printing and vacuum filtration (Zhou et al., 2006), dip coating (Song et al., 2006), sputtering (Fortunato et al., 2004), etc.). These include pre and post processing operations such as masking and etch-off as in lithography and other projection based methods (Rai-Choudhury, 1997 and Xia and Whitesides, 1998). In contrast to the aforementioned methods, direct-write inkjet printing requires only a single step for microdroplets patterns to be deposited with higher controllability, repeatability, and scalability. The inkjet process also minimizes the material wastage during the fabrication process as opposed to precious material loss during etching operations. There is limited literature (Song et al., 2008) demonstrating the use of direct inkjet printing of TFTs patterns onto substrates with the objective of evaluating their electronic characteristics. This chapter focuses on the fabrication of large scale (scalable) SWNTs based flexible TFT arrays.

5.2 Direct Write Inkjet Printing

Direct-write inkjet printing enables the deposition of miniscule fluid volumes at the pico and nano liter scales on different substrates. Thus, nanoparticulate colloids can be selectively deposited at target locations on the substrate in various patterned configurations using monodisperse microdroplets. Direct-writing is a non-contact method for feature deposition and does not contaminate the colloidal solutions during deposition.

Figure 5.1 depicts the direct-write inkjet system (MicroFab Technologies Inc., Plano, TX) that was used in this effort. The system included a JetDrive III waveform generator and amplifier, a pneumatics console, an optics system and a MJ-AT-01-30 piezoelectric (PZT) microvalve with an interchangeable orifice (i.e. nozzle) diameter of dimensions ranging in the orders of 10-80 microns. The 50 micron nozzle was used in the experiments reported in this chapter. The SWNT loading within the solvent determines the rheological properties of the printing fluid such as the viscosity and surface tension. A piezoelectric element is activated within the nozzle which propagates an acoustic wave to produce repeatable monodisperse drops. Depending on the underlying solid loading of the SWNTs within the fluid, different input parameters such as frequency, voltage and fluid pressure are manipulated to ensure optimal drop formations. An important aspect of jetting SWNT loaded solutions is the clogging of the nozzle orifice due to accumulation of the SWNT bundles at the tip. This issue was mitigated by sonicating the SWNT solutions (15-30 min) prior to deposition and thereby ensuring a homogenous colloid. Depicted in Figure 5.2 is an image of a SWNT laden microdroplet after ejection from the nozzle orifice captured by a CCD high speed camera.

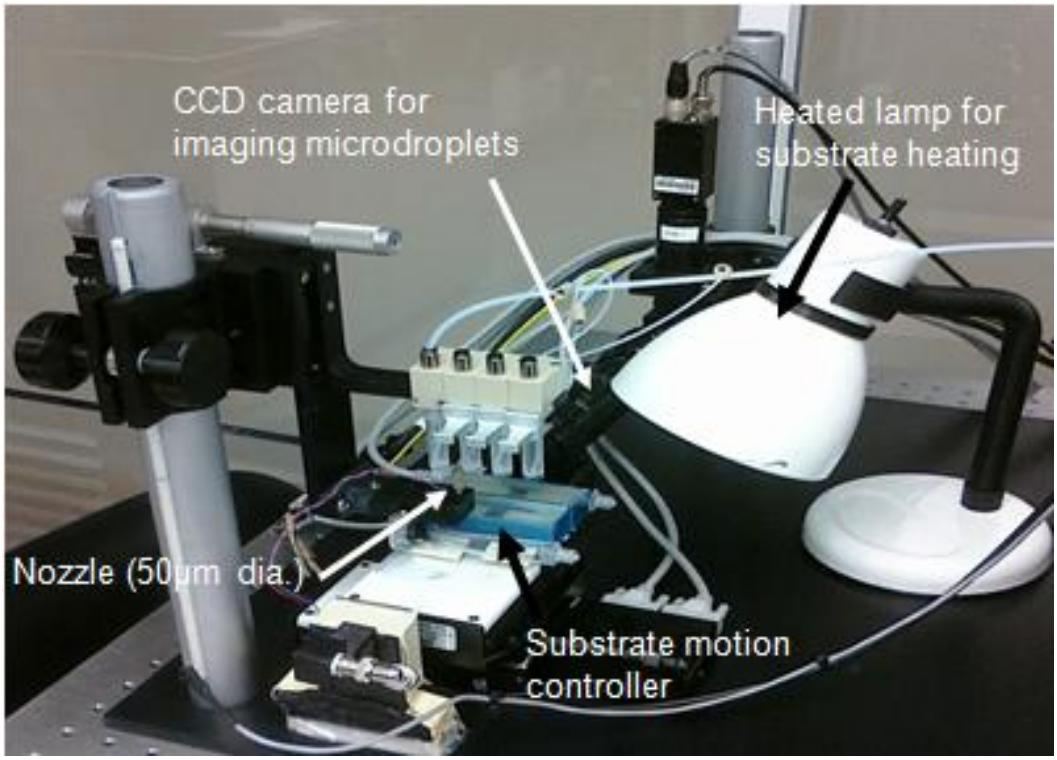

Figure 5.1. Direct write inkjet setup for f-TFTs.

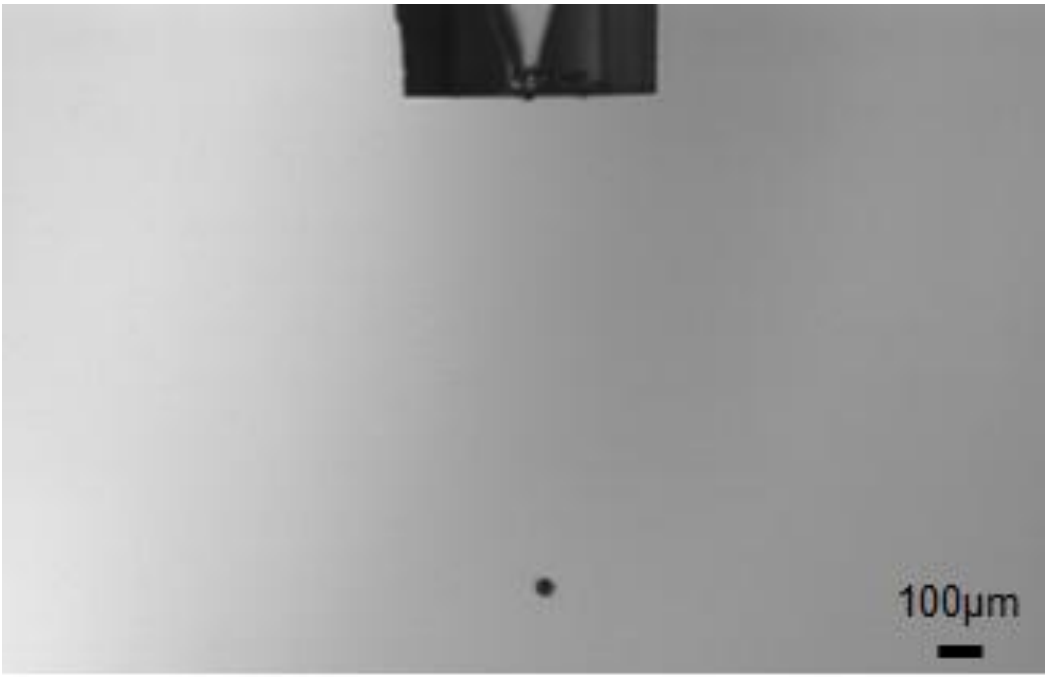

Figure 5.2. Image of SWNT microdroplet after ejection from nozzle.

5.3 Methodology

Carbon nanotubes were dispersed in a surfactant aqueous solution by use of a sonicator to break up bundles of nanotubes. The metallic and semiconducting carbon nanotubes were isolated using a proprietary (NanoTechLabs, Inc.) column chromatography separation procedure. Further, density gradient ultracentrifugation (Ghosh et al., 2010) was carried out to separate specific nanotube chiralities of the semiconducting single wall nanotubes (s-SWNTs). Figure 5.3a shows a colloidal solution of (6, 5) s-SWNTs evaluated using visible and ultraviolet spectroscopy. Polyethyleneimine (PEI) and tetracyanoquinodimethane (TCNQ) were dissolved in methanol and chloroform respectively. Ink jetted s-SWNT traces were immersed in solutions of PEI or TCNQ from 2-24 hours to dope (n and p-type) them. They were then transferred to multiple solvent baths to remove the residual dopant that had not adsorbed onto the nanotubes.

Prior to the deposition of SWNTs inks, substrates such as bare Kapton (Figure 5.3b) and 65nm thick gold coated Kapton (Figure 5.3c) were plasma etched (M4L, TePla) to remove contaminants. The plasma etching was conducted with argon (Ar) gas at a flow rate of 400SCCM and RF power of 200W for 5mins. The plasma etching process improved the s-SWNT trace deposition to bridge the gap between source and drain contacts. The Kapton substrates were cut into 10mm x 10mm coupons for device fabrication. Kapton substrates were inkjet printed with proprietary synthesized s-SWNT solutions on the source and drain contacts. A 90W incandescent light source was used to heat the substrate for solvent evaporation. The s-SWNT traces were then polymer

solution doped. A dielectric layer was deposited followed by a gate electrode. The fabricated f-TFTs made via enriched s-SWNTs inks were tested for their I-V and transport characteristics using a 4-probe station and 2 Keithley 2400 source meters.

(a) (b) (c)

Figure 5.3. (a) Colloidal solution of s-SWNT; (b) bare Kapton substrate with inkjet traces of SWNTs; (c) sample coupon of Kapton with Au contacts without SWNT traces.

5.4 Results and Discussion

The direct-write fabricated f-TFTs were evaluated for deposition accuracy, s-SWNT loadings and electronic characteristics.

5.4.1 Optical Deposition Characterization.

Figure 5.4a depicts an optical micrograph of s-SWNT trace printed from aqueous ink, forming a continuous network between source and drain electrodes. Aqueous solutions permitted significant higher concentrations (loadings) of nanotubes (s-SWNTs) as compared to conventional solvents. The higher loadings enabled less number of superimposed passes to achieve connectivity of the nanotube network as seen in Figure 5.4b.

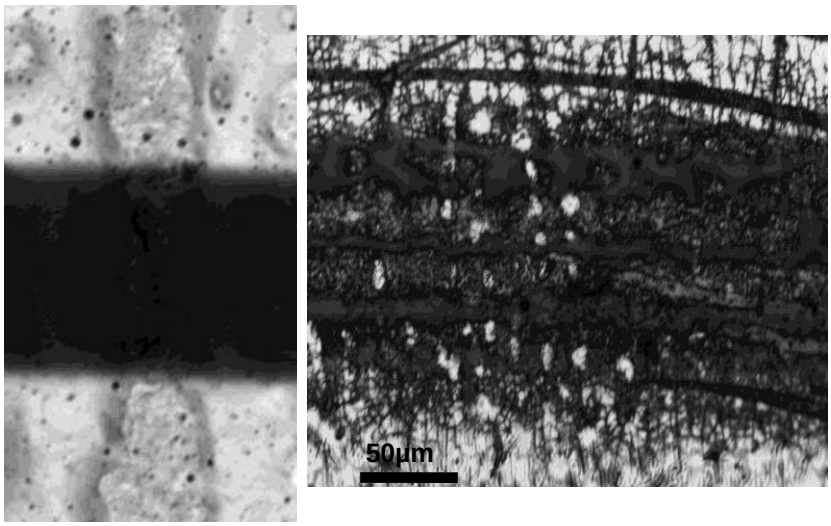

(a) (b)

Figure 5.4. (a) Optical micrograph of s-SWNT trace printed from aqueous ink, forming a continuous network between source and drain electrodes; (b) high magnification image of s-SWNT trace.

5.4.2 Atomic Force Microscopy of SWNT Traces.

Metallic SWNTs solutions were deposited to fabricate conductive traces for source and drain electrodes. Different numbers of overlay passes (50, 100, and 150) were deposited to evaluate the connectivity and resulting conductivity of the traces. The deposition pattern for 150 passes (Figure 5.5) revealed that the connected bundles of nanotubes were conductive. Figure 5.6 shows localized regions of nanotube clusters printed using 100 passes of nanotube colloid with lower connectivity as compared to the 150 pass configuration. At 50 passes of SWNT deposition, islands of nanotube bundles were observed (Figure 5.7) that led to non-conductive traces. These results demonstrate different thresholds of nanotube bundle connectivity for developing SWNT colloid based devices.

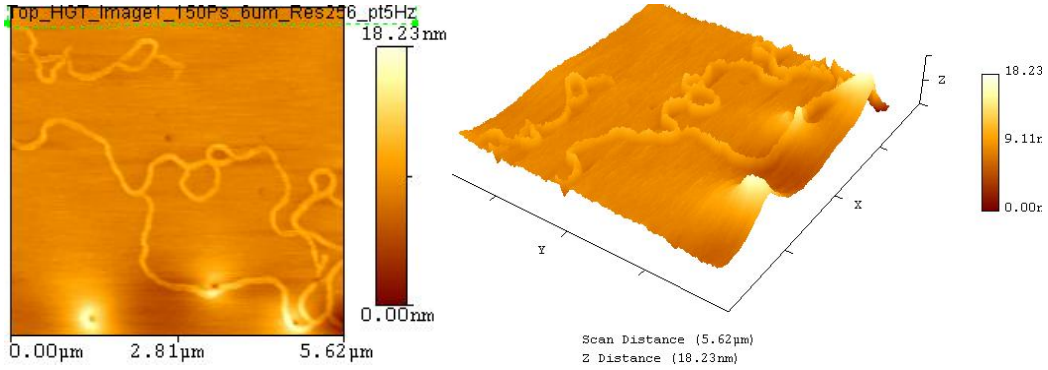

(a) (b)

Figure 5.5. Profile of 150 passes of nanotube colloid deposition (a) top view; (b) z-stack profile.

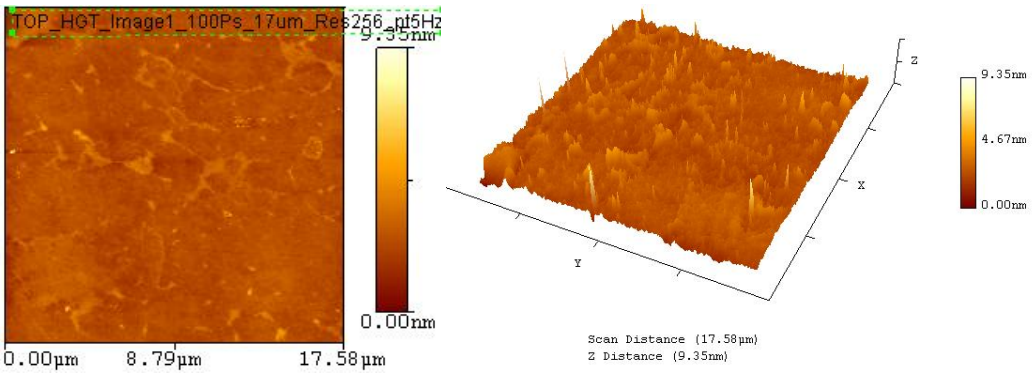

(a) (b)

Figure 5.6. Profile of 100 passes of nanotube colloid deposition (a) top view; (b) z-stack profile.

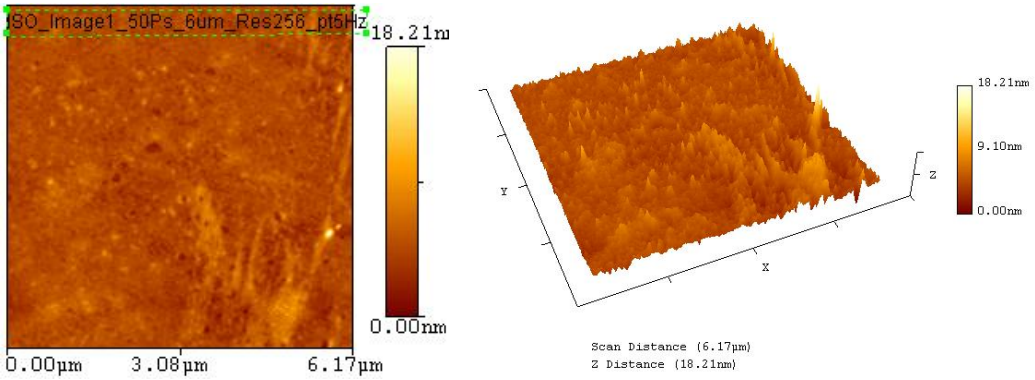

(a) (b)

Figure 5.7. Profile of 50 passes of nanotube colloid deposition (a) top view; (b) z-stack profile.

5.4.3 I-V Characterization and Transport Properties of f-TFTs.

Figure 5.8 shows the I-V data for two different nanocolloid traces and their suitability for thin-film transistor applications. Figure 5.8a demonstrates the conductivity of a graphene trace (15,200S/m) as compared to the higher conductivity values (34,000S/m) for a different graphene nanoplatelets trace (Figure 5.8b). The conductivity of SWNTs can be enhanced from 4,000S/m to as high as 96,000 S/m by enriching the metallic content of the SWNT fraction.

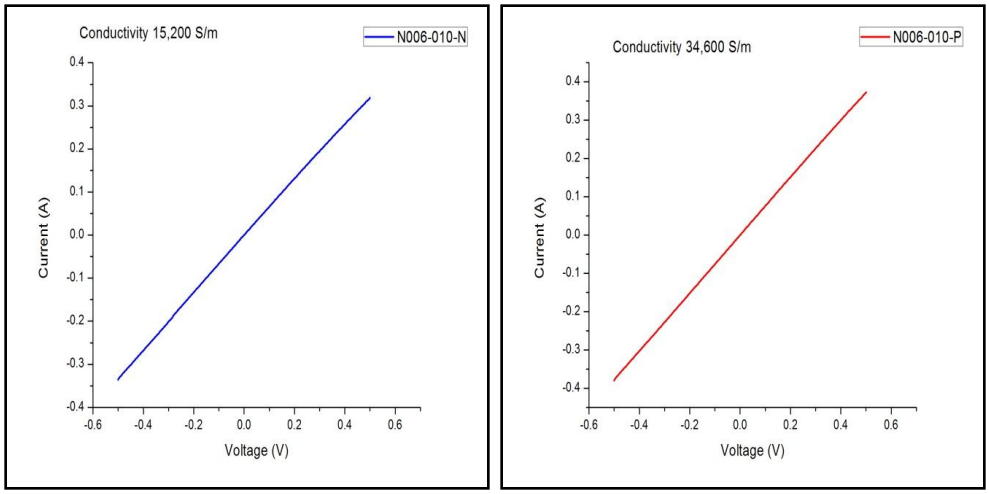

(a) (b)

Figure 5.8. Conductivities for two different nanocolloid traces (a) graphene; (b) higher conductivity graphene nanoplatelets.

Figure 5.9a illustrates the Current versus Voltage (I-V) measurement of two separate SWNT inks. The linear graph (ohmic) represents a nanocolloid that contains both metallic and semiconducting SWNTs. However, after separation and elimination of the metallic nanotubes from the semiconducting SWNTs we observe an S-shaped curve (Figure 5.9b) that has been printed on Au electrodes on Kapton (inset image). Depicted in Figure 5.9b is the semiconducting nature of the enriched s-SWNT ink which validates our separation scheme and demonstrates that functional device traces can be printed from these inks.

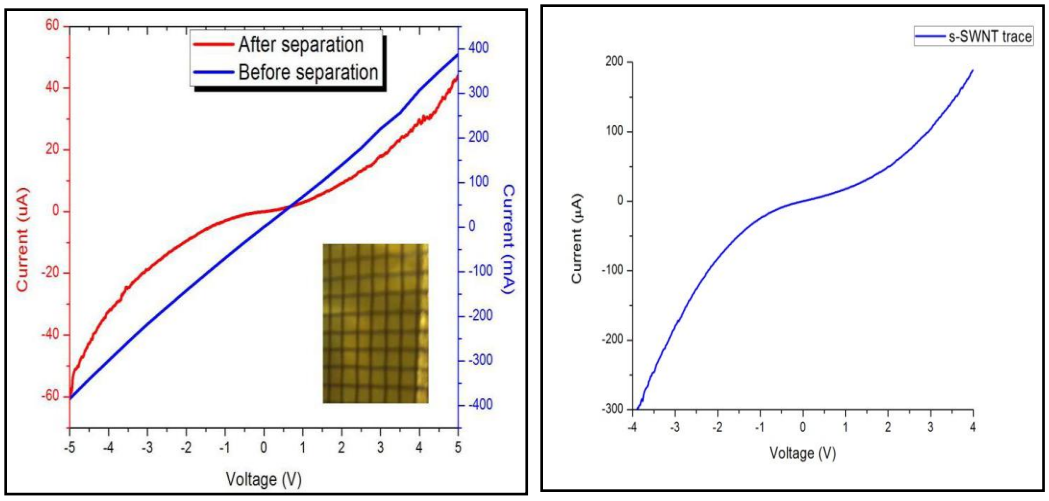

(a) (b)

Figure 5.9. (a) Current vs. voltage curves of SWNT traces before and after separation (inset is a Kapton substrate with gold contact pads); (b) a different I-V curve for semiconducting SWNT trace.

Flexible Field Effect Transistors (f-FETs) were tested using a current controlled voltage source and a Keithley 2400 SMU. (6, 5) enriched inks were used to fabricate flexible transistors that were doped by PEI and TCNQ. When fabricating the smaller coupon sizes, Ti/Au source, drain, and gate electrodes were evaporated. A 120nm zirconium silicate ($ZrSiO_4$) dielectric layer was evaporated because it has a dielectric constant between 7.3 and 12.7. Figure 5.10 shows that PEI doped s-SWNT flexible transistors exhibit modulation with a reverse bias on the gate. Figure 5.11 depicts the transfer curve of a PEI doped s-SWNT trace. Figure 5.12a reveals another flexible device's transport characteristics. Due to pinholes or inconsistencies in the vapor deposited dielectric layer, we observed a higher leakage current. The source, drain, deposited s-SWNT trace followed with a layer of dielectric polymer and gate electrode of the corresponding flexible transistor are shown in Figure 5.12b.

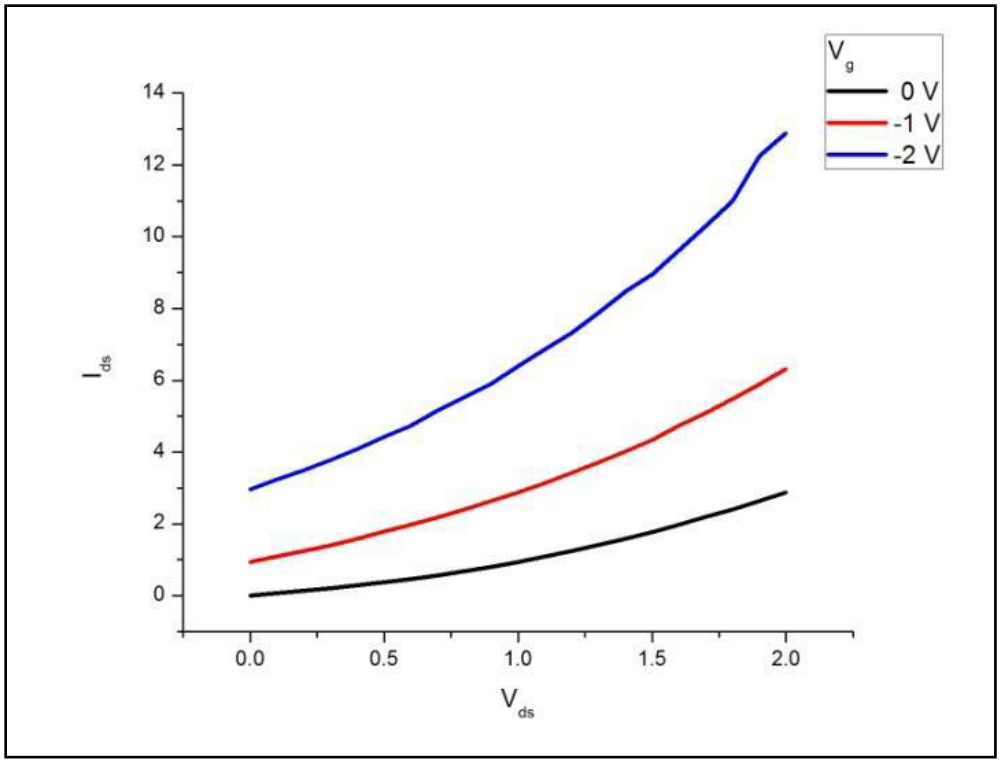

Figure 5.10. Transport characteristics of PEI doped flexible transistor fabricated from (6,5) enriched s-SWNTs. (Note: Source-drain voltage is on the x-axis, drain current is on the y-axis, and the legend shows the gate voltage).

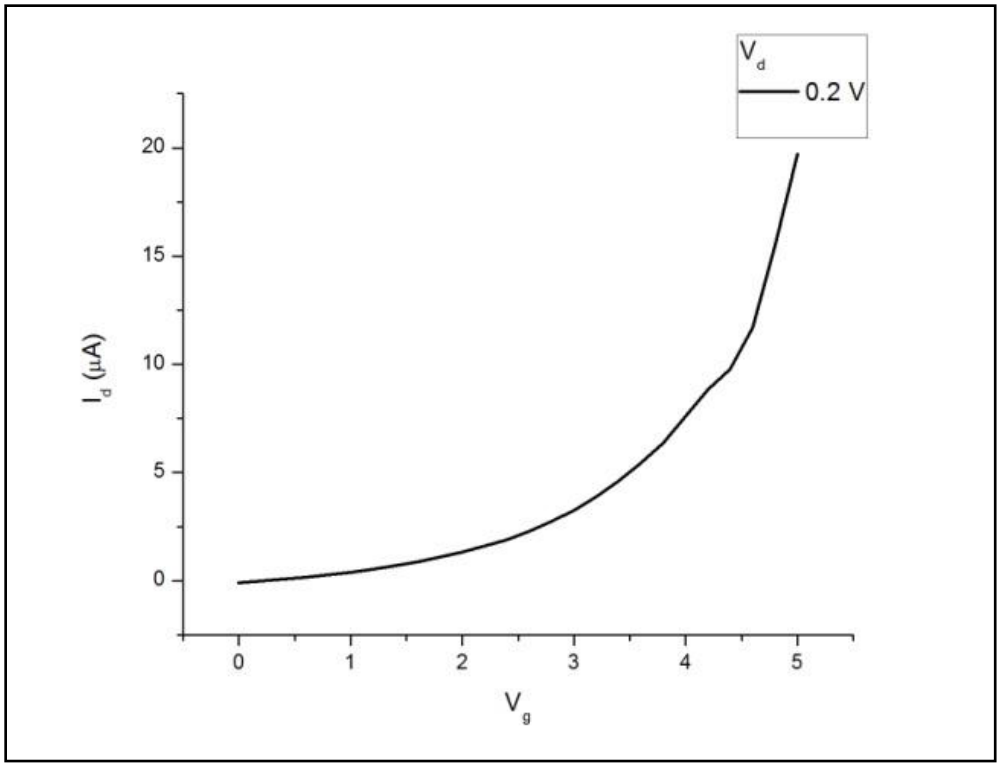

Figure 5.11. Transfer characteristics of a PEI doped s-SWNT transistor. (Note: The legend shows the drain Voltage, while the drain current is on the y-axis and the gate Voltage is on the x-axis).

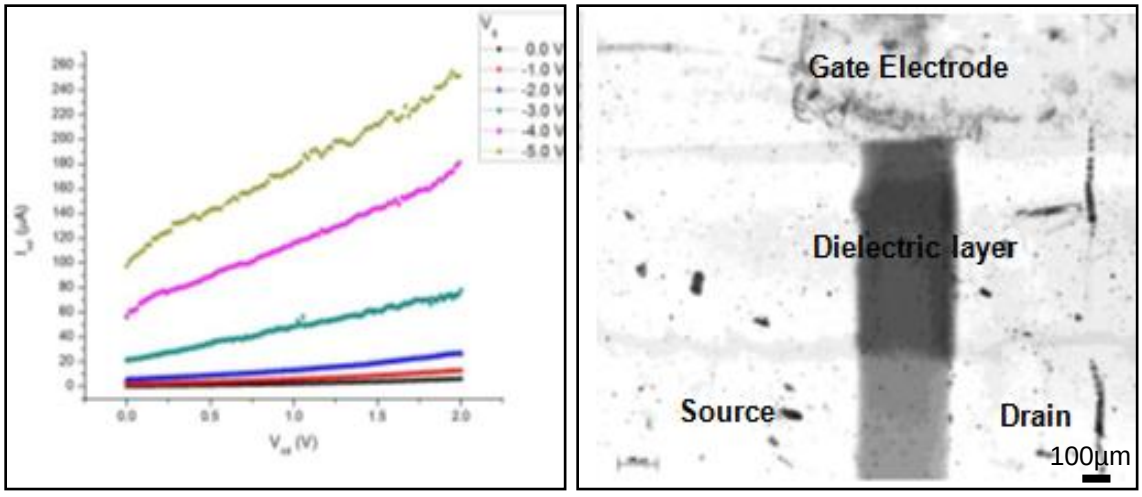

(a) (b)

Figure 5.12. (a) Transport characteristics of s-SWNT flexible TFT; (b) image of flexible s-SWNT transistor. (Note: scale bar is 100 micron).

5.5 Conclusion

In this study, we demonstrated the direct-write inkjet fabrication of flexible TFTs using s-SWNTs on Kapton substrates. Metallic and semiconducting (SWNTs) were effectively separated using column chromatography technique. Further, semiconducting nanotubes with (6, 5) chiralities were enriched and doped with PEI and TCNQ to obtain appropriate transistor properties. Plasma etched bare Kapton and gold coated Kapton substrates revealed better adhesion to the deposited SWNTs to bridge the gap between the source and drain electrodes. Optical and atomic force microscopy images indicated that 150 and 100 pass depositions exhibited connectivity and corresponding conductivity of nanotube bundles. M-SWNTs and graphene nanoplatelets traces were evaluated for respective conductivity (I-V) characteristics. Finally, a flexible field effect transistor device was fabricated and tested for its transport characteristics. Further improvements in device constructs can be affected by utilizing a different dielectric material, reducing channel width, and distance between the source and drain electrodes. The use of smaller nozzle sizes and higher concentration SWNT inks are viable approaches to further this work. This study provides a basis for fabricating large scale arrays of flexible TFTs using direct-write printing of SWNTs. Consequently, the objective of this dissertation can be realized by employing the combination of inkjet printing and laser to reduce the foot print of deposited features. The direct write system can be employed to eject nanotube solutions (i.e. the material used for fabricating f-TFTs) while the laser is impinged upon the microdroplets following ejection from the nozzle but prior to deposition on the substrate. The development of functional devices that was realized in this chapter enabled

the investigation conducted in Chapter 6 of understanding deposition characteristics of laser evaporated microdroplets on substrates. Thus, it provided an application of the concept of this research of controlled evaporation of microdroplets to achieve scalable micro/nano manufacturing of features.

CHAPTER 6

UNDERSTANDING DEPOSITION CHARACTERISTICS OF LASER EVAPORATED LIQUIDS

6.1 Overview

Based on the development in Chapter 5 that functional devices (i.e. thin film transistors) can be realized using carbon nanotubes, this chapter aims to investigate reducing the footprint of deposited features to enable scalable micro to nanomanufacturing. This was achieved using a unique approach which consisted of the combination of the direct write inkjet printing technique and the laser source. The direct write system was used to eject monodisperse microdroplets of two liquids (dye-saturated water and carbon nanotube colloid) while a 30W CO_2 laser was simultaneously applied to evaporate the droplets into smaller size dimensions prior to deposition on the substrate. A x-y linear stage motion controller was used for the deposition of monodisperse droplets to form line patterns of nanotubes on the substrate. The aim of this investigation was to demonstrate scalable manufacturing of micro and nano features on the same substrate based on utilization of the lasing source. The impact of the lasing source on deposited droplets on the substrate was compared to initial conditions (i.e. without the laser). Furthermore, the effect of lasing power (pulsed width modulation) at a lasing frequency of 5 kHz was assessed on diameter and surface area reduction of the microdroplet. The work in this chapter provided a basis for reducing the size of features towards scalable manufacturing of functional devices that can be fabricated using different colloidal suspensions.

6.2 Introduction

One of the most researched materials in recent years has been carbon nanotubes due to their immense applications across several industries. Carbon nanotubes remain popular due to their unique properties such as higher flexibility, excellent mechanical properties, electrical, and lower thermal expansion (Salvetat et al., 1999, Ruoff and Lorents, 1995, and Hone, 2004), as compared to conventional materials such as copper, aluminum, steel, and so forth. Many of their applications are being realized in the semiconducting industry in the form of functional devices such as microsensors (Mohr et al., 1991), microelectromechanical systems (MEMS) (Fujita, 1997), integrated circuits (Grochowski et al., 1997), and so forth. Additionally, there are numerous instances in which carbon nanotubes have been used to fabricate thin film transistors (Zhao et al., 2009, Wang et al., 2009, Snow et al., 2005, Han et al., 2007, LeMieux et al., 2008, and Ono et al., 2010). These devices are being formed mostly on semiconducting substrates of glass (Ren et al., 1998), silicon (Reichl, 1986), polymers (Ko et al., 2007), etc. The deposition of the carbon nanotubes employed in this work were deposited on silicon substrates. However, to make the notion of fabricating functional devices realizable, a process that enables controlled deposition of materials is essential. Printing of electronic devices has previously been explored and was found to achieve accurate deposition with minimal wastage of materials (Sirringhaus et al. (2000), Szczech et al. (2002), Burns et al. (2003), Shimoda et al. (2006), and Sirringhaus and Shimoda (2003)). The method has also been shown to exhibit high repeatability and controllability during the deposition process. Furthermore, the direct-write method is a non-contact method for feature

deposition and does not contaminate solutions during deposition. Therefore, the direct write inkjet printing technique was employed to eject monodisperse microdroplets of the nanotube solution. The droplets were then subjected to irradiation from a 30W CO_2 laser with the aim of reducing the size of droplets in-flight prior to deposition on the substrate such that the amount of the material deposited is significantly less than the initial droplet size. The objective of the work in this chapter was to demonstrate laser evaporation of two different liquids microdroplets towards manufacturing scalable micro to nano functional features.

6.3 Literature Review

Evaporation of microdroplets has been investigated by many researchers (Li et al. 2005, Maqua et al., 2008, Lim et al., 2009, Desai et al. (2010 and 2011), and Hallett et al., 2010). The increase of these investigations corresponds to the paradigm shift in manufacturing towards miniaturization of devices. The use of lasers towards achieving this feat has also been explored in recent years. For instance, Kiefer et al. (1997) studied Mie and Raman light scatterings (elastic and inelastic, respectively) from laser trapped microdroplets. The Raman data provided the chemical structure, size and refractive index of droplets which enabled the authors to determine that catechol evaporated faster than diethylene glycol. Ray and Devarakonda (1998) explored resonance-based light scattering techniques to measure evaporation rates of monodisperse droplets mixture containing ethanol and methanol generated through a modified vibrating orifice aerosol generator. Davis and Ray (1978) demonstrated evaporation of low-volatility liquid submicron droplets suspended in an electric field using a polarized laser beam. Droplets'

size was determined as a function of time and Mie theory was used to interpret the light-scattering data. Laser light scattering was used to measure the reduction in aerosol droplets size in the study of Roth and Fischer (1985). In perhaps one of the earliest attempts of laser characterization of droplet evaporation, Ro et al. (1968) explored evaporation rates of water droplets (dia. = 0.6mm-1.5mm) using the intensity variation of a laser beam at the droplet's center. Jia and Qiu (2002) proposed a novel method to measure the contact diameter, profile, and volume of liquid droplets on hot substrates using scattering patterns from laser beams. Although many of the previous studies only utilized lasers as a characterization method, they are still worthy of recognition because it demonstrates the capacity in which lasers can be incorporated in manufacturing systems to enable a hybrid approach. However, there are yet a few examples in which lasers were utilized specifically for microdroplet evaporation analogous to the intention of this investigation. The CO_2 laser, noted for its high output power and increased popularity for research in the both industry and academia (Mahalik, 2006), was the radiative source employed to achieve the objective in this study. Some notable efforts similar to this investigation, but lacking the focus of this research of controlled evaporation and deposition of a functional material (i.e. carbon nanotubes) are as follows. Michel et al. (1997) demonstrated evaporation of nano-sized zirconia particles using a CO_2 laser. A CO_2 laser was also employed by Kurland et al. (2007) for evaporating purposes to produce iron oxide nanopowders. The work of Moras et al. (2005) investigated an Nd:YAG laser as the evaporation mechanism towards the production of magnetic nanopowders for ferrofluids. The Nd:YAG laser was also employed by Essien et al.

(1993) to study the evaporation of dye-doped glycerin-water droplets. The impact of evaporation of a stainless steel fast moving target using a CO_2 laser was studied by Lisenkov et al. (2009). Lastly, the work of Hitoshi et al. (2006) investigated radiative evaporation of a single droplet of suspended alcohol fuel (i.e. ethanol) with the use of a CO_2 laser source. This work aimed to achieve controlled evaporation of microdroplets and their deposition towards micro to nano (i.e. scalable) manufacturing.

6.4 Methodology

A direct write inkjet printing setup (MicroFab Technologies Inc., Plano, TX) was employed in this investigation to deposit the candidate fluids on the substrate. The inkjet system was equipped with a JetDrive III waveform generator and amplifier to control jetting parameters (voltages and jetting frequency), a pneumatics console for supplying vacuum and pressure to the nozzle, an optics system and a MJ-AT-01-30 piezoelectric (PZT) microvalve with an interchangeable nozzle orifice. In this study, a 20µm nozzle orifice was employed for all experiments. A 30W CO_2 laser (Firestar Series V30, Synrad Inc., Mukilteo, WA) was then employed to impinge upon microdroplets ejected from the inkjet system to initiate droplet evaporation. The complete experimental setup is depicted in Figure 6.1. The laser source was operated at its default frequency of 5 kHz. The lasing frequency employed provided the greatest depth of modulation and enabled controlled evaporation of microdroplets. The impact of lasing power or pulse width modulation (PWM) was assessed on microdroplet evaporation. A blue color dye homogeneously mixed with deionized water was used as the initial fluid to study its deposition after laser irradiation on glass cover slip substrates (size: 22mm x 22mm). The initial fluid (i.e.

water and blue) was investigated as a proof of concept to provide the framework on how the ensuing carbon nanotube solution would evaporate towards smaller scale dimensions. The carbon nanotube solution was dispersed in a surfactant aqueous. A sonicator was used to break up bundles of the nanotubes, which were later isolated using a proprietary column chromatography separation method (courtesy of Nano TechLabs Inc., Yadkinville, NC). The solution consisted of metallic single wall nanotubes. Figure 6.2 below reveals a scanning electron microscopy (SEM) image or the nanotube networks and bundles inside a deposited carbon nanotube microdroplet on silicon substrate. Upon ejection from the inkjet system, the lasing power (i.e. PWM) was varied to evaporate the nanotube microdroplets en route to deposition on silicon substrates. The reduced droplets (i.e. after laser) of both candidate fluids were deposited on their respective substrates using an x-y motion controller (Newmark Systems, Rancho Santa Margarita, CA). The motion controller's velocity, determined by the jetting frequency and initial droplet size, was adjusted to ensure that the reduced droplets did not overlap on the substrate and deposited as isolated droplets in single line traces. Furthermore, the controller was programmed to ensure a 2mm spacing in between the columns (i.e. line traces) of the deposited droplets. The significance of depositing an individual droplet on the substrate was to ensure accurate measurement of the droplet diameter. Using the droplet diameter, the surface area of droplets was calculated. Prior to operating the laser source, initial droplets (i.e. before laser) were deposited on the substrate and their length (i.e. diameter) was measured using ImageJ, an image acquisition software from the national institute of health (NIH). Subsequently, the lasing output power was adjusted from 10% to 95% in

increments of 20% (i.e. 10, 30, 50, 70, and 95 %). The surface area of droplets at each lasing power was also measured and compared to the initial condition. Therefore, the reduction in diameter and subsequent surface area was attested to laser evaporation of the microdroplets.

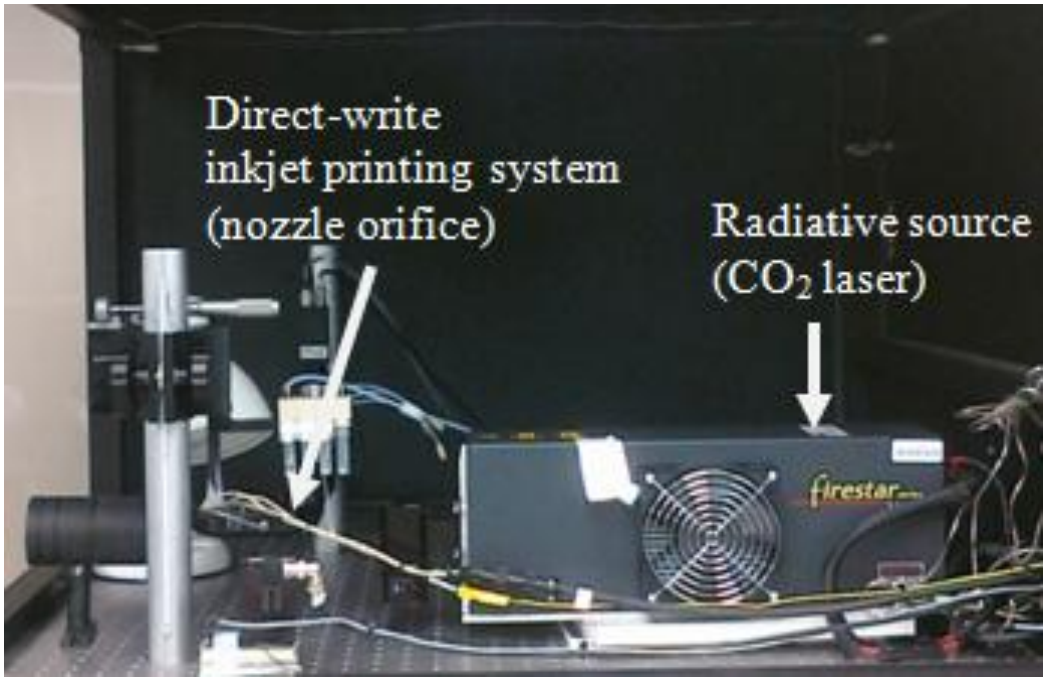

Figure 6.1. Inkjet printing system and laser source.

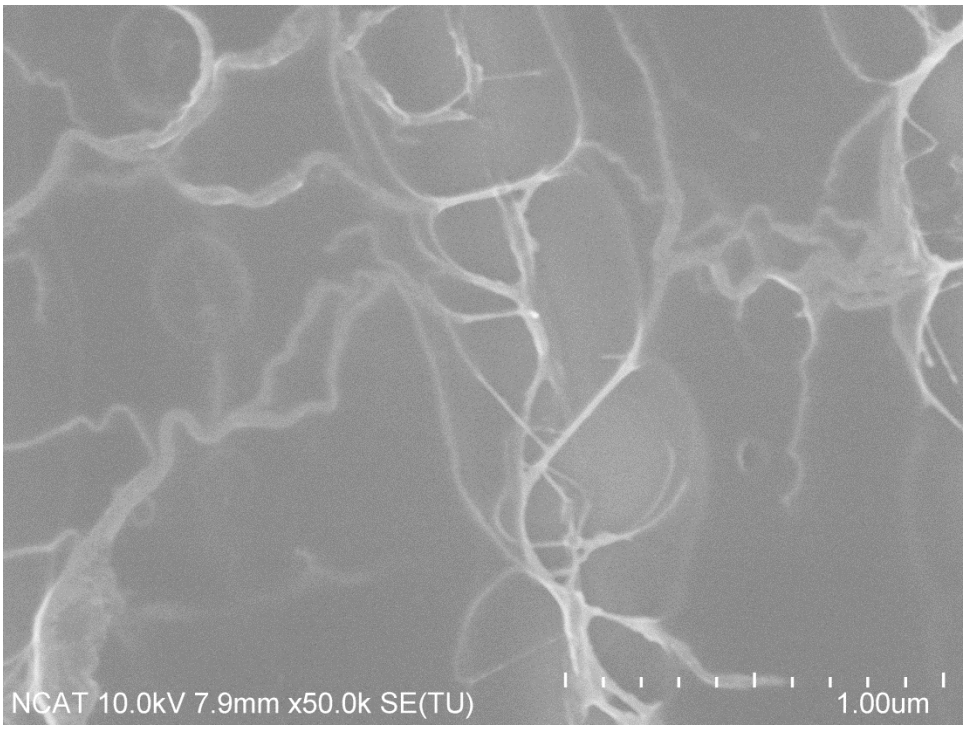

Figure 6.2. SEM image of nanotube network and bundles on silicon substrate.

6.5 Results

6.5.1 Reduction in Diameter of Deposited Microdroplets on Substrate.

The initial diameter of the deposited feature using the 20μm nozzle for the water and blue droplet measured approximately 144μm whereas the initial diameter for the carbon nanotube droplet was roughly 65μm. The differences in initial diameters of the deposited features can be attested to viscosity and surface tension differences of both fluids as well as substrate material that the fluids were deposited on (i.e. glass and silicon, respectively). Silicon substrates were used for the carbon nanotube experiments to facilitate characterization via SEM since silicon is a conducting material suitable for SEM imaging. These differences had an effect on the spreading characteristics of the droplets. Nevertheless, the reductions observed from both fluid types were comparable.

As the lasing output power was increased, the reduction in diameter also increased for both fluid types. For water and blue droplets, the initial diameter (i.e. 0% lasing power) of 144µm (Figure 6.3a) reduced to 35µm (Figure 6.3b) at 95% lasing power (see Table 6.1), equivalent to an overall reduction of 76% in diameter. Similarly, carbon nanotube droplets revealed an overall reduction in diameter of about 70% (see Table 6.2) since it reduced from an initial diameter of 65µm (Figure 6.4a) to roughly 20µm at 95% PWM (Figure 6.4b). Depicted in Figures 6.5 and 6.6 are graphical representations which demonstrates the impact of lasing power on diameters of blue and water and carbon nanotube microdroplets, respectively.

Table 6.1. Reduction in diameter for water and blue droplets.

Lasing Power (% PWM)	Diameter (µm)	Percentage Reduction in diameter (%)
0	143.48	100
10	85.33	59.47
30	76.09	53.03
50	65.22	45.45
70	57.61	40.15
95	35.60	24.81

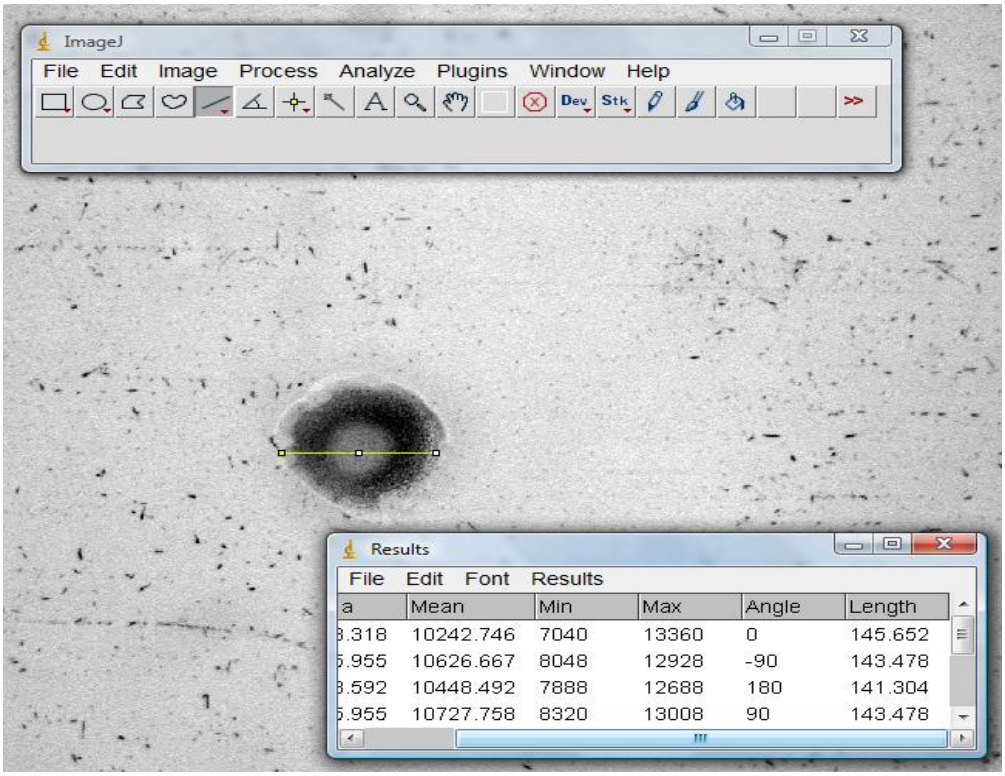

(a)

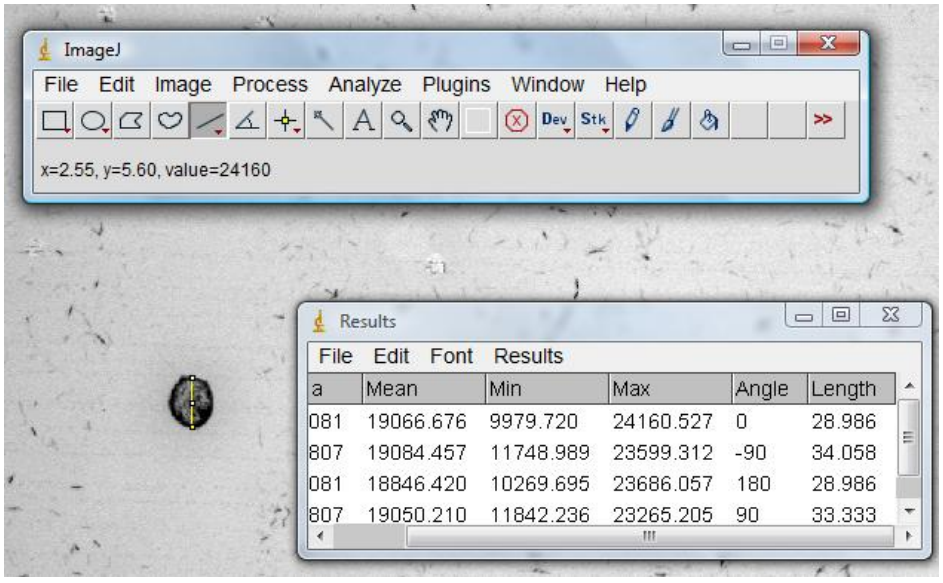

(b)

Figure 6.3. Water and blue experimental data (a) initial droplet diameter; (b) droplet diameter at 95% PWM.

Table 6.2. Reduction in diameter for carbon nanotube droplets.

Lasing Power (% PWM)	Diameter (μm)	Percentage Reduction in diameter (%)
0	64.67	100
10	45.38	70.17
30	40.49	62.60
50	32.61	50.42
70	26.63	41.18
95	19.97	30.88

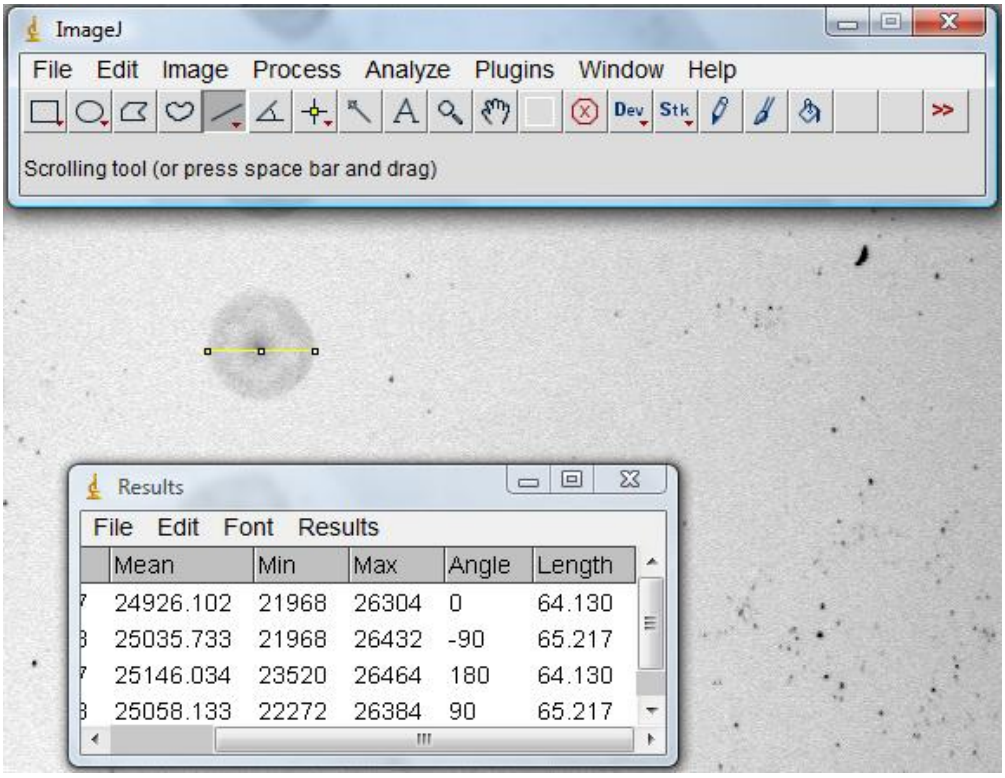

(a)

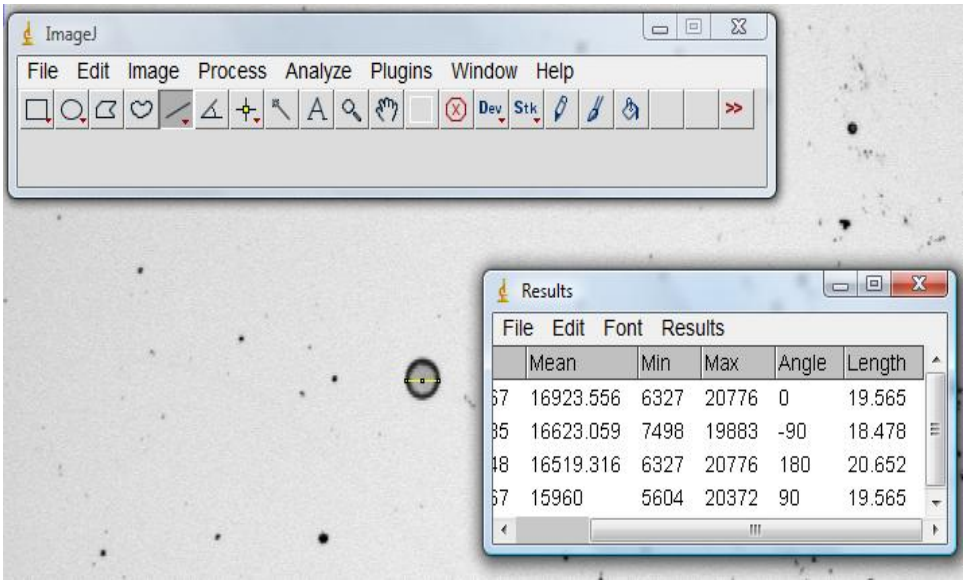

(b)

Figure 6.4. Carbon nanotube experimental data (a) initial droplet diameter; (b) droplet diameter at 95% PWM.

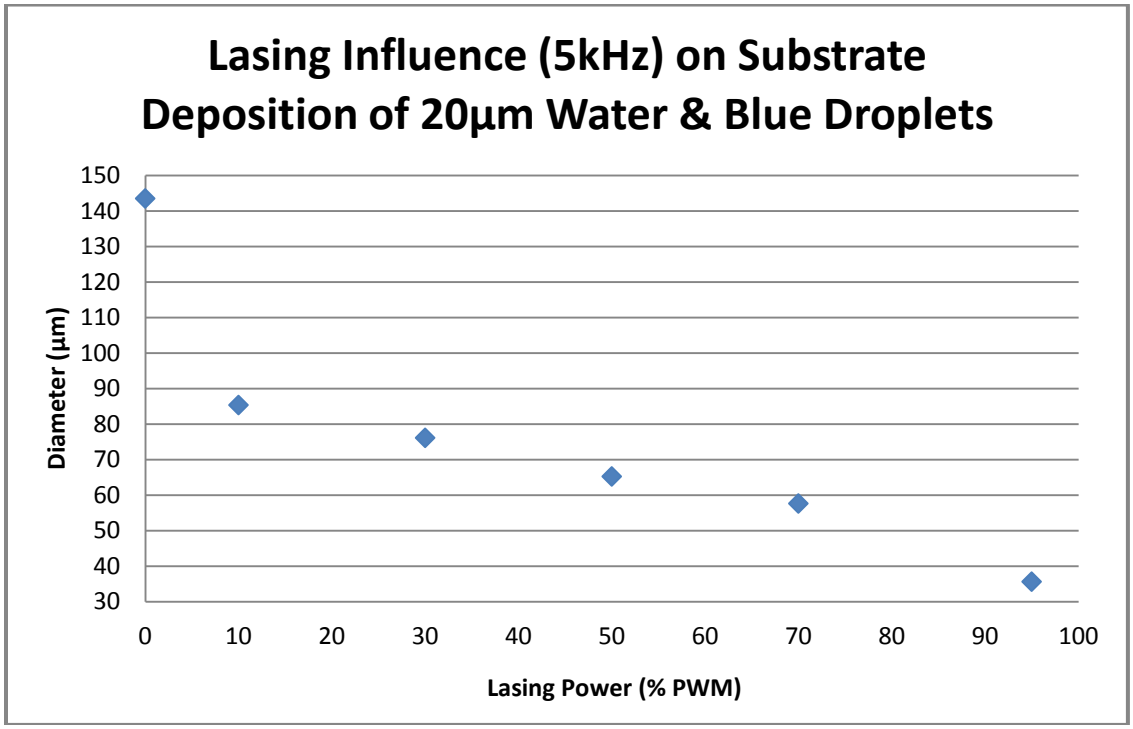

Figure 6.5. Impact of laser on diameter of deposited features using blue and water microdroplets.

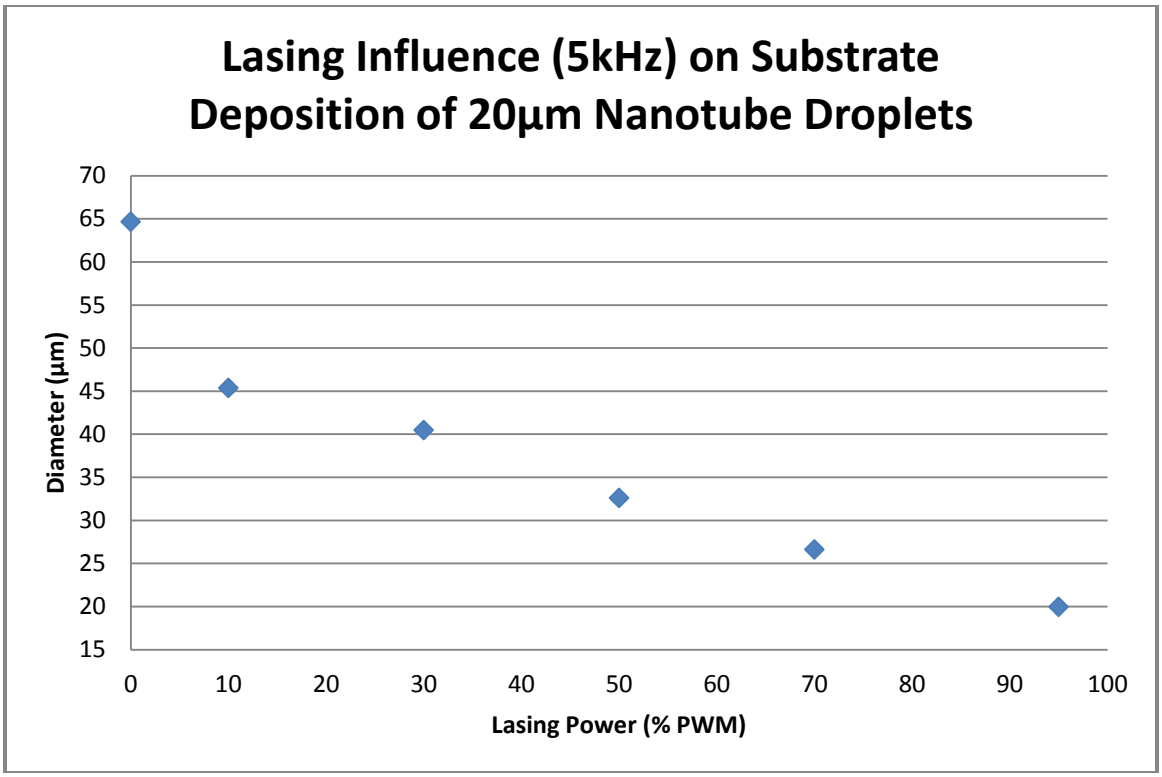

Figure 6.6. Impact of laser on diameter of deposited features using carbon nanotube microdroplets.

6.5.2 Surface Area Reduction of Deposited Microdroplets

The experimental data for the diameter (d) was subsequently used to calculate the surface area (πd^2) of the deposited feature from both fluid types. The reduction in surface area further emphasized the significance of the lasing power. The surface area reduction for water and blue microdroplets ranged from 63% to 93% (Table 6.3) at the highest lasing power. A graphical depiction of the effect of laser on evaporation of water and blue droplets is presented in Figure 6.7. Analogously, surface area reduction ranged from 50% to 90% for carbon nanotube microdroplets (Table 6.4). Figure 6.8 portrays the influence of laser evaporation of the carbon nanotube droplets. Consequently, as the laser

power was increased, the surface area reduction of microdroplets of both fluid types also increased.

Table 6.3. Reduction in surface area for water and blue droplets.

Lasing Power (% PWM)	Surface Area (picoliters)	Percentage Reduction in surface area (%)
0	64.67	-
10	23.30	63.97
30	18.36	71.62
50	13.50	79.13
70	10.50	83.76
95	4.45	93.12

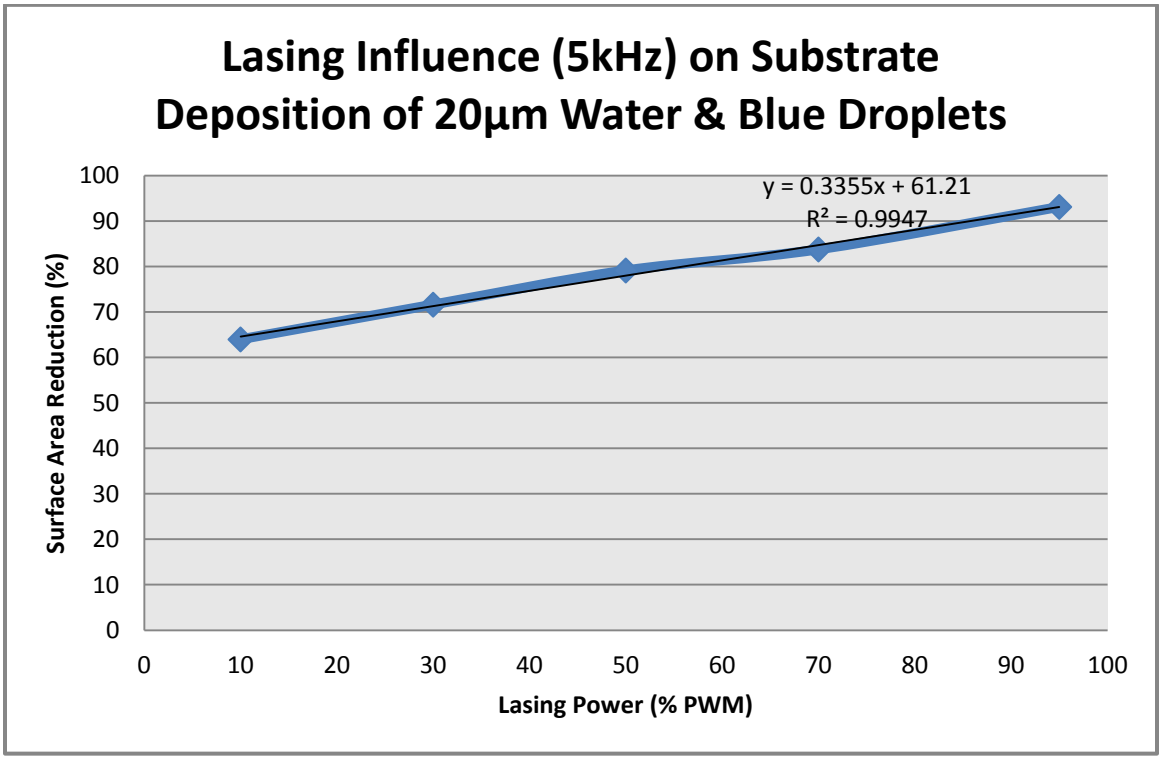

Figure 6.7. Effect of laser on surface area reduction of water and blue droplets.

Table 6.4. Reduction in surface area for carbon nanotube droplets.

Lasing Power (% PWM)	Surface Area (picoliters)	Percentage Reduction in surface area (%)
0	13.14	-
10	6.47	50.76
30	5.15	60.80
50	3.34	74.57
70	2.23	83.04
95	1.25	90.46

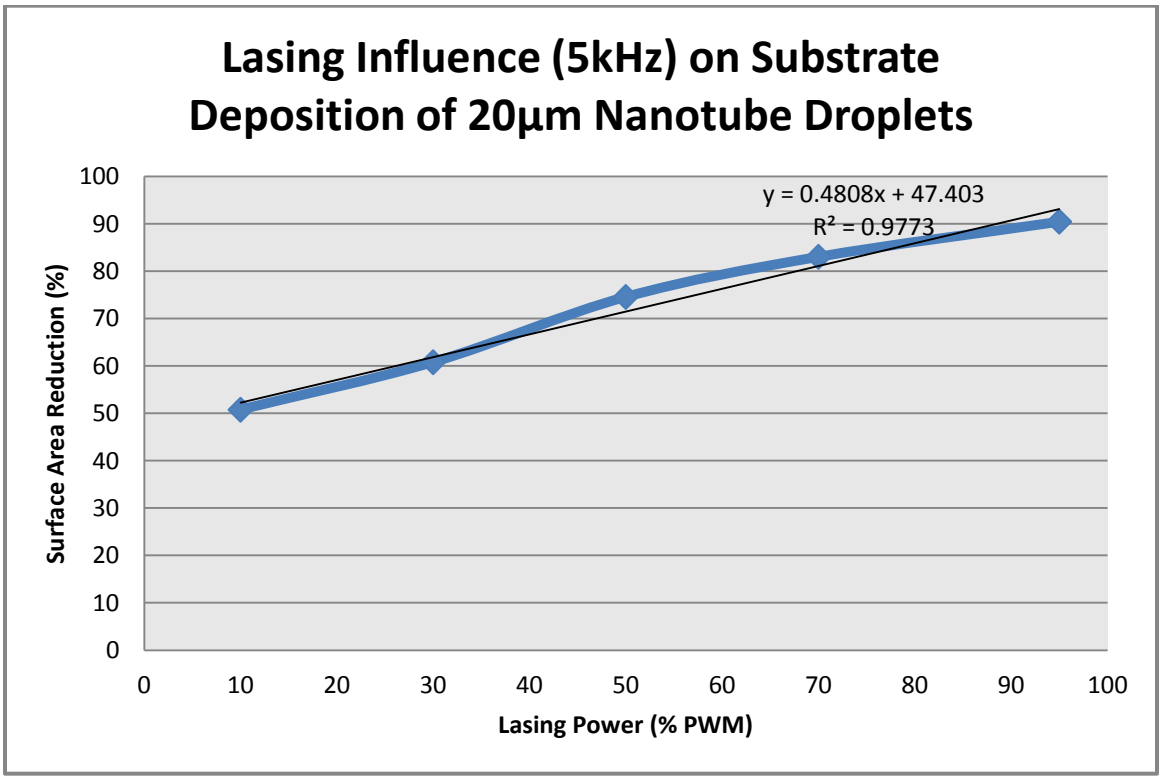

Figure 6.8. Effect of laser on surface area reduction of carbon nanotube droplets.

6.6 Conclusion

This chapter presented the results of an investigation on deposition of laser evaporated microdroplets. A mixture of water and blue color dye and carbon nanotube solution were the candidate fluids assessed to evaluate the impact of a 30W laser source on their diameter and surface area of the deposited features. As the lasing output power was increased, the diameter and surface area reductions of the deposited features from both fluid types also increased. The reductions for water and blue droplets were slightly higher than carbon nanotube droplets due to differences in viscosity, surface tension, and substrate material that each fluid was deposited upon. Furthermore, since the color of the water-dye solution was much darker as compared to the translucent nanotube solution it enabled it to absorb relatively higher heat from the laser source. This study provided a better understanding on the utilization of the laser and direct write inkjet printing towards the fabrication of micro and nanosized features. This is one of the first attempts towards controlled evaporation towards scalable micro/nano manufacturing. The research demonstrated that microdroplet can be controllably evaporated using a CO_2 laser source resulting in deposited features with varying sizes. The impact of using a smaller nozzle orifice (i.e. 10μm) will be investigated to assess if reductions at the nanoscale becomes realizable.

CHAPTER 7

CONCLUSION AND FUTURE WORK

7.1 Overview

The objective of this research was to investigate the controlled evaporation of microdroplets towards scalable droplet based manufacturing. The concept involved the use of a direct write inkjet printing technique to eject monodisperse microdroplets of different fluid types while simultaneously applying a heat source that would evaporate the droplets into smaller scale dimensions. Two heat sources were evaluated towards achieving the stated objective.

7.1.1 Resistive Heated Ring (Phase One)

The first phase of the research employed a convective source in the form of a resistive heated ring towards microdroplet evaporation. In this investigation, the evaporation characteristics for water and acetone microdroplets were studied as the temperature of the convective source was varied to understand the microdroplet size reduction phenomenon. A proportional reduction in the volume of water and acetone microdroplets was observed as the temperature of the resistive heating ring increased (i.e., increase in the heat flux). However, it was observed that acetone microdroplets exhibited a higher percentage volume reduction compared to water under the same experimental conditions. This observation was attested to the fact that acetone has a lower specific heat and higher volatility as compared to water. Two nozzle orifices (50μm and 30μm) in the direct write inkjet printing system were utilized in this study. The results revealed that microdroplets jetted with the higher diameter nozzle (50μm)

were observed to have higher percentage volume reductions than those jetted with the lower nozzle size (30μm) since the larger nozzle have a higher mass, the amount heat flux from the heated ring transferred to its microdroplets would be higher than those of the 30μm. Additionally, surface area to volume ratios were calculated for the reduced droplets in this study and the effects were evaluated. The findings revealed that droplets with higher surface area–to-volume ratio evaporated at a faster rate than their counterpart. Lastly, the experimental data of droplet size reductions were validated with a theoretical model (D^2 law). The model revealed that the experimental findings were in close agreement with the theoretical model. Therefore, the experiments conducted in this phase provided the promise that the second phase, which employed a radiative source (i.e. laser), would exhibit even further reductions. The evaporation realized in the first phase was due to heat transfer to the droplet's lateral periphery. However in the second phase, the laser's beam was focused to completely encapsulate the microdroplet which provided a more controlled evaporation towards achieving the primary objective of this research.

7.1.2 Radiative Laser Source (Phase Two)

The second phase towards the objective of this research involved the use of a radiative source (i.e. CO_2 laser) to initiate microdroplet evaporation. The experimental setup utilized in this phase was similar to that of the first phase. In contrast, a smaller nozzle orifice was introduced and two additional fluid types were evaluated. Microdroplet evaporation characteristics for water and acetone were studied after being subjected to laser irradiation. Furthermore, the impact of adding a color additive to both fluids was also investigated. This enabled the evaluation of the impact of the darker color

on heat absorption and consequent reductions in microdroplet shrinkage. The results revealed as well as concurred with the observation of the first phase that acetone microdroplets have higher percentage volumetric reductions as compared to water microdroplets under equivalent conditions. However, acetone with the color addition reduced at slightly higher evaporation rates compared to plain acetone droplets. This observation revealed the fact that darker colored liquids absorb more heat as compared to clear liquids. Droplets ejected from the smallest nozzle size (20µm) revealed higher percentage reductions in volume as compared to the larger nozzle sizes of 50µm and 30µm for all fluid types. This was due to the lower mass of the smaller microdroplets thereby resulting in faster evaporation rates for the equivalent amount of heat flux subjected by the laser beam. The observation was opposite the findings of the first phase which revealed that microdroplets from higher nozzle orifice evaporated more than droplets ejected out of the smaller orifice. The contradiction in the findings between the first two phases was due to the differences in the heat transfer of both sources since the resistive heating ring transferred heat to microdroplets' periphery while the laser source transferred heat to totally encapsulate the microdroplets. Furthermore, as the lasing output power and lasing frequency were increased, there was a rapid increase in surface area-to-volume ratio for droplets ejected from the smaller nozzle orifice (20µm) due to superheating of the fluid. In contrast to the initial phase (resistive heating ring experiments), significantly higher reductions in microdroplet volumes using CO_2 lasers were realized. The use of laser beam enabled "on-the-fly" manipulation of the microdroplet size based on modulation of parameters. This phase enabled the subsequent

investigation of depositing evaporated carbon nanotube solutions onto a substrate with the aim of achieving scalable manufacturing of functional devices. Specifically, the fabrication of thin film transistors was realized and discussed subsequently.

7.1.3 Fabrication of a Functional Device

Following the findings from phase one and two of this research that controlled evaporation was feasible, fabrication of functional devices using carbon nanotubes was investigated. In this study, the direct write inkjet printing technique was used to manufacture flexible thin film transistors (f-TFTs) using semiconducting single walled nanotubes (s-SWNTs) deposited on Kapton substrates. The substrate, Kapton, was plasma etched and gold coated to enable better adhesion to the deposited SWNTs to tighten the gap between source and drain electrodes. Optical and atomic force microscopy (AFM) images indicated that 150 and 100 pass depositions exhibited connectivity and revealed conductivity of the deposited nanotube bundles. In addition, metallic SWNTs and graphene nanoplatelets traces were evaluated for respective conductivity (I-V) characteristics. Finally, a flexible field effect transistor device was fabricated and tested for its transport characteristics. The advancement of this work towards large scale fabrication will be realized by utilizing a different dielectric material, reducing channel width as well as the distance between the source and drain electrodes. Furthermore, the use of smaller nozzle sizes (i.e. 10 and 20μm) and higher concentration SWNT inks are viable approaches to further this work. However, the investigation provided a basis for fabricating large scale arrays of flexible TFTs using direct write inkjet printing of carbon nanotubes. This effort demonstrated that functional devices such

as transistors can be fabricated using the inkjet printing technique. Consequently, this research provides foundation for reducing the foot print of deposited features via controlled microdroplet evaporation using the inkjet printing and laser setup.

7.1.4 Laser Evaporation of Deposited Droplets on Substrate

As a result of the success in fabricating thin film transistors using carbon nanotubes (Chapter 5), the next step of the research focused on studying the reduction characteristics of laser evaporated liquids. The aim of this investigation was to examine the deposition characteristics of features using carbon nanotubes colloids for fabricating functional materials. The inkjet printing system was employed to eject nanotube solutions (i.e. the material used for fabricating f-TFTs) while the laser was impinged upon microdroplets following ejection from the nozzle but prior to deposition on the substrate. This investigation enabled a direct application of the concept of this dissertation of controlled evaporation of microdroplets to achieve scalable micro/nano manufacturing of features. In this study, a mixture of water and blue color dye and carbon nanotube solution were the two fluids assessed to evaluate the impact of the 30W laser source on their diameter and surface area. The water and blue fluid was used for proof-of-concept purposes to observe reduction and deposition behavior and provide insight on how the carbon nanotube solution would behave. Experimental results revealed that as the lasing output power was increased, the diameter and surface area reductions of the microdroplets from both fluid types also increased. However, the reductions for water and blue droplets were slightly higher than carbon nanotube droplets due to differences in viscosity, surface tension, and substrate material that each fluid was deposited upon. This

study provided a better understanding on the utilization of the approach (i.e. laser and direct write inkjet printing) towards the fabrication of micro and nanosized features because it was one of the first attempts aimed at achieving controlled evaporation towards scalable micro/nano manufacturing. The research demonstrated that microfeatures can be controllably evaporated using the CO_2 laser source. The impact of using a smaller nozzle orifice (i.e. 10μm) will be investigated to assess if reductions at the nanoscale becomes realizable.

In summary, this research has provided a framework for achieving controlled evaporation of features at the micrometer range with the aim of transforming those features to the nanoscale. A unique approach was demonstrated to realize this objective by using both a convective heat transfer source and a radiative source. Furthermore, fabrication of functional devices has been demonstrated (i.e. flexible thin film transistors) using the direct-write inkjet approach. However, to advance the efforts of this research, there are some future efforts that should be investigated to make the objective of this work more realizable. The following efforts are recommended to ensure the possibility of attaining reductions at the nanoscale.

7.2 Future Work

- Use of smaller micro nozzles should be investigated (i.e. 1-10μm)
- Use of higher output CO_2 laser source ($\geq$ 1kW)
- Replicate thin film transistor fabrication by incorporating the laser to reduce the size of microdroplets prior to deposition on substrates.
    - This would enable reduction of features of the printed transistor

- Response surface analysis of factors should be conducted
    - To determine the combination of factors required to obtain the optimum desired controlled evaporation of features towards nanoscale manufacturing
- Hybrid approach (direct write inkjet printing and nano-imprint lithography)
    - In the hybrid approach, the laser source will reduce microdroplets ejected from inkjet system which will then be deposited on nanosized patterns created by NIL

REFERENCES

Abramoff, M.D., Magalhaes, P.J., and Ram, S.J. (2004). Image Processing with ImageJ. *Biophotonics International*, volume 11, issue 7, 36-42.

Acronym Finder. (n.d.). Retrieved September 3, 2010, from The Acronym Finder: http://www.acronymfinder.com/LASER.html

Arnold, C.B., Serra, P., and Piqué, A. (2007). Laser direct-write techniques for printing of complex materials. *MRS Bulletin*, 23-31.

Ashkin, A. and Dziedzic, J.M. (1987). Optical trapping and manipulation of viruses and bacteria. *Science*, 1517–1520.

Berns, M.W., Wright, W.H., and Steubing, R.W. (1991). Laser microbeam as a tool in cell biology. *International Review of Cytology*, 1-44.

Bieri, N. R., Chung, J., Poulikakos, D., and Grigoropoulos, C. P. (2004). Manufacturing of nanoscale thickness gold lines by laser curing of a discretely deposited nanoparticle suspension. *Superlattices and Microstructures*, 437-444.

Bortolani, F. and Dorey, R. (2009). Synthesis of spherical lead zirconate titanate (PZT) nanoparticles by electrohydrodynamic atomization. *Advances in Applied Ceramics*, 108(6), 332–337.

Brinley, E., Babu, K., and Seal, S. (2007). The solution precursor plasma spray processing of nanomaterials. *JOM*, 54-59.

Brody, T. P. (1984). The Thin Film Transistor - A Late Flowering Bloom. *IEEE Transactions on Electron Devices*, 31 (11), 1614–1628.

Burns, S.E., Cain, P.,Mills, J.,Wang, J. and Sirringhaus, H. (2003). Inkjet printing of polymer thin-film transistor circuits. *Materials Research Society Bulletin*, 28(11), 829–834.

Busnaina, A. (2007). Nanomanufacturing Handbook. New York: CEC Press.

Cardinaud, C., Peignon, M. C., and Tessier, P. Y. (2000). Plasma etching: principles, mechanisms, application to micro- and nano-technologies. *Applied Surface Science*, 72-83.

Chen, C. T., Tseng, F.G., and Chieng, C.C. (2006). Evaporation evolution of volatile liquid droplets in nanoliter wells. *Sensors and Actuators A*, 12-19.

Chen, J., Doumanidis, H., Lyons, K., Murday, J., and Roco, M. (2007). *Manufacturing at the Nanoscale: National Nanotechnology Initiative Workshop Report*.

Chen, R.H., Phuoc, T.X., and Martello, D. (2010). Effects of nanoparticles on nanofluid droplet evaporation. *International Journal of Heat and Mass Transfer (Article in Press)*, 1-6.

Chou, S. Y., Krauss, P. R., and Renstrom, P. J. (1996). Nanoimprint lithography. *Journal of Vacuum Science Technology B*, 4129-4133.

Chrisey, D.B. (2000). Materials processing: the power of direct writing. *Science*, 289(5481), 879–881.

Colina, M., Duocastella, M., Fernández-Pradas, J.M., Serra, P., and Morenza, J.L. (2006). Laser induced forward transfer of liquids: study of the droplet ejection process. *Journal of Applied Physics*, 1-7.

Colina, M., Serra, P., Fernández-Pradas, J.M., Sevilla, L., and Morenza, J.L. (2005). DNA deposition through laser induced forward transfer. *Biosensors and Bioelectronics*, 1638–1642.

Crafton, E. F. and Black, W. Z. (2004). Heat transfer and evaporation rates of small liquid droplets on heated horizontal surfaces. *Heat and Mass Transfer*, 1187-1200.

Creighton, J. R. and Ho, P. (2001). Introduction to Chemical Vapor Deposition (CVD). *ASM International- Chemical Vapor Deposition*, 1-9.

Davis, E. James and Ray, Asit K. (1978). Submicron droplet evaporation in the continuum and non-continuum regimes. *Journal of Aerosol Science*, 411-422.

Desai, S., Esho, T., and Kaware, R. (2010). Understanding Microdroplet Evaporation towards Scalable Micro/Nano Fabrication. *Proceedings of the Industrial Engineering Research Conference*, (pp. 1-6). Cancun, Mexico.

Desai S., Esho T., and Kaware, R. (2011). Experimental Investigation of Controlled Microdroplet Evaporation Towards Scalable Micro/Nano Manufacturing. *IIE Transactions*, 44, 155-162.

Duocastella, M, Fernández-Pradas, J.M., Morenza, J.L., Zafra, D, and Serra, P. (2010). Novel laser printing technique for miniaturized biosensors preparation. *Sensors and Actuators B: Chemical*, 596-600.

Eddy, D. S. and Sparks, D. R. (1998). Application of MEMS technology in automotive sensors and actuators. *Proceedings of the IEEE*, 1747 – 1755.

Essien, M., Armstrong, R. L., and Gillespie, J. B. (1993). Lasing emission from an evaporating layered microdroplet. *Optics Letters*, 762-764.

Faeth, G.M. (1977). Current status of droplet and liquid combustion. *Progress in Energy and Combustion Science*, 3(4), 191–224.

Feynman, R. (1961). There's plenty of room at the bottom. New York: Reinhold.

Fieberg, C. (2003). Experimental Investigation of Droplet Evaporation Under Hot Temperature and High Pressure Conditions. Diploma Thesis.

Fong, C., Black, N., Kiefer, P. and Shaw, R. (2007). An experiment on the Rayleigh instability of charged liquid drops. *American Journal of Physics*, 75(6), 499–503.

Fortunato, E., Barquinha, P., and Pimentel, A. (2004). Wide-bandgap high-mobility ZnO thin-film transistors produced at room temperature. *Applied Physics Letters*, 85(13), 2541-2543.

Fujita, H. (1997). A decade of MEMS and its future. *Proceedings of IEEE, Tenth Annual International Workshop on Micro Electro Mechanical Systems*, 1-7.

Furukawa, Y., Yonezu, H., and Wakahara, A. (2007). Monolithic integration of light-emitting devices and silicon transistors. *Micro/Nano Lithography*, 9-14.

Garcia, C., Murtazin, A., Groh, S., Becker, M., and Niemax, K. (2010). Characterization of particles made by desolvationof monodisperse microdroplets of analyte solutions and particle suspensions for nanoparticle calibration in inductively coupled plasma spectrometry. *Spectrochimica Acta Part B: Atomic Spectroscopy*, 80-85.

Ghosh, S., Bachilo, S., and Weisman, B. (2010). Advanced sorting of single-walled carbon nanotubes by nonlinear density-gradient ultracentrifugation. *Nature Nanotechnology*, 5, 443–450.

Girshick, S. (2008). Aerosol processing for nanomanufacturing. *Journal of Nanoparticle Research*, 935–945.

Greiner, A., Wendorff, J., Yarin, A., and Zussman, E. (2006). Biohybrid nanosystems with polymer nanofibers and nanotubes. *Applied Microbiology and Biotechnology*, 387–393.

Grochowski, A., Bhattacharya, D., Viswanathan, T. R., and Laker, K. (1997). Integrated Circuit Testing for Quality Assurance in Manufacturing: History, Current Status, and Future Trends. *IEEE Transactions on Circuits and Systems—II: Analog and Digital Signal Processing*, 610-633.

Guijt, R. and Breadmore, M. (2008). Maskless photolithography using UV LEDs. *Lab Chip*, 1402–1404.

Hallett, W.L.H and Beauchamp-Kiss, S. (2010). Evaporation of single droplets of ethanol–fuel oil mixtures. *Fuel*, 2496-2504.

Han, S.I. and Jeong, S.H. (2004). Laser-assisted chemical vapor deposition to directly write three-dimensional microstructures. *Journal of Laser Applications*, 154-159.

Han, X., Janzen, D.C., Vaillancourt, J., and Lu, X. (2007). Printable high-speed thin-film transistor on flexible substrate using carbon nanotube solution. *Micro and Nano Letters*, 2, 96–98.

Heston, S. (2004) Linear quadrupole focusing for high resolution microdroplet-based fabrication. M.S. Thesis, University of Pittsburgh, Pittsburgh, PA.

Hitoshi, T., Hiroshi, N., and Yasushige, U. (2006). Droplet Evaporation of Alcohol Fuel by Radiative Heating. *Japan Science and Technology Agency*, 19-24.

Hoffmann, F. (1996). Laser microbeams for the manipulation of plant cells and subcellular structures. *Plant Science*, 1-11.

Hohn, K.K.B., Li, L., and Hutchings, I.M. (2008). Direct writing technology – Advances and developments. *CIRP Annals - Manufacturing Technology*, 601-620.

Hone, J. (2004). Carbon Nanotubes: Thermal Properties. *Dekker Encyclopedia of Nanoscience and Nanotechnology*, 603-610.

Hornak, L. A., Brown, K., Taylor, B., and Barr, J. C. (1997). Polymer Guided Wave Integrated Optics: An Enabling Technology for Micro-Opto-Electro-Mechanical Systems (invited paper), in *Miniaturized Systems with Micro-Optics and Micromechanics II, Proc SPIE*, 3008 124-135.

Huang, Y., Wen, X., Goswami, B. and Chrisey, D. (2007). Direct writing biological patterns & constructs onto fabrics. National Textile Center Research Briefs: June 2007, NTC Project: F06-CL02, 1–3.

Jang, J. and Liccardo, D. (2007). Small UAV Automation Using MEMS. *Aerospace and Electronic Systems Magazine-IEEE*, *30*-34.

Jia, W. and Qiu, H. (2002). Fringe probing of an evaporating microdroplet on a hot surface. *International Journal of Heat and Mass Transfer*, 4141-4150.

Jones, T., Gunji, M., Washizu, M. and Feldman, M. (2001). Dielectrophoretic liquid actuation and nanodroplet formation. *Journal of Applied Physics*, 89(2), 1441–1448.

Kaehr, B., Ertas, N., Nielson, R., Allen, R., Hill, R.T., Plenert, M., and Shear, J.B. (2006). Direct-write fabrication of functional protein matrixes using a low-cost Q-switched laser. *Analytical Chemistry*, 3198–3202.

Kattamis, N.T., Purnick, P.E., Weiss, R., and Arnold, C.B. (2007). Thick film laser induced forward transfer for deposition of thermally and mechanically sensitive materials. *Applied Physics Letters*, 1-3.

Kiefer, W., Popp, J., Lankers, M., Trunk, M., Hartmann, I., Urlaub, E., and Musick, J. (1997). Raman-Mie scattering from single laser trapped microdroplets. *Journal of Molecular Structure*, 113-120.

Ko, S., Pan, H., Grigoropoulos, C., Luscombe, C., Fréchet, J., and Poulikakos, D. (2007). All-inkjet-printed flexible electronics fabrication on a polymer substrate by low-temperature high-resolution selective laser sintering of metal nanoparticles. *Nanotechnology*, 1-8.

Kurland, HD., Grabow, J., Staupendahl, G., Andra, W., Dutz, S., and Bellemann, M. E. (2007). Magnetic iron oxide nanopowders produced by CO_2 laser evaporation. *Journal of Magnetism and Magnetic Materials*, 73-77.

Lamanna, G., Sun, H.; Weigand, B., Magatti, D., Micciche, P., and Ferri, F. (2005). Measurements of droplet vaporisation by means of light scattering. *Colloids and Surfaces A*, 153–161.

Langmuir, I. (1918). The evaporation of small spheres. *Phys. Rev.*, 368-370.

Lee, J.S., Kim, Y.J., Kang, B.G., Kim, S.Y., Park, J., Hwang, J. and Kim, Y.J. (2009) Electrohydrodynamic jet printing capable of removing substrate effects and modulating printing characteristics, in Proceedings of the IEEE 22nd *International Conference on Micro Electro Mechanical Systems*, IEEE, Piscataway, NJ, pp. 487–490.

LeMieux, M.C., Roberts, M., Barman, S., Jin, Y., Kim, J., and Bao, Z. (2008) Self-Sorted, Aligned Nanotube Networks for Thin-Film Transistors. *Science*, 321, 101-104.

Li, K.Y., Tu, H. and Ray, A.K. (2005) Charge limits on droplets during evaporation. *Langmuir*, 21(9), 3786–3794.

Li, Y., Shawgo, R., Tyler, B., Henderson, P., Vogel, J., Rosenberg, A., Storm, P., Langer, R., Brem, H., and Cima, M. (2004). In vivo release from a drug delivery MEMS device. *Journal of Controlled Release*, 211-219.

Lim, E.W.C., Koh, S.H., Lim, L.K., Ore, S.H., Tay, B.K., Ma, Y., and Wang, C-H. (2008). Experimental and computational studies of liquid aerosol evaporation. *Aerosol Science*, 618-634.

Lim, T., Han, S., Chung, J., Chung, J. T., Ko, S., and Grigoropoulos, C. P. (2009). Experimental study on spreading and evaporation of inkjet printed pico-liter

droplet on a heated substrate. *International Journal of Heat and Mass Transfer*, 431-441.

Lin, Y., Hong, M.H., Chen, G.X., Lima, C.S., Tan, L.S., Wang, Z.B., Shi, L.P., and Chong, T.C. (2007). Hybrid laser micro/nanofabrication of phase change materials with combination of chemical processing. *Journal of Materials Processing Technology*, 340-345.

Lin, Y., Huang, Y., and Chrisey, D. B. (2009). Droplet formation in matrix-assisted pulsed-laser evaporation direct writing of glycerol-water solution. *Journal of Applied Physics*, 1-6.

Lisenkov, V. V., Osipov, V. V., and Shitov, V. A. (2009). Research of Laser Evaporation of Fast-Moving Target. *Laser Physics*, 1192-1197.

Liu, Y., Cui, T. and Varahramyan, K. (2003). All-polymer capacitor fabricated with inkjet printing technique. *Solid-State Electronics*, 47(9), 1543–1548.

Lu, G., Peng, X. and Wan, X. (2009). An experimental investigation on spreading of droplets with evaporation and nucleation. *Heat Transfer, Asian Research*, 38(1), 40–50.

Mahalik, N. (2006). Micromanufacturing and Nanotechnology. Germany: Springer.

Maqua, C., Castanet, G., Grisch, F., Lemoine, F., Kristyadi,T., and Sazhin, S.S. (2008). Monodisperse droplet heating and evaporation: Experimental study and modelling. *International Journal of Heat and Mass Transfer*, 3932–3945.

Michel, G., Staupendahl, G., Eberhardt, G., Muller, E., and Oestreich, C. (1997). Production of nanosized zirconia-particles by CO_2 laser evaporation. *Proceedings of the 1997 5th Conference and Exhibition of the European Ceramic Society*. Trans Tech Publication, 161-164.

Mijatovic, D., Eijkel, J.C.T., and van den Berg, A. (2005). Technologies for nanofluidic systems: top-down vs. bottom-up - a review. *Lab on a chip*, 492-500.

Mikkilineni, S., Landry, E.S. andMcGaughey, A.J.H. (2007). Subcritical and supercritical nanodroplet evaporation: a molecular dynamics investigation, in *Proceedings of the ASME-JSME Thermal Engineering Summer Heat Transfer Conference*, 775–782.

Mohr, J., Bley, P., Burbaum, C., Menz, W., and Wallrabe, U. (1991). Fabrication of microsensor and microactuator elements by the LIGA-process. *International Conference on Solid-State Sensors and Actuators*, 607-609.

Moras, K., Schaarschuch, R., Riehemann, W., Zinoveva, S., Modrow, H., and Eberbeck, D. (2005). Production and characterisation of magnetic nanoparticles produced by

laser evaporation for ferrofluids. *Journal of Magnetism and Magnetic Materials*, 119-126.

Müller-Fiedler, R. and Knoblauch, V. (2003). Reliability aspects of microsensors and micromechatronic actuators for automotive applications. *Microelectronics Reliability*, 1085-1097.

Neev, J., Da Silva, L.B., Feit, M.D., Perry, M.D., Rubenchik, A.M., and Stuart, B.C. (1996). Ultrashort pulse lasers for hard tissue ablation. *IEEE Journal of Quantum Electronics (Selected Topics)*, 790- 800.

Nelson, J.S. and Berns, M.W. (1989). Laser application in biomedicine. Part II: Clinical applications. *Journal of Laser Application*, 9-20.

Ng, J., Desmulliez, M., Lamponi, M., Moffat, B., McCarthy,A., Suyal, H., Walker, A., Prior, K., and Hand, D. (2009). A direct-writing approach to the micro-patterning of copper onto polyimide. *Circuit World*, 3 – 17.

Nikolopoulos, N., Theodorakakos, A., and Bergeles, G. (2007). A numerical investigation of the evaporation process of a liquid droplet impinging onto a hot substrate. *International Journal of Heat and Mass Transfer*, 303-319.

Odde, D.J. and Renn, M.J. (1999). Laser-guided direct writing for applications in biotechnology. *Trends in Biotechnology*, 385-389.

Odde, David J. and Renn, Michael J. (2000). Laser-Guided Direct Writing Living Cells. *Biotechnology and Bioengineering*, 312-318.

Ono, Y., Kishimoto, S., Ohno, Y., and Mizutani, T. (2010). Thin film transistors using PECVD-grown carbon nanotubes. *Nanotechnology*, 21, 1-4.

Palm, L. and Nilsson, J. (1998). Impact of droplet placement on paper by the level of droplet flight from stability in a continuous ink jet printer. *International Symposium on Silver Halide Imaging*, 42(6), 483–533.

Park, J., Hardy, M., Kang, S.B., Adair, K., Mukhopadhyay, D., Lee, C., Strano, M., Alleyne, A., Georgiadis, J., Ferreira, P. and Rogers, J. (2007) High-resolution electrohydrodynamic jet printing. *Nature Materials*, 6(10), 782–789.

Pena, A., Wang, Z., Whitehead, D., and Li, L. (2010). Direct writing of micro/nano-scale patterns by means of particle lens arrays scanned by a focused diode pumped Nd:YVO4 laser. *Applied Physics A: Materials Science & Processing*, 287-295.

Photolithography. http://www.ece.gatech.edu/research/labs/vc/theory/photolith.html

Pique, A. and Chrisey, D.B. (2002) Direct write technologies for rapid prototyping applications, in *Direct Write Technologies for Rapid Prototyping Applications*, Academic Press, San Diego, CA, pp. 1–10.

Polla, D.L. (2001). MEMS technology for biomedical applications. I*nternational Conference Proceedings on Solid-State and Integrated-Circuit Technology*, 19-22.

Rai-Choudhury, P. (1997). Chapter 5 – Photomask Fabrication Procedures and Limitations. Handbook of Microlithography, Micromachining, & Microfabrication Vol. 1: Microlithography, Washington USA, SPIE Press.

Ray, A. K. and Devarakonda, V. (1998). Evaporation of multicomponent microdroplets of volatile constituents. *Journal of Aerosol Science*, 585-586.

Reid, J. and Mitchem, L. (2006). Laser probing of single-aerosol droplet dynamics. *Annu. Rev. Phys. Chem.*, 245–71.

Reichl, H. (1986). Silicon Substrates for Chip Interconnection. *Microelectronics International*, 5 – 7

Ren, Z. F., Huang, Z. P., Xu, J. W., Wang, J. H., Bush, P., Siegal, M. P., and Provencio, P. N. (1998). Synthesis of Large Arrays of Well-Aligned Carbon Nanotubes on Glass. *Science*, 1105-1107.

Ro, P. S., Fahlen, T. S., and Bryant, H. C. (1968). Precision Measurements of Water Droplet Evaporation Rates. *Applied Optics*, 883-890.

Roth, P. and Fischer, R. (1985). An experimental shock wave study of aerosol droplet evaporation in the transition regime. *Physics of Fluids*, 1665-72.

Ruoff, R. and Lorents, D. (1995). Mechanical and thermal properties of carbon nanotubes. *Carbon*, 33, 925-930.

Salaita, K., Wang, Y., and Mirkin, C. A. (2007). Applications of dip-pen nanolithography. *Nature Nanotechnology*, 145 – 155.

Salvetat, J., Bonard, J., Thomson, N., Kulik, A., Forr´o, L., Benoit, W., and Zuppiroli, L. (1999). Mechanical properties of carbon nanotubes. *Applied Physics A: Materials Science & Processing*, 69, 255-260.

Sangiovanni, J. and Labowsky, M. (1982). Burning times of linear droplet arrays: a comparison of experiment and theory. *Combustion and Flame*, 15-30.

Sefiane, K. and Bennacer, R. (2009). Nanofluids droplets evaporation kinetics and wetting dynamics on rough heated substrates. *Advances in Colloid and Interface Science*, 263-271.

Sele, C.W., Werne, T. V., Friend, R.H. and Sirringhaus, H. (2005). Lithography-free self-aligned inkjet printing with sub-hundred nanometer resolution. *Advanced Materials*, 17(8), 997–1001.

Shimoda, T.,Matsuki,Y., Furusawa,M., Aoki, T.,Yudasaka, I., Tanaka, H., Iwasawa, H., Wang, D., Miyasaka, M. and Takeuchi, Y. (2006). Solution-processed silicon films and transistors. *Nature*, 440(7085), 783–786.

Sirringhaus, H., Kawase, T., Friend, R.H., Shimoda, T., Inbasekaran, M., Wu,W., and Woo, E.P. (2000) High-resolution inkjet printing of all-polymer transistor circuits. *Science*, 290(5499), 2123–2126.

Sirringhaus, H. and Shimoda, T. (2003). Inkjet printing of functional materials. *Materials Research Society Bulletin*, 802-806.

Skrabalak, S.; and Xia, Y. (2009). Pushing Nanocrystal Synthesis toward Nanomanufacturing, *ACS Nano*, 3(1), 10-15.

Snow, E.S., Campbell, P.M., Ancona, M.G., and Novak, J.P. (2005). High-mobility carbon-nanotube thin-film transistors on a polymeric substrate. *Applied Physics Letters*, 86, 1-3.

Song, J.W., Kim, J., Yoon, Y.H., Choi, B.S., Kim, J.H., Han, C.S. (2008). Inkjet printing of single-walled carbon nanotubes and electrical characterization of the line pattern. *Nanotechnology*, 19, 1-6.

Song, Y.I., Kim, G.Y., Choi, H.K., Jeong, H.J., Kim, K.K., Yang, C.M., Lim, S.C., An, K.H., Jung, K.T., and Lee, Y.H. (2006). Fabrication of Carbon Nanotube Field Emitters Using a Dip-Coating Method. *Chemical Vapor Deposition*, 12, 375-379.

Stutzmann, N., Friend, R.H. and Sirringhaus, H. (2003) Self-aligned, vertical channel, polymer field effect transistors. *Science*, 299(5614), 1881–1885.

Swindal, J., Chen, G., Scheschak, K., Chang, R., and Jackson, T. (1996). Measurement of the evaporation rates of closely spaced flowing droplets by optical cavity resonances. *Atomization and Sprays*, 331-351.

Szczech, J.B., Megaridis, C.M., Gamota, D.R. and Zhang, J. (2002) Fineline conductor manufacturing using drop-on demand PZT printing technology. *IEEE Transactions on Electronic Packaging Manufacturing*, 25(1), 26–33.

Tanaka, T., Urabe, Y., Nishide, D., and Kataura, H. (2009). Continuous Separation of Metallic and Semiconducting Carbon Nanotubes using Agarose Gel. *Applied Physics Express*, 2, 125002.

Tang, W. C. and Lee, A. P. (2001). Defence applications of MEMS. *MRS Bulletin*, 318-319.

Taniguchi, N. (1983). Current status in, and future trends of ultrprecision machining and ultrafine material processing. *Annals of CIRP*, 573-582.

Tay, B. Y. and Edirisinghe, M. J. (2002). Time-Dependent Geometrical Changes in a Ceramic Ink Droplet. *Proceedings: Mathematical, Physical and Engineering Sciences,* London: The Royal Society, 2039-2051.

Tseng, C.C. and Viskanta, R. (2006). Enhancement of water droplet evaporation by radiation absorption. *Fire Safety Journal*, 236-247.

Varghese, S. K. and Gangamma, S. (2007). Evaporation of Water Droplets by Radiation: Effect of Absorbing Inclusions. *Aerosol and Air Quality Research*, 95-105.

Venkatesan, T. and Green, S. (1996). Pulsed Laser Deposition: Thin Films in a Flash. *American Institute of Physics*, 22-24.

Wang, C., Zhang, J., Ryu, K., Badmaev, A., Gomez De Arco, L., and Zhou, C. (2009). Wafer-Scale Fabrication of Separated Carbon Nanotube Thin-Film Transistors for Display Applications. *Nano Letters*, 9, 4285-4291.

Wang, J.Z., Gu, J., Zenhausern, F. and Sirringhaus, H. (2006) Low-cost fabrication of submicron all polymer field effect transistors. *Applied Physics Letters*, 88(13), 133502 (3 pages).

Webster's Online Dictionary: http://www.merriam-webster.com.

Xia, Y. and Whitesides, G.M. (1998). Soft lithography. Angew. Chem. Int. Ed.550-575.

Xu, J., Zhong, C., and Fu, C. (2007). Novel method for printing high-quality metal wires. *Micro/Nano Lithography*, 1-2.

Yatsuzuka, K., Saito, K. and Asano, K. (1997) Aero-dynamical motion of charged droplets ejected from the 26 μm nozzle, in *Proceeding of the IEEE Industry Applications Society Annual Meeting*, IEEE, Piscataway, NJ, 1845–1850.

Yoon, J. B., Han, C. H., Yoon, E., and Kim, C. K. (1998). Novel and high-yield fabrication of electroplated 3D micro-coils for MEMS and microelectronics. *Part of the SPIE Conference on Micromachining and Microfabrication Process Technology IV*, 233-240.

Zhang, X.R. and Xu, X. (2004). Development of a biosensor based on laser-fabricated polymer microcantilevers. *Applied Physics Letter*, 2423–2425.

Zhao, J., Lee, C.W., Han, X., Chen, F., Xu, Y,, Huang, Y., Chan-Park, M., Chen, P., and Li, L.J. (2009). Solution-processable semiconducting thin-film transistors using single-walled carbon nanotubes chemically modified by organic radical initiators. *Chemical Communications*, 46, 7182-7184.

Zhou, Y., Hu, L., and Grüner, G. (2006). A method of printing carbon nanotube thin films. *Applied Physics Letters*, 88, 1-3.

APPENDIX

RANDOMIZED FACTORIAL DESIGN

Multilevel Factorial Design

```
Factors:       4     Replicates:      2
Base runs:    54     Total runs:    108
Base blocks:   1     Total blocks:    1

Number of levels: 2, 3, 3, 3

Design Table (randomized)
```

Run	Blk	A	B	C	D
1	1	2	1	2	3
2	1	1	1	3	1
3	1	2	1	2	3
4	1	2	1	1	1
5	1	1	2	1	2
6	1	2	2	1	2
7	1	1	2	1	1
8	1	1	1	1	1
9	1	2	2	1	1
10	1	2	3	2	1
11	1	1	2	2	3
12	1	1	3	2	1
13	1	2	1	3	3
14	1	1	3	1	3
15	1	1	3	2	3
16	1	2	1	3	3
17	1	2	2	2	1
18	1	1	3	2	2
19	1	1	2	1	1
20	1	2	2	2	2
21	1	1	2	1	2
22	1	2	3	2	1
23	1	2	3	3	1
24	1	1	3	2	1
25	1	2	1	3	2
26	1	2	2	3	1
27	1	1	3	2	2
28	1	1	2	3	2
29	1	2	3	1	1
30	1	2	3	3	3
31	1	2	2	3	2
32	1	2	2	1	3
33	1	2	3	2	2
34	1	1	1	2	1
35	1	1	1	2	2
36	1	2	1	1	3
37	1	1	2	2	1
38	1	1	2	3	3
39	1	1	2	1	3
40	1	1	1	1	1

41	1	1	1	2	3
42	1	1	2	3	2
43	1	2	2	3	3
44	1	2	1	1	3
45	1	1	1	3	1
46	1	1	1	3	3
47	1	2	3	1	3
48	1	1	3	2	3
49	1	2	1	1	1
50	1	2	3	1	3
51	1	2	3	2	2
52	1	1	1	2	2
53	1	2	3	2	3
54	1	2	1	1	2
55	1	1	2	1	3
56	1	2	2	2	3
57	1	2	2	3	2
58	1	1	3	1	1
59	1	1	1	3	2
60	1	1	2	3	1
61	1	1	3	3	3
62	1	1	1	2	1
63	1	2	2	1	3
64	1	2	3	2	3
65	1	2	2	3	3
66	1	2	2	2	3
67	1	1	3	3	2
68	1	2	2	1	2
69	1	2	2	3	1
70	1	2	3	1	1
71	1	2	1	2	1
72	1	1	3	1	3
73	1	2	2	1	1
74	1	1	3	3	3
75	1	1	3	1	2
76	1	1	2	2	3
77	1	2	2	2	1
78	1	1	1	3	2
79	1	1	1	1	3
80	1	2	1	3	2
81	1	1	1	2	3
82	1	1	1	1	2
83	1	1	1	1	2
84	1	1	3	1	1
85	1	1	3	1	2
86	1	1	3	3	1
87	1	2	3	3	2
88	1	2	1	2	2
89	1	2	1	3	1
90	1	2	3	3	3
91	1	2	1	3	1
92	1	1	2	3	1
93	1	2	3	3	2
94	1	1	1	3	3
95	1	1	1	1	3
96	1	2	3	1	2
97	1	2	2	2	2
98	1	1	2	3	3
99	1	1	3	3	2
100	1	1	2	2	1

```
101     1   1   2   2   2
102     1   1   2   2   2
103     1   2   3   3   1
104     1   2   1   2   1
105     1   1   3   3   1
106     1   2   1   2   2
107     1   2   3   1   2
108     1   2   1   1   2
```

Note: A: Fluid Type (1=Water, 2=Acetone); B: Lasing Power (1= 10%, 2= 50%, 3= 95%), C: Lasing Frequency (1 = 5 kHz, 2 = 10 kHz, 3 = 20 kHz); D: Nozzle Size (1= 20µm, 2= 30µm, 3= 50µm)

Factorial Design Data

No.	Fluid Type	Laser Power	Laser Frequency	Nozzle Size	% Volume Reduction
1	Acetone	10	10	50	21.65
2	Water	10	20	20	36.77
3	Acetone	10	10	50	34.20
4	Acetone	10	5	20	29.76
5	Water	50	5	30	46.64
6	Acetone	50	5	30	47.12
7	Water	50	5	20	50.87
8	Water	10	5	20	31.20
9	Acetone	50	5	20	48.14
10	Acetone	95	10	20	82.76
11	Water	50	10	50	32.10
12	Water	95	10	20	74.76
13	Acetone	10	20	50	24.16
14	Water	95	5	50	46.00
15	Water	95	10	50	48.28
16	Acetone	10	20	50	37.51
17	Acetone	50	10	20	51.99
18	Water	95	10	30	60.51
19	Water	50	5	20	52.32
20	Acetone	50	10	30	57.73
21	Water	50	5	30	49.86
22	Acetone	95	10	20	83.62
23	Acetone	95	20	20	81.72
24	Water	95	10	20	76.62
25	Acetone	10	20	30	39.52
26	Acetone	50	20	20	65.30
27	Water	95	10	30	70.85
28	Water	50	20	30	55.99
29	Acetone	95	5	20	84.39
30	Acetone	95	20	50	64.23

31	Acetone	50	20	30	56.72
32	Acetone	50	5	50	31.98
33	Acetone	95	10	30	75.14
34	Water	10	10	20	26.12
35	Water	10	10	30	36.68
36	Acetone	10	5	50	24.47
37	Water	50	10	20	53.27
38	Water	50	20	50	39.42
39	Water	50	5	50	27.92
40	Water	10	5	20	33.01
41	Water	10	10	50	18.85
42	Water	50	20	30	55.99
43	Acetone	50	20	50	48.20
44	Acetone	10	5	50	21.08
45	Water	10	20	20	38.50
46	Water	10	20	50	25.89
47	Acetone	95	5	50	60.03
48	Water	95	10	50	48.28
49	Acetone	10	5	20	43.01
50	Acetone	95	5	50	58.56
51	Acetone	95	10	30	81.00
52	Water	10	10	30	30.48
53	Acetone	95	10	50	59.55
54	Acetone	10	5	30	36.83
55	Water	50	5	50	26.89
56	Acetone	50	10	50	50.38
57	Acetone	50	20	30	59.51
58	Water	95	5	20	73.71
59	Water	10	20	30	39.51
60	Water	50	20	20	56.81
61	Water	95	20	50	59.88
62	Water	10	10	20	42.41
63	Acetone	50	5	50	44.58
64	Acetone	95	10	50	68.24
65	Acetone	50	20	50	48.20
66	Acetone	50	10	50	44.27
67	Water	95	20	30	69.17
68	Acetone	50	5	30	59.36
69	Acetone	50	20	20	67.91
70	Acetone	95	5	20	79.49
71	Acetone	10	10	20	46.59
72	Water	95	5	50	41.69

73	Acetone	50	5	20	64.30
74	Water	95	20	50	47.75
75	Water	95	5	30	58.74
76	Water	50	10	50	32.10
77	Acetone	50	10	20	63.15
78	Water	10	20	30	37.20
79	Water	10	5	50	16.69
80	Acetone	10	20	30	45.51
81	Water	10	10	50	22.31
82	Water	10	5	30	25.74
83	Water	10	5	30	25.74
84	Water	95	5	20	74.66
85	Water	95	5	30	66.51
86	Water	95	20	20	77.71
87	Acetone	95	20	30	83.50
88	Acetone	10	10	30	38.52
89	Acetone	10	20	20	43.06
90	Acetone	95	20	50	65.01
91	Acetone	10	20	20	41.19
92	Water	50	20	20	59.45
93	Acetone	95	20	30	76.79
94	Water	10	20	50	22.50
95	Water	10	5	50	15.55
96	Acetone	95	5	30	76.48
97	Acetone	50	10	30	54.97
98	Water	50	20	50	36.45
99	Water	95	20	30	65.39
100	Water	50	10	20	53.27
101	Water	50	10	30	46.90
102	Water	50	10	30	59.62
103	Acetone	95	20	20	84.98
104	Acetone	10	10	20	34.62
105	Water	95	20	20	78.57
106	Acetone	10	10	30	39.81
107	Acetone	95	5	30	77.86
108	Acetone	10	5	30	33.36